Simple Conceptual Models for Tropical Ocean-Atmosphere Interactions on Interannual Timescales

Diplomarbeit

Malte Jansen

Leibniz-Institut für Meereswissenschaften
an der Universität Kiel

Mathematisch-Naturwissenschaftliche Fakultät
der Christian-Albrechts-Universität zu Kiel

June 15, 2007

Abstract

The parameters of simple conceptual models for the coupled atmosphere-ocean dynamics in the tropics are fitted to observational data and it is analyzed how well the fitted models reproduce observed statistical properties from stochastic excitation, representing short-timescale "weather noise".

The El Niño Southern Oscillation (ENSO) is well described by the linear recharge oscillator model. In the recharge oscillator picture, the oscillation is explained by the recharging (discharging) of equatorial heat content during a La Niña (El Niño) event. On the other hand, the delayed action oscillator, in which the oscillation is due to equatorial wave travel times, turns out to be the less reasonable approximation. The observed skewness and kurtosis of eastern Pacific (Niño3) sea surface temperature (SST) timeseries can be explained by nonlinear coupling of SST on thermocline depth anomalies and effects of seasonality.

The observed dynamics of the equatorial Atlantic also turns out to be described well by the recharge oscillator model. An oscillatory mixed ocean dynamics-SST mode exists in boreal spring and summer, while the system is overdamped in fall and winter. No oscillatory coupled mode is found in the Indian Ocean. Instead, Indian Ocean SST seems to be well described by a red noise process forced by ENSO.

Fitting a simple model for the interactions of the tropical Indian and Atlantic Oceans with ENSO to observational data, it is found that the Indian Ocean tends to damp the ENSO oscillation and is responsible for a frequency shift to shorter periods. However, forecast prediction skills can hardly be improved by explicitly including the Indian Ocean SST, since the latter is strongly related to ENSO. The interactions between the Atlantic Ocean and ENSO are generally weaker than between Indian Ocean and ENSO. But some feedback from the Atlantic on ENSO seem to exist, which could improve forecast prediction skills.

Zusammenfassung

Die Parameter von einfachen konzeptionellen Modellen für die gekoppelte Dynamik von Ozean und Atmosphäre in den Tropen werden an Beobachtungsdaten angepasst. Es wird analysiert wie gut die Modelle, angetrieben von stochastischer Anregung, die das kurzzeitskalige "Wetter-Rauschen" darstellen soll, beobachtete statistische Eigenschaften des Systems reproduzieren.

Die El Niño Southern Oscillation (ENSO) wird gut durch das lineare "recharge oscillator" Modell beschrieben. Im "recharge oscillator" Bild wird die Oszillation durch das Aufladen bzw. Entladen des äquatorialen Wärmeinhaltes während eines La Niña bzw. El Niño Ereignisses bedingt. Das "delayed action oscillator" Modell hingegen, bei dem die Oszillation durch die Propagationszeit äquatorialer Wellen bedingt ist, erweist sich als weniger sinnvolle Approximation. Die beobachtete Schiefe und Kurtosis der Ost-Pazifischen (Niño3) Meeresoberflächentemperatur (SST) Zeitreihe kann durch nichtlineare Kopplung der SST an Anomalien in der Tiefe der Thermokline und durch die Saisonabhängigkeit der Variabilität erklärt werden.

Auch die beobachtete Dynamik im Gebiet des äquatorialen Atlantiks lässt sich gut durch das "recharge oscillator" Modell beschreiben. Ein gedämpft schwingender gekoppelter Ozean Dynamik-SST Mode existiert im borealen Frühling und Sommer, während das System in Herbst und Winter überdämpft ist. Im Indischen Ozean kann kein gekoppelter periodischer Mode gefunden werden. Stattdessen ist die SST des Indischen Ozeans gut beschrieben durch einen von ENSO angetriebenen "red-noise" Prozess.

Mit Hilfe eines einfachen Modelles für die Wechselwirkung des tropischen Indischen beziehungsweise Atlantischen Ozeans mit ENSO wird gezeigt dass der Indische Ozean dämpfend auf ENSO wirkt und für eine erhöhte ENSO-Frequenz verantwortlich ist. Dennoch kann die Qualität von ENSO-Vorhersagen durch die explizite Berücksichtigung des Indischen Ozeans kaum verbessert werden, da dieser selbst stark vom ENSO Signal dominiert ist. Die Wechselwirkungen zwischen dem Atlantik und ENSO sind allgemein schwächer als zwischen dem Indischen Ozean und ENSO. Jedoch scheint ein gewisser Einfluss des Atlantiks auf ENSO zu existieren, der die Vorhersagbarkeit von ENSO verbessern könnte.

Contents

Introduction

The tropical atmosphere plays a dominant role as a driving force for the planetary atmospheric circulation. Therefore disturbances in the tropics can lead to significant climate variability nearly all over the globe.

The most prominent interannual tropical climate fluctuation is the El Niño Southern Oscillation (ENSO). The El Niño phenomenon manifests as a warm sea surface temperature anomaly (SSTA) in the tropical eastern Pacific which alters the atmospheric Walker circulation. The changed winds in turn influence the ocean dynamics, causing a fast positive feedback and a delayed negative feedback, the latter beeing responsible for the observed quasi-periodic behaviour (e.g. Neelin et al. (1998) and references therein). Via atmospheric teleconnections ENSO has impacts in many regions all over the globe. Particularly the tropical Indian Ocean and parts of the tropical Atlantic region are strongly influenced by ENSO (e.g. Latif and Barnett (1995), Enfield and Mayer (1997), Latif and Grötzner (2000)).

The Indian and Atlantic Oceans might as well have intrinsic coupled Ocean-Atmosphere dynamics analog to the Pacific ENSO phenomenon. But the feedbacks are weaker and, especially in the Indian Ocean, the SSTA is dominated by the ENSO signal. The role of the intrinsic coupled dynamics in these regions is therefore harder to quantify. This explains why divergent opinions exist on the role of intrinsic coupled dynamics in these basins (e.g. Keenlyside and Latif (2007), Dommenget and Latif (2002) and references therein).

The tropical Indian and Atlantic Ocean SSTA in turn are supposed to have large-scale atmospheric teleconnections themselves. Recently, different studies investigated a possible feedback of the Indian and Atlantic Oceans on the Pacific. However, they came to different conclusions about the tropical Indian and Atlantic Oceans' influence on the ENSO cycle (e.g. Dommenget et al. (2006) and references therein).

To improve the understanding of the mechanisms responsible for the ENSO dynamics, models of different complexity have been used. They are sometimes classified into the following classes: The most complex ones are coupled Atmosphere-Ocean general circulation models (GCMs). Hybrid coupled models consist of an ocean GCM (OGCM) coupled to a simpler atmospheric model. Intermediate coupled models (ICMs) are usually based on a reduced gravity ocean model, a steady-state shallow water model

for the atmosphere and some additional parameterizations. Finally, simple conceptual models have been proposed, consisting of no more than a few box-averaged variables. This last class of models defines the scope of this study. The most prominent are the delayed action oscillator of Suarez and Schopf (1988) and Battisti and Hirst (1989) and the recharge oscillator of Jin (1997). The model parameters are usually roughly estimated from physical considerations, or derived more strictly from more complex models.

In this study an inverse modelling approach is used: Simple models are used as a hypothesis for the coupled dynamics and the model parameters are fitted to observational data. It is analyzed how well the fitted models describe the observations, which reveals whether the important interactions neceassary to describe the observed dynamics are included in the models. Examination of the fitted models finally offers a deeper understanding of the observed dynamics. Simple conceptual models are thus used as a statistical tool to systematically analyze observational data with regard to the existence of particular mechanisms described by the models.

After a short discussion of the data and methods which is given in chapter 1, this study is separated into three major parts. In chapter 2, different existing conceptual models for ENSO are analyzed and modifications are proposed. Chapter 3 analyzes whether mechanisms analog to ENSO also play a role in the Atlantic and Indian Oceans. Finally, the feedback from the Indian and Atlantic Oceans on the Pacific and their influence on the ENSO cycle is investigated in chapter 4. Each chapter contains a separate introduction and discussion of the results.

Chapter 1

Data and Methods

1.1 Data

Observational SST data is taken from the HADISST data set (Rayner et al. (2003)). This is a gridded data set based on an EOF reconstruction of observational data back till 1870. Since very little real observational thermocline depth data is available, we use 20^{o}C isotherm depth data from an NCEP-forced simulation of the MPI-OM OGCM (Marsland et al. (2003)) for the period 1950 to 2001, using standard bulk formulas for the calculation of heat fluxes and a weak relaxation of surface salinity to the Levitus et al. (1994) climatology. At some points real observational 20^{o}C isotherm depth data from the BMRC data set, is shown for comparison. This is a gridded data set based on an interpolation using data from the TAO array and ship measurements. Since all models used in this study describe interannual variability and are formulated as anomaly models, all observational/forced GCM data is linearly detrended and the seasonal cycle is removed.

1.2 Fitting Methods

Parameters for the models were obtained by performing fits minimizing the root-mean-square (rms) error of one month forecast of monthly mean data. Two different fitting methods were applied here. One is a linear regression method having the advantage of being an analytical method that provides unambiguous solutions and confidence intervals. However, it has the disadvantage that since it can only be applied to equations that are linear in the parameters it can only be applied to fit a model using one time-step per month. To overcome this problem a numerical least-squares fit is also applied. Here the time-stepping can be chosen arbitrarily. Both methods are described and discussed in detail in the following three subsections.

Both methods were applied for non-seasonal fits using the whole data set, and for seasonal dependent fits. The seasonal fits provide one set of parameters for each calendar month. In order to increase the sampling size, a 3 months moving block of data was used for the fit of each month. The seasonal fit is described in more detail in section 1.2.4.

1.2.1 The Linear Regression

Suppose a response variable Y is given by a mean depending linearly on k factors X_l, $l = 1, ..., k$ plus an error term E, so that a set of n observations Y_t and X_{lt}, t = 1,...,n is given by

$$Y_t = \sum_l a_l X_{lt} + E_t \,, \tag{1.1}$$

where E_t are independent random variables with mean zero and variance σ_E. Then the least-squares estimator for the parameter-vector $\underline{a}$ is given by

$$\underline{\hat{a}} = (\underline{\underline{X}}^T \underline{\underline{X}})^{-1} \underline{\underline{X}}^T \underline{Y}. \tag{1.2}$$

The $p \cdot 100\%$ confidence interval for the parameter a_l is given by

$$\left(\hat{a}_l - \frac{t_{(1+p/2)} \hat{\sigma}_E}{\underline{X}_l^T \underline{X}_l} \,,\; \hat{a}_l + \frac{t_{(1+p)/2} \hat{\sigma}_E}{\underline{X}_l^T \underline{X}_l} \right) , \tag{1.3}$$

where $\hat{\sigma}_E$ is the estimator for the standard deviation of E and $t_{(1+p)/2}$ denotes the accordant quantile of the students t-distribution with $n - k$ degrees of freedom (see von Storch and Zwiers (1999)).

Assume a model can be written in the form

$$\frac{d\underline{X}}{dt} = \underline{\underline{a}}\, \underline{X} + \underline{\xi} \,, \tag{1.4}$$

where $\underline{X}$ denotes the vector of variables with mean zero, contained in the model, $\underline{\underline{a}}$ is a matrix containing the parameters and $\underline{\xi}$ are the residuals that are assumed to be white noise. This prognostic equation can be approximated by its discrete analogue with an explicit time step of one month as

$$\underline{X}_{t+1} - \underline{X}_t = \Delta t\, \underline{\underline{a}}\, \underline{X}_t + \underline{\xi}_t \,, \tag{1.5}$$

where $\underline{X_t}$ denotes the vector of monthly mean values[1] of month t and $\Delta t = 1\,\text{month}$. If all variables are normalized by their standard deviatons, the parameters of $\underline{\underline{a}}$ are given in units of months^{-1}. Assuming that the model contains m different variables, equation (1.5) can be written in form of m linear equations

$$X_{j,t+1} - X_{j,t} = \sum_l a_{j,l} X_{l,t} + \xi_{j,t} \quad j = 1, ..., m. \tag{1.6}$$

Defining $Y_{j,t} = X_{j,t+1} - X_{j,t}$, the linear regression can be applied separately for each equation with fixed j.

However, for some models discussed in the following, parameters occurring in different equations are set to be identical. For example, in the simplest recharge oscillator model (which is explained in detail in section 2.4) ω_0 occurs in both, the SST and the thermocline depth equation. In this case the different variables are interpreted as elements of one dataset. For simplicity this is only explained for the example of the simplest recharge oscillator model. The model can be written as

$$\begin{array}{ll} \frac{d}{dt} T_P = \omega_0 h_P - 2\gamma_P T_P + \xi_T \\ \frac{d}{dt} h_P = -\omega_0 T_P \qquad\quad + \xi_h \end{array} \tag{1.7}$$

The reader might verify that for a time-series of length τ this model with discrete explicit time stepping can be written in the form:

$$\begin{pmatrix} \Delta T_1 \\ \vdots \\ \Delta T_{\tau-1} \\ \Delta h_1 \\ \vdots \\ \Delta h_{\tau-1} \end{pmatrix} = \begin{pmatrix} -2T_1 & h_1 \\ \vdots & \vdots \\ -2T_{\tau-1} & h_{\tau-1} \\ 0 & -T_1 \\ \vdots & \vdots \\ 0 & -T_{\tau-1} \end{pmatrix} \begin{pmatrix} \gamma \\ \omega_0 \end{pmatrix} + \begin{pmatrix} \xi_{T,1} \\ \vdots \\ \xi_{T,\tau-1} \\ \xi_{h,1} \\ \vdots \\ \xi_{h,\tau-1} \end{pmatrix} \tag{1.8}$$

where $\Delta T_t = T_{t+1} - T_t$ and $\Delta h_t = h_{t+1} - h_t$.

This can be written in the form

$$\underline{Y_t} = \underline{\underline{X}}\,\underline{a} + \underline{E}\,, \qquad Y, E \in \mathbb{R}^{2(\tau-1)}\,,\ X \in \mathbb{R}^{2\times 2(\tau-1)}\,,\ a \in \mathbb{R}^2 \tag{1.9}$$

or:

[1]The dimensionless monthly noise ξ_t is given as the monthly mean of ξ times one month

$$Y_t = \sum_{l=1,2} a_l X_{lt} + E_t, \qquad t = 1..2(\tau - 1) \tag{1.10}$$

which is similar to equation 1.1. The linear regression can now be applied to find least-squares estimates for γ and ω_0. However, even if h and T are normalized to have the same variance, this does not necessarily apply fo ξ_h and ξ_T and thus for the E_t. It should be mentioned that in this case the least-squares estimator is no longer the best fit in the sense that the variance of the parameter estimates is minimal.

Finally, some models are used where one predictor variable is evaluated at some time lag. This time lag is not a linear parameter and thus cannot be fitted by linear regression. Instead it has to be estimated or fitted using the numerical fit described in the following section and has to be taken as a constant for the linear regression.

1.2.2 The Numerical Least-Squares Fit

If a model using only one time step per month is fitted to observational data it will have a systematic bias compared to a continuous model (or a model using much shorter time steps). That is why it is desirable to fit parameters to a model, using more than one time step per month. But, any model given by a system of linear differential equations will become nonlinear in the parameters if more than one timestep shall be used. Still, all models used in this study can be written as

$$\underline{X}_t = f(\underline{a}, \underline{X}_{t-1}) + \underline{\xi}\,, \tag{1.11}$$

where $\underline{a}$ denotes the parameter vector and $\underline{X}_t$ denotes the vector containing the model variables at month t. Thus, given an estimator for the parameter vector $\underline{\hat{a}}$, an estimator for the model variables for the next timestep is given by

$$\underline{\hat{X}}_t = f(\underline{\hat{a}}, \underline{X}_{t-1})\,. \tag{1.12}$$

A least square estimator for the elements of $\underline{a}$ can generally be found by numerically minimizing[2]

$$\sum_t (\underline{X}_t - \underline{\hat{X}}_t)^2 = \sum_t (\underline{X}_t - f(\underline{\hat{a}}, \underline{X}_{t-1}))^2\,. \tag{1.13}$$

Again it should be mentioned that this is not necessarily the best fit in the sense that the variance of the parameter estimates is minimal. Further it should be mentioned

[2]Here the matlab routine "fminsearch" is used to estimate the minimum.

that solutions are generally not definite, so the results might depend on the starting values of the numerical minimization. However, it turns out that for most of the models and the number of time steps used in this study the results are unambiguous and in general agreement with the results of the linear regression for all physically reasonable starting values. Ten time steps were used for one month forecasts in all numerical fits presented in this study.

1.2.3 A Monte Carlo Experiment to Review Fitting Methods

A Monte Carlo experiment is performed to test the fitting methods. The major goal is to estimate the systematic bias of the linear regression due to the fact that only one time step per month is used, and to check the reliability of the significance intervals given by the linear regression.

A number of artificial data sets is constructed using the recharge oscillator with stochastic excitation. It can be written as

$$\frac{d}{dt}\begin{pmatrix} T_E \\ h \end{pmatrix} = \begin{pmatrix} a_{11} & a_{12} \\ a_{21} & a_{22} \end{pmatrix}\begin{pmatrix} T_E \\ h \end{pmatrix} + \begin{pmatrix} \xi_T \\ \xi_h \end{pmatrix}, \tag{1.14}$$

where T_E is the equatorial eastern Pacific SSTA and h is the zonally averaged equatorial thermocline depth anomaly. The terms ξ_T and ξ_h denote stochastic excitation due to short time scale "weather" noise, which is approximated as white noise. The model will be discussed in detail in section 2.3.

Equation (1.14) is integrated using 10 time steps per month with parameters given in table 1.1.

a_{11}	a_{12}	a_{21}	a_{22}
-0.08	0.13	-0.14	-0.01

Table 1.1: Parameters used for the construction of an artificial data set, units are month^{-1}.

These parameter values are based on parameter fits to Pacific observational data. The noise forcings are fitted to mimic statistical properties of observed data.

An ensemble of 10000 runs was performed. Each run was integrated for 52 years, the usual length of observational data used in this study. Then a recharge oscillator model was fitted to each 52 year-output using the two methods described above. Table 1.2 shows the averaged results of the numerical fit and the linear regression to these artificial data sets. Additionally, the third column shows the confidence interval of each numerical fit, calculated from the 0.025 and 0.975 quantiles of the

ensemble. Since in practical applications only one dataset is available, such an ensemble based estimation of the confidence intervals cannot be made. Instead, due to its computational simplicity it is practicable to calculate error estimates using the linear regression. The mean confidence intervals estimated by linear regression are given in the last column of table 1.2.

	Numerical Fit	Linear Regression	2.5% and 97.5% quantiles of Num. Fit	95% conf. Int. estimated with Lin. Regr.
a_{11}	-0.083	-0.088	$\hat{a}_{11} - 0.033$; $\hat{a}_{11} + 0.026$	$\hat{a}_{11} \pm 0.028$
a_{12}	0.131	0.125	$\hat{a}_{12} - 0.028$; $\hat{a}_{12} + 0.030$	$\hat{a}_{12} \pm 0.028$
a_{21}	-0.141	-0.135	$\hat{a}_{22} - 0.021$; $\hat{a}_{22} + 0.019$	$\hat{a}_{22} \pm 0.019$
a_{22}	-0.011	-0.019	$\hat{a}_{21} - 0.022$; $\hat{a}_{21} + 0.019$	$\hat{a}_{21} \pm 0.019$

Table 1.2: Parameters and confidence intervals resulting from the numerical fit and the linear regression. All values are ensemble mean values, except for the confidence intervals calculated from the quantiles of the ensemble given in the 3rd column. all values are ensemble mean values.

The averaged results of the numerical fit are in good agreement with the original parameters used by the stochastic model with which the data sets were constructed. This was to be expected, since the model used for the numerical fits is exactly the same as the model used to produce the data. On the other hand there is a systematic bias of the parameters fitted with the linear regression of 0.005-0.009 month^{-1}. The error is smaller than the significance interval for the parameters, but since the values given in table 1.2 are calculated as a mean of 10000 fits, it definetely reveals a systematic bias. This is due to the fact that the linear regression uses only one time step per month.

According to the ensemble size, the quantiles of the ensemble of numerical fits can be assumed to be accurate to ± 1 for the last given digit. The confidence intervals estimated by linear regression are in adequate agreement with the corresponding intervals estimated from the ensemble. So assuming that the model perfectly describes the underlying physics and that the noise forcing for different months is independent, the confidence intervals from the linear regression are a useful estimator. However, errors that are due to unconsidered dynamics with timescales of more than one month might lead to an underestimation of the confidence intervals.

In the following, the results of the numerical fit are given as the fitted value, whereas the confidence intervals of the parameters are estimated based on the linear regression, for want of a more accurate estimation. The confidence intervals of eigenvalues that are presented in this study are estimated based on a Monte Carlo experiment, assuming a Gaussian probability distribution for the parameter values.

1.2.4 Seasonal Dependent Parameter Fits

For some models presented in the following, seasonal dependent parameter sets shall be fitted. However, if parameters are fitted separately for each calendar month the effective sample size is only one twelfth of the sample size available for non-seasonal-dependent fits. To attain maximum sample size retaining maximum seasonal resolution, a 3 month moving data block is used to fit monthly parameters. This means that parameters for a calendar month m are fitted using data of the calendar months m-1, m, and m+1 modulo 12. For example, for the January parameter-values all data of December, January and February is used for the parameter fit. For the February parameters, January, February and March data is used and so forth.[3]

[3]Strictly speaking the predictor data set is formed of data containing months (m-1, m, m+1)mod12. The response variable for month t is constructed as $Y_t = X_{t+1} - X_t$.

Chapter 2

Simple Models for ENSO

2.1 Introduction

Our understanding of the coupled atmosphere-ocean dynamics in the tropical Pacific, responsible for the well known El Niño events, began with the results of Bjerknes (1964). He discovered the positive feedback mechanism between eastern Pacific SSTA, zonal wind stress anomalies and ocean dynamics. However, for the observed quasi-periodic development and decay of ENSO anomalies a delayed negative feedback is also necessary. An early model study of the dynamics resposible for ENSO was performed by Zebiak and Cane (1987). They were able to reproduce the irregular recurrence of warm events with a preferred period of three to four years in a coupled model of intermediate complexity (ICM). To improve the understanding of the basic mechanisms responsible for ENSO, even more simple conceptual models were proposed that condense the dynamics to ordinary differential equations (ODE) or delay differential equations (DDE). This class of ENSO models defines the scope of this study.

Suarez and Schopf (1988) first presented the delayed action oscillator, consisting of one DDE for eastern equatorial Pacific SSTA. The oscillation in this model is explained by equatorial wave transport processes. A positive (negative) SSTA in the equatorial eastern Pacific induces a positive (negative) zonal wind stress anomaly in the central Pacific. This causes downwelling (upwelling) Kelvin waves travelling to the East and upwelling (downwelling) Rossby waves travelling to the West. The Kelvin waves are therefore responsible for a downwelling (upwelling) in the eastern basin which in turn causes a warming (cooling) of SST. This is the positive Bjerknes feedback. The oscillation is due to the reflection of the Rossby waves at the western boundary into upwelling (downwelling) Kelvin waves, inducing the transition to a La Niña (El Niño) event. The SSTA is assumed to be in equilibrium with thermocline depth anomalies in this model. Battisti and Hirst (1989) (hereinafter BH89) find the same equation by following a more strict derivation. They suggest quite differ-

ent parameter sets, though, corresponding to different regimes, as will be shown in the next section. More generally, lively discussion exists whether ENSO reveals a self-sustained and irregular behaviour due to nonlinear dynamics within the "slow" components of the coupled system, whether the oscillation is sustained by uncoupled short timescale "weather noise", or whether the oscillation is self-sustained but the irregularity is due to the "weather noise" (see Neelin et al. (1998) an references therein).

Jin (1997) proposes the recharge oscillator model, which can be written in terms of two linear first order ODEs for eastern Pacific SSTA and thermocline depth anomaly. The oscillation in this model is explained by discharging (recharging) of equatorial heat content during an El Niño (La Niña) event. Equatorial wave travel times are not explicitly considered in this model. Burgers et al. (2005) perfom a parameter fit of the recharge oscillator model to observational SST and thermocline depth data. Based on the results of their fit they suggest a further simplification of the recharge oscillator model to a simple damped harmonic oscillator with SSTA playing the role of momentum and thermocline depth playing the role of position.

One of the shortcomings of all these models is that they do not reproduce the observed kurtosis and skewness of eastern Pacific SSTA, with extreme events being more likely than for an ordinary Gaussian distribution and El Niño events being stronger than La Niña events.

It has been known for long that ENSO is strongly locked to the seasonal cycle, with El Niño events usually peaking towards the end of the year - after all, El Niño owes its name to this fact. Jin et al. (1996) also discuss a possible influence of seasonality on ENSO periodicity and its regularity via frequency locking to rational multiples of one year. They find a quasi-biennial and a $\frac{4}{3}$-year peak next to the dominating 4-year period, in an ICM if the annual cycle is included. The predictability of ENSO does also largely depend on the time of the year, with the prominent prediction barrier in boreal spring (e.g. McPhaden (2003)). However, controversial discussion exists on whether the explicit consideration of seasonality in simple statistical ENSO prediction models allows for better forecasts (see for example Xue et al. (2000) and references therein).

In this study, the parameters of different conceptual models for ENSO, accounting for different physical key mechanisms, are fitted to observational data. The different models are then compared in terms of their capability to reproduce observed statistical properties of ENSO, if excited by stochastic forcing, representing short timescale uncoupled "weather-noise". Further their predictive skills as forecast models are examined.

Sections 2.2 to 2.4 discuss the delayed action oscillator and the recharge oscillator model. In section 2.5, a simple unification of the delayed action oscillator and the recharge oscillator is proposed.

The observed skewness and kurtosis of Niño3 SSTA timeseries is explained by the nonlinear coupling of SSTA on thermocline depth anomalies and effects of seasonality in section 2.6.

In section 2.7, seasonality is included in the recharge oscillator model by allowing for seasonal dependent parameters. It is analyzed whether the observed seasonality can be reproduced by such a model and whether the annual mean statistics are influenced by the locking to the seasonal cycle. Finally the predictive skill of the seasonal dependent recharge oscillator is examined.

2.2 The Delayed Action Oscillator

2.2.1 Model Description

The "oldest" conceptual model being discussed in this study is the delayed action oscillator that was first presented by Suarez and Schopf (1988) and BH89. The linear version of the delayed oscillator model can be written as

$$\frac{dT}{dt}(t) = -bT(t-\tau) + cT(t)\,. \tag{2.1}$$

The equation describes the SST anomaly (T) averaged over a box in the eastern equatorial Pacific which is influenced by a fast feedback represented by $cT(t)$ and a delayed effect represented by the term $bT(t-\tau)$. The term $cT(t)$ includes the effects of thermal damping, upwelling/downwelling Kelvin waves, coastal upwelling and horizontal advection. The term $bT(t-\tau)$ accounts for the effects of Rossby waves reflected as Kelvin waves at the western boundary. τ is thus given by the travel times of equatorial waves and is estimated to be 180 days in BH89.

It should be stressed that for the parameters proposed by both groups the linear model reveals infinite growth. Thus a nonlinear extension is necessary to avoid infinite growth.

Using the approach $T = T_0 \exp(\lambda t)$ for (2.1) the eigenvalues λ are given by the implicit equation

$$\lambda = -b\exp(-\lambda\tau) + c\,. \tag{2.2}$$

The solutions of 2.2 are discussed in detail in BH89. Here, a simple way to approximate the delayed oscillator shall be presented.

The slowly oscillating weakly damped/growing solutions where $|\lambda| << \tau^{-1}$ (τ is

estimated to be 180 days here whereas the El Niño period seems to be about 4 years) can be found by approximating $T(t-\tau)$ by its Taylor expansion:

$$T(t-\tau) = T(t) - \frac{dT}{dt}\tau + \frac{1}{2}\frac{d^2T}{dt^2}\tau^2 + O(\tau^3)\,. \tag{2.3}$$

Therefore, neglecting third and higher order terms, equation (2.1) can be approximated as

$$\frac{dT}{dt} = -b(T - \tau\frac{dT}{dt} + \frac{\tau^2}{2}\frac{d^2T}{dt^2}) + cT\,. \tag{2.4}$$

This can be rewritten in the classical form of a damped harmonic oscillator

$$\frac{d^2T}{dt^2} = -\omega_0^2 T - 2\gamma\frac{dT}{dt} \quad with \quad \omega_0^2 = \frac{2(b-c)}{b\tau^2} \quad and \quad \gamma = \frac{1-b\tau}{b\tau^2}\,. \tag{2.5}$$

The eigenvalues of (2.5) are given by

$$\lambda_{1/2} = -\gamma \pm \sqrt{\gamma^2 - \omega_0^2}\,. \tag{2.6}$$

These eigenvalues can be obtained by using the approach $T = T_0\exp(\lambda t)$ and solving (2.5) for λ or by rewriting (2.5) into a system of two first order ODEs and calculating the eigenvalues of the matrix describing the time derivation, as explained in appendix A. It should be noted that the same solution as in (2.6) is obtained if the exponential function in (2.2) is replaced by its Taylor expansion up to the order τ^2. Equation (2.2), however, has multiple solutions. The general solution of (2.1) is given by an infinite sum of sinusoidal solutions and is thus generally not exactly sinusoidal itself. Equation (2.6) provides an approximation for the "slowest" mode, which turns out to be dominant.

It shall especially be pointed out here that the original model described by equation (2.1) as well as the approximation given by (2.5) both reveal a similar division into four different parameter regimes. The four regimes and the corresponding parameter ranges in equation (2.5) are given as[1]:

Damped solutions	for	$\gamma > 0$	and	$\gamma^2 > \omega_0^2$
Damped oscillatory solutions	for	$\gamma > 0$	and	$\gamma^2 < \omega_0^2$
Growing oscillatory solutions	for	$\gamma < 0$	and	$\gamma^2 < \omega_0^2$
At least 1 purely growing solution	for	$\gamma < 0$	and	$\gamma^2 > \omega_0^2$

[1]Strictly speaking this is only valid if ω_0^2 is positive. If ω_0^2 is negative, there is always a purely growing mode.

The four different regimes in the parameter space of the harmonic oscillator are shown in figure 2.1. In the growing regimes the addition of nonlinear terms is necessary to get realistic behaviour. The simplest nonlinear extension of the delayed oscillator model is the addition of a term proportional to $-T(t)^3$ in equation (2.1). The equation is then similar to the delayed action oscillator model presented by Suarez and Schopf (1988). BH89 give physical justifications for the different nonlinear extensions. However, many aspects are quite similar in the nonlinear system. The oscillation period differs only slightly between the nonlinear model and its linear counterpart and most importantly there are still four different regimes in the nonlinear model. The "growing oscillation" is replaced by a self sustained oscillation (the amplitude is limited by the nonlinear damping). And instead of the "purely growing" phase one finds a regime with two stable fixpoints (where the positive linear feedback and the negative nonlinear feedback are in balance).[2]

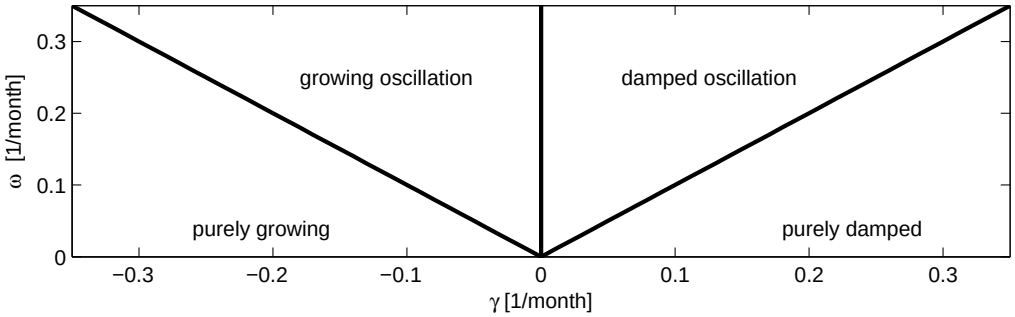

Figure 2.1: The four parameter regimes of the damped harmonic oscillator.

Suarez and Schopf propose parameters that belong to the purely growing regime in the linear version but still reveal oscillations between two unstable fixpoints in the nonlinear model (an "El Niño" and a "La Niña" state). Estimating the parameters on the base of an ICM, BH89 find parameters belonging to the growing oscillatory phase, which becomes a self-sustained oscillation in the nonlinear model. More recently it was proposed (e.g. Penland and Sardeshmukh (1995)) that the system is in the regime of a damped oscillation, forced by uncoupled short timescale variability that acts as a white noise forcing on longer timescales.

2.2.2 Parameter Fit to Niño3 Observational Data

The parameters of the linear delayed oscillator, as described in the previous section are fitted to observational Niño3 (5^oS–5^oN, 150^oW 90^oW) SST data, described in

[2]It should be noted that the parameters where these bifurcations occur are not exactly the same in the nonlinear model and in its linear counterpart.

section 1.1, by minimizing the rms error of one month forecasts. The fit routines are described in section 1.2.

Parameters and prediction skills are cross-validated by first using the time period from 1950 to 1975 for the parameter fit and the period from 1976 to 2001 for the evaluation of the forecast skill and vice versa.

Table 2.1 shows the fitted values for the parameters resulting from the numerical fit and the 95% significance intervals estimated from the linear regression. There is no error estimate for the timelag, since this cannot be fitted using the linear regression.

	1950-1975	1976-2001	1950-2001
b	0.13 ± 0.09	0.13 ± 0.07	0.13 ± 0.06
c	-0.03 ± 0.09	-0.01 ± 0.07	0.0 ± 0.06
τ	$6,4$	$5,7$	$5,9$

Table 2.1: Fitted parameters of the linear delayed action oscillator model for the Pacific. b and c are given in units [month^{-1}], τ is given in month. The upper row gives the time periods of observational data used for the fits.

The fitted parameter values for the different periods are equal within the 95% significance interval given by the linear regression. This suggests that the physical processes described by this model can be assumed to be stationary. It should be mentioned that the results for the numerical fit – especially the result for τ – depend on the value of τ used to initialize the numerical fit. However, in the realistic range of initialization values the result for τ lies between sligthly less than five and slightly more than six months, while the other parameters are not influenced significantly. A timelag τ of six month is also consistent with the estimation of BH89 based on a Zebiak and Cane (1987) -type model. Considering equation (2.5), the fitted model can be approximated by a damped oscillator with $\gamma \approx 0.05$ month^{-1} and $\omega \approx 0.24$ month^{-1}. This would reveal a damped oscillation with a period of about two years and a damping timescale of 20 months.

Suarez and Schopf (1988) analyze the behavior of the delayed oscillator model with an additional nonlinear term proportional to T^3. Based on physical arguments, the model dynamics are discussed for the parameter range $0 < \alpha = b/c < 1$. In this parameter range the linear approximation reveals infinite growth and no oscillation. With an additional nonlinear damping, the equation has an unstable fixpoint at $T = 0$ and two 'outer' fixpoints symmetric to $T = 0$, belonging to a cold and a warm state. These solutions are unstable as well for some sets of parameters, and an oscillation between the warm and the cold state can occur, given an additional nonlinear damping.

BH89 derive the parameters of the linear delayed oscillator model from an interme-

diate complex coupled model. They find parameters $b = 3.9\,\mathrm{yr}^{-1} \simeq 0.33\,\mathrm{month}^{-1}$, $c = 2.2\,\mathrm{yr}^{-1} \simeq 0.18\,\mathrm{month}^{-1}$ and $\tau = 180\,\mathrm{days} \simeq 6\,\mathrm{months}$. In this parameter range the model reveals a growing oscillation with a dominating period of 3 years. This is in good agreement with the intermediate complex model that is used to derive these parameters, which also reveals a growing oscillation in its linearized approximation.

The fits performed in this study suggest a damped oscillatory parameter regime. To exclude the possibility that the linear damping/amplification c is underestimated, due to the lack of an explicit consideration of a nonlinear damping, parameter fits with an additional term proportional to T^3 were also performed. In contrast to the assumptions of Suarez and Schopf (1988) and BH89 that the linear approximation reveals a purely growing or growing oscillatory mode, which is damped by nonlinear effects, the nonlinear parameter fit results in a linear damping (i.e. $c < 0$) and no significant nonlinear damping or amplification[3]. For this reason this nonlinear extension is not discussed in more detail here.

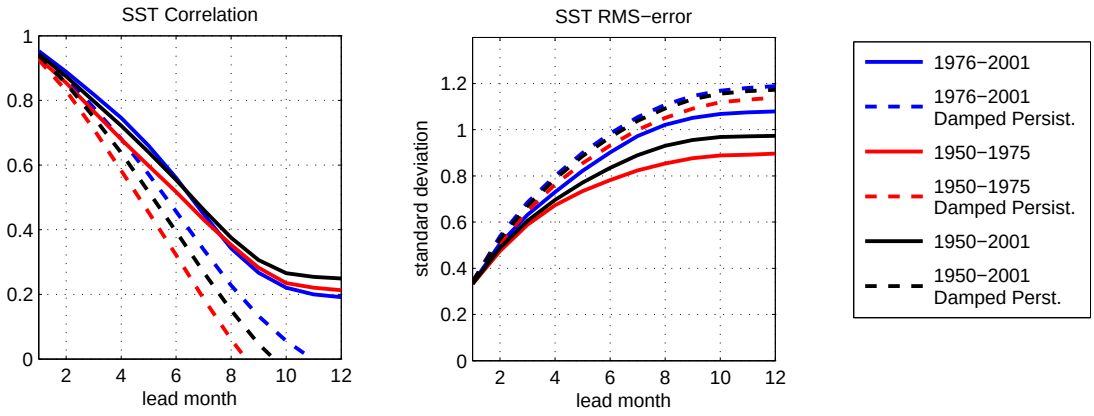

Figure 2.2: Forecast skill of the delayed action oscillator model for the Pacific. The colored lines show cross-validated forecast skills. The time intervals given in the legend refer to the period used for the forecast skill evaluation, while in each case the other interval was used to fit the parameters. For the black line the whole time period was used for the parameter fit and for the evaluation of forecast skill. Left: Anomaly correlation between predictions and observations. Right: rms error of predictions in units of one standard deviation.

Figure 2.2 shows the forecast skill of the linear delayed oscillator for Niño3 SSTA for the time period 1950 to 2001 and the cross-validated forecast skills for the first and second half of the timeseries. Shown is the correlation between predictions and observations as well as the rms-error of predictions. The damped persistence skill of a fitted AR1-process is shown for comparison. It should be noted that an AR1-process does not have any correlation-skill above persistence, which means that its

[3]Indeed the fits of the nonlinear model reveal an (unsignificant) nonlinear amplification. Due to the positive nonlinear term, this model reveals infinite growth, once T exeeds a certain limit, which is not physically reasonable.

correlation skill is simply the auto-correlation of the timeseries. On the other hand, the rms-error of (undamped) persistence forecasts, which converges towards $\sqrt{2}$ times the standard deviation, is always higher than the rms-error of an AR1-process, which converges towards one standard deviation for long lead times. This should also be kept in mind if the forecast skill of a GCM is compared to any damped model or to ensemble predictions. While the rms-error of single GCM runs also converges towards $\sqrt{2}$ times the standard deviation for long "unpredictable" lead times, the skill of any damped model or of a large ensemble mean converges towards one standard deviation. They will therefore naturally have a smaller rms-error, especially for long lead times, than a single GCM run even if this is not the case for the correlation skill, which is sometimes not clearly pointed out in literature.

Significant forecast skill above damped persistence is found for both cross-validated timeseries using the delayed action oscillator model. The small difference between the cross-validated skills and the skill of the not cross-validated run using the whole timeseries for the parameter fits and for the evaluation suggests that 26 years provide sufficient data for the fits and that there is very little artificial skill.

2.2.3 The Delayed Oscillator Excited by Stochastic Forcing

With the parameters fitted in the previous section, the model reveals damped oscillatory behaviour. To retain variance the model, which shows damped oscillatory behaviour for the parameters fitted in the previous section, is excited by stochastic exitation as proposed for example by Jin (1997) for the recharge oscillator model. Physically, the noise forcing represents short timescale uncoupled variability, that is assumed to be representable by white noise forcing on the timescales of the coupled atmosphere-ocean dynamics described by the model (see also Hasselmann (1976)). The equation for the delayed oscillator excited by stochastic forcing can then be written as

$$\frac{dT}{dt}(t) = -bT(t-\tau) + cT(t) + \xi(t)\,, \tag{2.7}$$

where $\xi(t)$ represents the white noise forcing.

This model is integrated for $3 \cdot 10^4$ years using 10 time steps per month. The parameters fitted in the previous section to 1950 to 2001 observational data and white noise forcing with the amplitude fitted to mimic the variance of Niño3 SST is used. Figure 2.3 compares the resulting power spectrum and the frequency distribution of monthly mean values to observational Niño3 SST data from 1870 to 2003. Looking at the power spectral density we find a major peak of the model spectrum at a period of little more than two years, in accordance with the estimate in the previous section. This major peak is shifted to higher frequencies compared to the observational spectrum where it lies at frequencies corresponding to four or five year periods. A minor peak can be identified at a period of little less than six months. This second peak fits

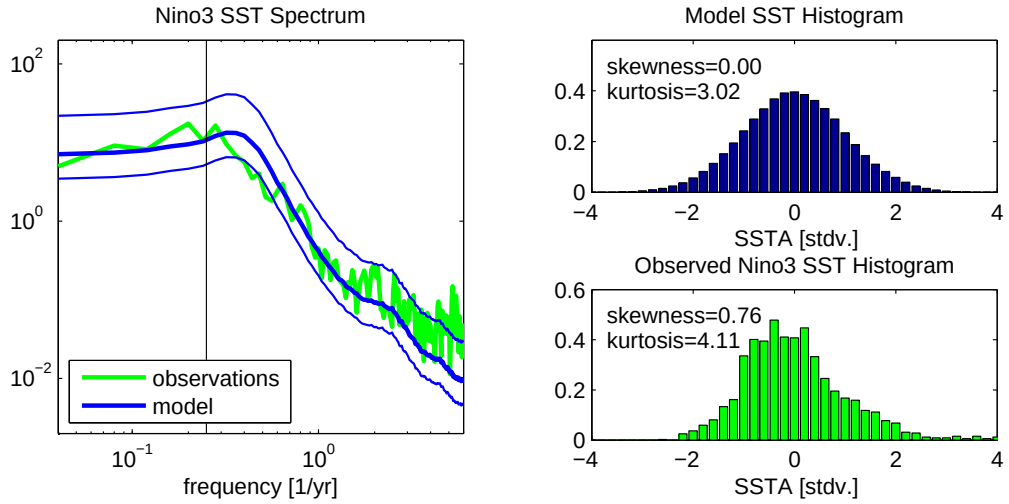

Figure 2.3: Spectra and frequency distribution of the linear delayed action oscillator model excited by stochastic noise forcing and observed Niño3 SST timeseries. The thin blue lines show 95% confidence levels. The thin black vertical line in the spectral density plot denotes a period of four years. The SSTA in the frequency distributions is normalized by the standard deviation of Niño3 SST.

well with observations. For very high frequencies there is significantly more variance in the observational timeseries. This might indicate a failure of the model to reproduce the variability on monthly timescales but it might as well an aliasing effect due to sparse sampling especially of the older observational data. If only the last 30 years of observational data are used for a power spectrum, less variance is found on short timescales as well. The frequency distribution of the model is nearly Gauss shaped whereas the observed frequency distribution of Niño3 SST has significant skewness and kurtosis. This is due to seasonal and nonlinear effects that are not contained in this model. They are discussed in detail in section 2.6.

2.3 The Recharge Oscillator

2.3.1 Model Description

The linear recharge oscillator introduced by Jin (1997) can be written in the form of two prognostic and two diagnostic equations:

$$\begin{aligned} \tfrac{d}{dt}h_W &= -rh_W - \alpha\tau \\ \tfrac{d}{dt}T_E &= -cT_E + \gamma h_E \\ \tau &= bT_E \\ h_E &= h_W + \tau\,, \end{aligned} \tag{2.8}$$

where h_W and h_E are the equatorial western and eastern Pacific thermocline depth anomalies, T_E is the equatorial eastern Pacific SST anomaly and τ represents the zonally integrated wind-stress anomaly in the equatorial Pacific.

The first equation describes the response of western Pacific thermocline depth to equatorial wind stress forcing. The second equation gives the response of eastern Pacific SST to eastern Pacific thermocline depth anomalies. The third equation states an instantaneous response of the averaged wind stress forcing to eastern Pacific SST anomalies and the last equation states an instantaneous adjustment of the thermocline tilt to the wind stress. Equatorial wave travel times are thus not explicitely considered here. As mentioned in Burgers et al. (2005) this system of equations can be transformed to a system of equations of the following form:

$$\frac{d}{dt}\begin{pmatrix} T_E \\ h \end{pmatrix} = \begin{pmatrix} a_{11} & a_{12} \\ a_{21} & a_{22} \end{pmatrix}\begin{pmatrix} T_E \\ h \end{pmatrix}, \tag{2.9}$$

where $h = 0.5(h_E + h_W)$, which is approximately the zonally averaged equatorial thermocline depth and the parameters are given as

$$a_{11} = -c + \gamma\frac{b}{2}\,, \quad a_{12} = \gamma\,, \quad a_{21} = r\frac{b}{2} - \alpha b - c\frac{b}{2} + \gamma\frac{b^2}{4}\,, \quad a_{22} = -r + \gamma\frac{b}{2}\,. \tag{2.10}$$

The damping terms a_{11} and a_{22} include the direct damping terms[4] $-c$ and $-r$ and the indirect amplification due to the atmosphere-ocean coupled feedback, first hypothesized by Bjerknes (1969). Oscillatory behaviour can occur due to the surface-subsurface coupling terms a_{12} and a_{21} of which a_{12} is apparently the direct coupling

[4]Here c already contains a temperature advection and coastal upwelling term that is mentioned separately in Jin (1997)

of surface temperature to the subsurface watermass that is considered to be relatively warm when the thermocline is deep, and cold when the thermocline is shallow. The coupling of thermocline depth to SST on the other hand is only via the atmospheric bridge as expected, which can be seen by the occurence of b in all terms of a_{21} in (2.10) and is, as suggested by parameter fits, dominated by the negative terms. This allows for the 'recharge mechanism', which means that the mean thermocline raises and the equatorial heat content discharges during an El Niño event, allowing for the transition to a La Niña, whereas equatorial heat content recharges during a La Niña event, allowing for the transition towards an El Niño. This recharge-discharge mechanism was shown to be necessary for the El Niño oscillation by Zebiak and Cane (1987) and it is confirmed by analysis of observational data by Meinen and McPhaden (2000).

It should be stressed that equation (2.8) could also be transformed into an equation similar to (2.9) with h being replaced by h_E or h_W and with different parameters a_{ij}. The averaged thermocline depth, however, turns out to be a very useful predictor variable.

Equation (2.9) can be transformed into one second order ODE for T_E. Defining $\gamma = -\frac{1}{2}(a_{11} + a_{22})$ and $\omega_0^2 = a_{11}a_{22} - a_{12}a_{21}$, it has the common form of the damped oscillator equation

$$\frac{d^2T_E}{dt^2} = -\omega_0^2 T_E + 2\gamma \frac{dT_E}{dt}\,. \tag{2.11}$$

Thus, the discussion of the four parameter regimes in section 2.2 is equally valid for the recharge oscillator model.

As explained in Appendix A the eigenvalues of the recharge oscillator are given by the eigenvalues of the matrix in 2.9 as

$$\lambda_{1,2} = \frac{1}{2}(a_{11} + a_{22}) \pm \sqrt{\frac{(a_{11} - a_{22})^2}{4} + a_{12}a_{21}}\,. \tag{2.12}$$

So the criterion for oscillatory behaviour is

$$-a_{12}a_{21} > \frac{(a_{11} - a_{22})^2}{4}\, y \tag{2.13}$$

and in the oscillatory regime the criterion for growth (what corresponds to a self-sustained oscillation in the nonlinear extension) is given by

$$a_{11} + a_{22} > 0\,. \tag{2.14}$$

2.3.2 Parameter Fit to Observational Data

The parameters of the recharge oscillator as written in equation (2.9) are fitted using HADISST Niño3 SST data for T_E and 20^oC isotherm GCM data averaged over the equatorial Pacific (120^oE 80^oW) for h. The data is described in detail in section 1.1 and the parameter fits are explained in section 1.2.

Parameters and prediction skills are cross-validated by first using the time period from 1950 to 1975 for the parameter fit and the period from 1976 to 2001 for the evaluation of the forecast skill and vice versa. Additionally a "best fit" was performed using the whole data set from 1950 to 2001.

The following table shows the fitted parameter values in units of month^{-1} resulting from the numerical fit and the 95% confidence intervals estimated from the linear regression.

	1950-1975	1976-2001	1950-2001
a_{11}	-0.10 ± 0.04	-0.06 ± 0.03	-0.08 ± 0.03
a_{12}	0.12 ± 0.04	0.14 ± 0.04	0.13 ± 0.03
a_{21}	-0.16 ± 0.03	-0.12 ± 0.02	-0.14 ± 0.02
a_{22}	0.00 ± 0.03	-0.01 ± 0.02	-0.01 ± 0.02

Table 2.2: Fitted parameters and 95% significance intervals of the recharge oscillator model for the Pacific in [month^{-1}]. The upper row gives the time periods of observational data used for the fits.

As for the delayed oscillator model, the fitted parameter values for the different periods are consistent within the 95% confidence levels. This suggests that the physical processes described by this model can be assumed to be stationary. Looking at the parameter values one can see that the value of a_{22} is not significantly different from zero and the absolute value of a_{21} is not significantly different from a_{12}. This is in agreement with Burgers et al. (2005) who used this result as a justification for the simplest recharge oscillator model. Also the parameter values are, within the given 95% intervals, in agreement with the results of Burgers et al. (2005) although they used real observational thermocline depth data for the time period from 1980 to 2003 for their parameter fits.

Considering equation (2.13) we find that the fitted set of parameters belongs to a damped oscillatory regime with an eigenfrequency corresponding to a period of about 4 years $\pm$ 9 months and a damping timescale of around 2 years (22 +15/-6 months). This is in agreement with the eigenfrequency estimated from the power spectrum of observed data.

As explained in Appendix A, the solutions of (2.9) are given by $exp(\lambda_i) * v_i$, where

λ_i are the eigenvalues and v_i are the corresponding eigenvectors. If the criterion for oscillation (2.13) is fulfilled, one pair of complex conjugated eigenvalues and eigenvectors is found, from which the phase relation of T_E and h can be determined. For the fitted parameters thermocline depth anomalies lead SSTA by about 75^o, and SSTA lead thermocline depth anomalies of opposite sign by 105^o. This phase difference describes the heating/cooling of SST due to thermocline depth anomalies and the recharging/discharging of heat content during a La Niña/El Niño event which is essential for the oscillation. For an undamped oscillation the phase difference is exactly 90^o.

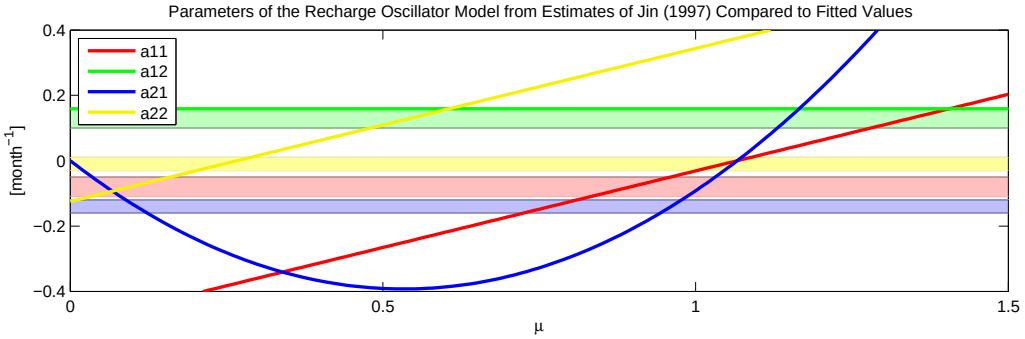

Figure 2.4: Parameters of the recharge oscillator model as written in equation (2.9), derived from the parameters discussed by Jin (1997), plotted against the tuning parameter μ which characterizes the strength of air-sea coupling. The shaded areas denote the 95% confidence intervals of the corresponding parameters resulting from the fits performed in this study.

Jin (1997) estimates parameters for the recharge oscillator model from rough physical considerations. The properties of equations (2.8) are discussed for $c = 0.5\,month^{-1}$, $\gamma = 0.01875\,\frac{K}{m\,month}$[5], $r = 0.125\,month^{-1}$, $\alpha = 0.0625\,month^{-1}$ and $b = b_0\,\mu$ with $b_0 = 50\,\frac{m}{K}$. μ is a tuning parameter characterizing the strength of air-sea coupling and is varied between 0 and 1.5. Using (2.10) and rescaling with the observed standard deviation of SSTA $\sigma_T = 0.86\,K$ and thermocline depth $\sigma_h = 7.3\,m$, the corresponding parameters of (2.9) in [month^{-1}] are $a_{11} = -0.5 + 0.47\mu$, $a_{12} = 0.16$, $a_{21} = -1.47\mu + 1.38\mu^2$ and $a_{22} = -0.125 + 0.468\mu$. These parameters are plotted against μ in figure 2.4. For comparison the 95% confidence intervals of the fitted parameters are shown by the shaded areas. No value of μ exists where the whole set of parameters discussed by Jin (1997) is in agreement with the results of the parameter fits performed in this study. But it should be noted that if the parameters proposed by Jin (1997) are varied by ± 50% the fitted parameter set can be reproduced. This stresses that the parameters used by Jin (1997) are rough physical estimates that have to be regarded as orders of magnitude rather than exact values. The parameters proposed in this study, on the other hand, are gained by straightforward fits to observational data and

[5]This value for γ is used in the discussion of Jin (1997), even though the parameter value that is physically motivated in his paper is higher by a factor of 4 (see Appendix B)

therefore allow for conclusions about the actual parameter regime describing ENSO.

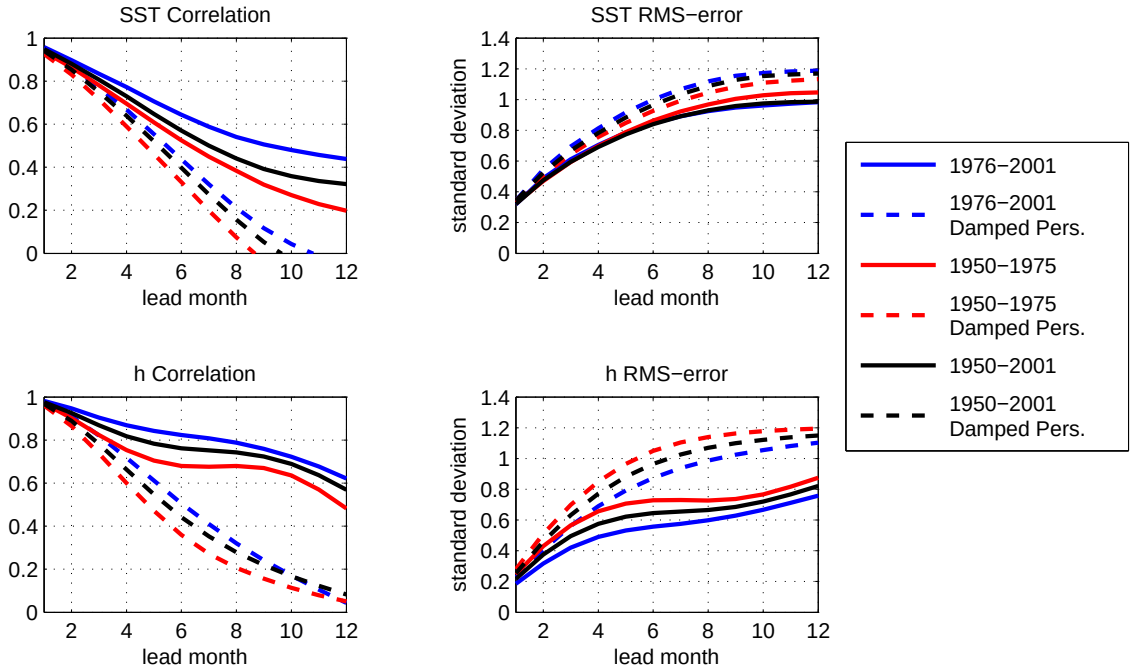

Figure 2.5: Forecast skill of the recharge oscillator model for Niño3 SSTA (top) and equatorial Pacific thermocline depth anomalies (bottom). The coloured lines show cross-validated forecast skills. The time intervals given in the legend refer to the period used for the forecast skill evaluation, while in each case the other interval was used to fit the parameters. For the black lines the whole time period was used for the parameter fit and for the evaluation of forecast skill. Left: Anomaly correlation between predictions and observations. Right: rms error of predictions in units of one standard deviation.

Figure 2.5 shows the forecast skill of the recharge oscillator model for Niño3 SSTA and for the equatorial averaged depth of the 20°C thermocline for the time period 1950 to 2001 and the cross-validated forecast skills for the first and second half of the timeseries. As for the delayed action oscillator, the small difference between the cross-validated skills and the skill of the not cross-validated run using the whole timeseries for the parameter fits and for the evaluation suggests that 26 years provide sufficient data for the fits and that there is very little artificial skill. Even though GCM thermocline depth data is used here, the correlation-skill for SST predictions is better than that of the delayed oscillator model. The rms-error of the delayed action oscillator strongly varies between the different time periods, but for the 1976-2001 time period, which probably contains the most reliable data, the recharge oscillator predictions also have a smaller rms-error. This suggests that the averaged thermocline depth is a more valuable predictor than the lagged Niño3 SSTA. The prediction skill for averaged thermocline depth is generally better than the skill of SST predictions,

indicating that the signal in the first is less noisy. It should be stressed, however, that this might be different if real observational data is used for thermocline depth, instead of GCM data.

2.3.3 The Recharge Oscillator Excited by Stochastic Forcing

Analogue to section 2.2.3 the model is excited by stochastic forcing. The major effects of short timescale weather fluctuations on the eastern Pacific SSTA and averaged heat content are via air temperature variability and via variations of the wind stress forcing, with the first acting on SSTA and the latter acting on both[6]. The model with stochastic excitation can be written as:

$$\frac{d}{dt}\begin{pmatrix} T_E \\ h \end{pmatrix} = \begin{pmatrix} a_{11} & a_{12} \\ a_{21} & a_{22} \end{pmatrix}\begin{pmatrix} T_E \\ h \end{pmatrix} + \begin{pmatrix} \xi_T \\ \xi_h \end{pmatrix} \tag{2.15}$$

where ξ_T and ξ_h are the net forcings acting on eastern Pacific SST and averaged thermocline depth. However, as indicated above, ξ_T and ξ_h can generally not be assumed to be independent even if wind stress and air temperature anomalies are assumed to be independent.

Assuming that ξ_T and ξ_h are correlated in phase, which means that the cross spectral density $P_{\xi_T\xi_h}$ is real, the power spectral density of SST and thermocline depth for the model given by equations (2.15) can be calculated analytically as[7]

$$P_{TT}(\omega) = \frac{a_{12}^2 P_{\xi_h\xi_h} + (\omega^2 + a_{22}^2)P_{\xi_T\xi_T} - 2a_{12}a_{22}P_{\xi_h\xi_T}}{(\omega^2 + a_{12}a_{21} - a_{11}a_{22})^2 + (a_{11} + a_{22})^2\omega^2} \tag{2.16}$$

and

$$P_{hh}(\omega) = \frac{a_{21}^2 P_{\xi_T\xi_T} + (\omega^2 + a_{11}^2)P_{\xi_h\xi_h} - 2a_{21}a_{11}P_{\xi_h\xi_T}}{(\omega^2 + a_{12}a_{21} - a_{11}a_{22})^2 + (a_{11} + a_{22})^2\omega^2}\ . \tag{2.17}$$

Since $a_{12}a_{22} < 0$ while $a_{21}a_{11} > 0$ it can be seen that a positive correlation between ξ_h and ξ_T increases the variance of T while it decreases the variance of h. For uncorrelated forcing the total variance of h is too high compared to observations for any finite variance of ξ_h. Thus a correlation between the two noise forcings of 0.32 (corresponding to 10% explained variance) is chosen for the following experiments, to mimic the total variance of observed Niño3 SST and averaged thermocline depth with still a reasonable amount of noise on the thermocline depth. The variances of the noise forcings meet $\sigma_{\xi_T} = 1.5\,\sigma_{\xi_h}$. The choice of the correlation and the total

[6]Since the thermocline tilt is assumed to be in equilibrium with the wind stress in this model, there is also quite a large effect of wind stress forcing on eastern Pacific SSTA.

[7]Regard appendix C for a cautionary note on the definition of spectra for processes continuous in time.

variance of the noise forcings is somewhat arbitrary, since three degrees of freedom (σ_{ξ_T}, σ_{ξ_h} and the correlation) exist while only the two total variances of T and h are fitted to observations. However, the qualitative results presented in the following are not altered if the correlations and variances are chosen in a reasonable range.

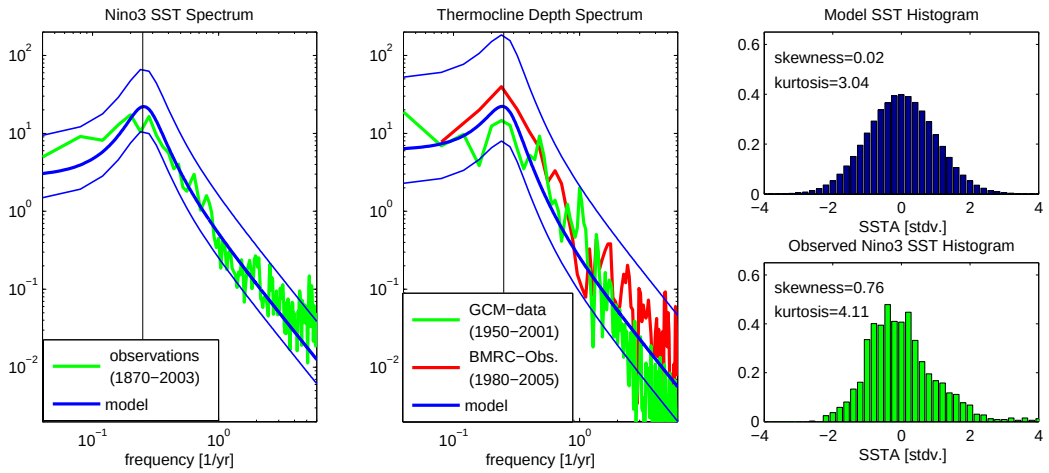

Figure 2.6: Left: Power spectral density of eastern Pacific SST time series from the recharge oscillator model compared to observed Niño3 SST data. The thin blue lines denote 95% confidence levels. The thin vertical line denotes a period of four years. Center: The same for the model thermocline depth and 20^{o}C isotherm depth from a GCM run forced with NCEP data and from BMRC observational data. The thin blue lines show 95% confidence levels based on the time period of the GCM data. Right: Niño3 SSTA frequency distribution of the recharge oscillator model (top) and from observations (bottom). The SSTA is normalized by the standard deviation of Niño3 SST.

Figure 2.6 shows the model power spectra, calculated from equations (2.16) and (2.17) as well as the SST frequency distribution resulting from a numerical $3 \cdot 10^4$ year model integration similar to section 2.2.3. The model SST spectrum fits well with observations, especially on longer timescales. However, the minor peak at a period of about 6 months, that can be identified in the observational spectrum and that was reproduced by the delayed oscillator model, is naturally not included in the recharge oscillator model, since the latter describes a damped harmonic oscillation. The high variance on the high frequency end of the spectrum of the observed timeseries has already been discussed in section 2.2.3. The spectrum of the model thermocline depth timeseries has a too pronounced peak at the El Niño period and too much variance on shorter timescales compared to the NCEP forced GCM data. The real observational BMRC timeseries on the other hand shows a more pronounced peak and more variance on shorter timescales as well. Generally, differences are hardly significant and statements about the observational thermocline depth spectrum are very speculative since too little data exists. As for the delayed oscillator, the frequency distribution of the model SST is, unlike the observations, nearly Gauss shaped. For further discussion about the reasons for skewness and kurtosis in the observed Niño3

timeseries see section 2.6.

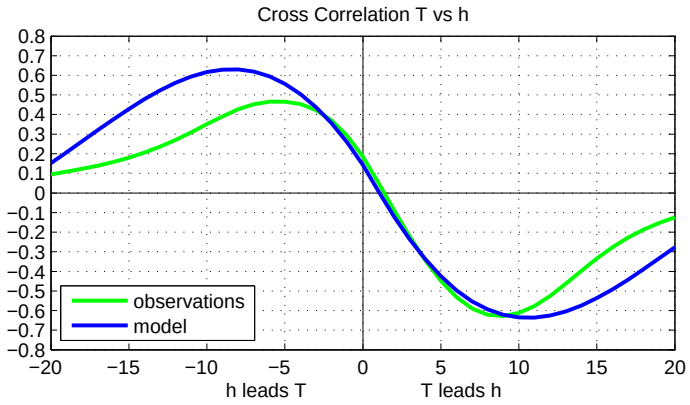

Figure 2.7: Cross correlation between Niño3 SSTA and thermocline depth anomalies averaged over the equatorial Pacific from 1950 to 2001 observational/forced GCM data (green) compared to the results of the recharge oscillator model (blue). Correlations above 0.27 a significant on are 95% level assuming 52 degrees of freedom, for the observational data.

Figure 2.7 shows the cross-correlation between Niño3 SSTA (T) and thermocline depth anomalies averaged over the equatorial Pacific (h) from the recharge oscillator model integration, compared to observational/forced GCM data. The observed cross-correlation has maxima with thermocline depth anomalies leading SSTA by about 6 months and with SSTA leading thermocline depth anomalies of opposite sign by about 9 months. The first describes the coupling of SSTA on thermocline depth anomalies while the second describes the recharging (discharging) of equatorial heat content during a La Niña (El Niño) event. These are the key mechanisms responsible for the oscillation in the recharge oscillator picture. Further, this correlations explain the relevance of averaged thermocline depth as a predictor for Niño3 SSTA and vice versa. The cross-correlation is generally reproduced well by the recharge oscillator model, even though correlations for long lead times tend to be too high. Especially, the recharge oscillator model reaches a maximum correlation slightly above 0.6 for thermocline depth leading SSTA by about 9 months, while the maximum is reached for thermocline depth leading SSTA by only about 6 months and is beneath 0.5 in the observational/forced GCM data.

2.4 The Simplest Recharge Oscillator

Burgers et al. (2005) suggest that the recharge oscillator model described above can again be simplified. They fit the recharge oscillator model to observational data finding that if Niño3 SST and equatorial averaged thermocline depth time series are

normalized by their standard deviation the damping of thermocline depth a_{22} can be neglected and the surface-subsurface coupling parameters a_{12} and a_{21} can assumed to be equal. This is supported by the parameter fits presented in section 2.3. The recharge oscillator model can thus be simplified to

$$\frac{d}{dt}\begin{pmatrix} T_E \\ h \end{pmatrix} = \begin{pmatrix} -2\gamma & \omega_0 \\ -\omega_0 & 0 \end{pmatrix}\begin{pmatrix} T_E \\ h \end{pmatrix} \tag{2.18}$$

which has the same form as the equation of a damped harmonic oscillator with h playing the role of position and T_E playing the role of momentum.

It should be stressed that the justification for this simplification of the recharge oscillator model is based on the results of parameter fits only and is not legitimated physically in any way.

A parameter fit for the simplest recharge oscillator as suggested in equation (2.18) is performed using the same data as for the recharge oscillator model in the previous section. The fitting methods are described in section 1.2. Table 2.3 shows the fitted parameter values resulting from the numerical fit and the 95% confidence levels estimated from the linear regression.

	1950-1975	1976-2001	1950-2001
γ	0.055 ± 0.018	0.030 ± 0.013	0.040 ± 0.011
ω_0	0.140 ± 0.024	0.131 ± 0.020	0.133 ± 0.015

Table 2.3: Fitted parameters and 95% confidence levels of the simplest recharge oscillator model for the Pacific in [month^{-1}]. The upper row gives the time periods of observational data used for the fits.

If γ is compared to $\frac{1}{2}a_{11}$ and ω_0 is compared to a_{12} and a_{21} in the recharge oscillator, it is found that these results are in good agreement with the parameter fits of section 2.3.2. However, the error estimates are smaller than those for the recharge oscillator model, which reflects the fact that this model includes only half as much parameters. The forecast skill of this model (not shown) is identical to that of the recharge oscillator model. Expectedly the statistical properties of the simplest recharge oscillator model (not shown) forced by stochastic excitation do not show any significant differences to the recharge oscillator model presented in the previous section.

2.5 The Delayed Recharge Oscillator

2.5.1 Model Description

In this section a model is proposed that includes the direct effects of the delay due to travel times of equatorial waves and the recharge mechanism as a natural unification of the delayed action oscillator and the recharge oscillator model. It will be shown that the delayed oscillator and the recharge oscillator both follow from two limit cases of this model.

The linear delayed recharge oscillator model is given by

$$\begin{aligned} \tfrac{d}{dt}T_E &= -\gamma_T T_E + c h_E \\ \tfrac{d}{dt}h_E &= -\gamma_h h_E + \tilde{k}\tau - \tilde{r}\tau(t-\delta) \\ \tau &= b T_E \,, \end{aligned} \tag{2.19}$$

where T_E is the eastern Pacific SSTA, h_E is the eastern Pacific thermocline depth anomaly and τ denotes the anomalous zonal wind stress in the central Pacific, which is simply assumed to be proportional to the eastern Pacific SSTA. The eastern Pacific SSTA equation is analogue to the SST equation of the recharge oscillator model (equation 2.8). The eastern Pacific thermocline depth equation contains a damping term, a "fast" Kelvin wave response on central Pacific wind stress anomalies and a delayed response via the reflection of Rossby waves at the western boundary. The time delay due to wave travel times is denoted here by δ to avoid confusion with the wind stress forcing, however it is basically the same as the time delay τ in the delayed oscillator equation (2.1). In the "fast SST adjustment" limit the first equation of (2.19) degenerates to the purely diagnostic equation

$$T_E = \frac{c}{\gamma_T} h_E \,. \tag{2.20}$$

With the second and third equation of (2.19) an equation similar to the delayed oscillator equation (2.1) is obtained. In the "fast wave" limit ($\delta = 0$) on the other hand, equations (2.19) become similar to the recharge oscillator model.[8]

[8] equations (2.19) with $\delta = 0$ and (2.8) are similar in that both can be transformed to a system of equations of the form:

$$\frac{d}{dt}\begin{pmatrix} T_E \\ h_E \end{pmatrix} = \begin{pmatrix} a_{11} & a_{12} \\ a_{21} & a_{22} \end{pmatrix} \begin{pmatrix} T_E \\ h_E \end{pmatrix} \tag{2.21}$$

2.5.2 Parameter Fit to Observational Data

Equations (2.19) can be rewritten as

$$\begin{aligned} \frac{d}{dt}T_E &= -\gamma_T T_E + c h_E \\ \frac{d}{dt}h_E &= -\gamma_h h_E + k T_E - r T_E(t-\delta) \end{aligned} \tag{2.22}$$

To avoid problems with the fitting routines the time lag δ was not fitted here but fixed to 6 months as found for the wave delay time in the delayed oscillator model. The other parameters of (2.22) are fitted to HADISST Niño3 SST data for T_E and 20^oC isotherm depth GCM data averaged over the eastern equatorial Pacific (Niño3) for h_E. The data is described in detail in section 1.1 and the fitting methods are explained in section 1.2. As done before, parameters and prediction skills are cross-validated by first using the time period from 1950 to 1975 for the parameter fit and the period from 1976 to 2001 for the evaluation of the forecast skill and vice versa. Additionally a "best fit" is performed using the whole data set from 1950 to 2001. Table 2.4 shows the fitted parameter values resulting from the numerical fit and the 95% significance intervals estimated from the linear regression.

	1950-1975	1976-2001	1950-2001
γ_T	0.18 ± 0.06	0.17 ± 0.05	0.17 ± 0.04
c	0.14 ± 0.06	0.19 ± 0.06	0.16 ± 0.04
γ_h	0.11 ± 0.05	0.09 ± 0.05	0.10 ± 0.04
k	0.10 ± 0.06	0.05 ± 0.05	0.07 ± 0.04
r	0.18 ± 0.04	0.13 ± 0.04	0.16 ± 0.03

Table 2.4: Fitted parameters and 95% confidence intervals of the linear delayed recharge oscillator model for the Pacific in [month^{-1}]. The upper row gives the time periods of observational data used for the fits.

As for the other models it can be verified that the fitted parameter values for the different periods are equal within the 95% confidence levels given by the linear regression, suggesting that the physical processes described by this model can be assumed to be stationary. Comparison of the temperature damping parameter γ_T to the absolute value of a_{11} in the recharge oscillator (2.9) suggests that the damping timescale of SST anomalies is significantly shorter in this model than in the recharge oscillator formulation. This is due to the fact that the positive Bjerknes feedback, which is the positive feedback between eastern Pacific SSTA and thermocline tilt, due to zonal wind stress anomalies, is implicitly included in the a_{11} term in (2.9) while in (2.22) SST couples explicitly to eastern pacific thermocline depth anomalies. For the second equation of (2.22), the results of the parameter fits show that for a given SSTA the

delayed Rossby wave effect (given by $-rT_E(t-\delta)$) finally dominates the direct Kelvin wave effect (given by $+kT_E$). This allows for the delayed recharging.

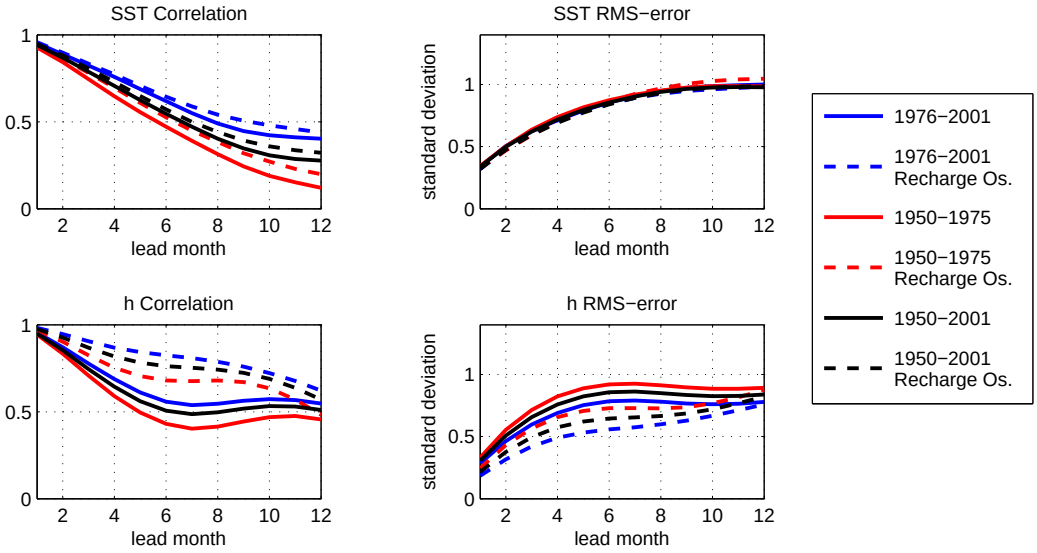

Figure 2.8: As 2.5 but for the linear delayed recharge oscillator model (solid) compared to the recharge oscillator model (dashed). h denotes eastern Pacific thermocline depth for the delayed recharge oscillator, but equatorial averaged thermocline depth for the recharge oscillator model.

Figure 2.8 shows the forecast skill of the delayed recharge oscillator model for Niño3 SSTA and for the eastern equatorial thermocline depth (solid lines) compared to the forecast skills of the recharge oscillator model (dashed lines). The thermocline depth forecast of the recharge oscillator model however is for equatorial averaged thermocline depth. Thus, comparison to the Niño3 thermocline depth forecast skill of the delayed recharge oscillator suggests that averaged thermocline depth is easier to forecast than eastern Pacific thermocline depth. This might be explained by the fact that the latter consists of a smaller averaging area and can therefore be expected to be more noisy. However there might be additional physical reasons.

The SST prediction skill of the delayed recharge oscillator model is also worse than that of the recharge oscillator model. This is due to the fact that, additional to Niño3 SSTA, the thermocline depth averaged over the whole equatorial strip is a better predictor variable than eastern Pacific thermocline depth. Figure 2.9 shows the cross-correlation function of the mean equatorial thermocline depth and Niño3 SST (red) compared to the cross-correlation function of the eastern Pacific thermocline depth and Niño3 SSTA (green). It can be seen that eastern Pacific thermocline depth is highly correlated with Niño3 SSTA, with little time lag, therefore it is not a very useful additional predictor variable to SSTA. The mean thermocline depth on the other hand has a maximum lead correlation of little less than 0.5 with thermocline depth leading SSTA by about 6 months. And, as discussed in section 2.3, it is

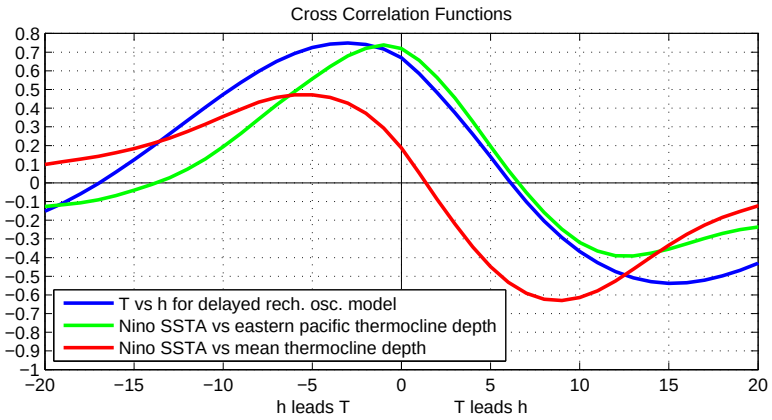

Figure 2.9: Observed cross-correlation of HADISST Niño3 SST and Niño3 GCM thermocline depth anomalies compared to the results of the delayed recharge oscillator model, and to the observed cross-correlation of HADISST Niño3 SST and GCM thermocline depth anomalies averaged over the whole equatorial Pacific. All observational data is for the period from 1950 to 2001. Correlations above 0.27 are significant on a 95% level assuming 52 degrees of freedom.

this phase shift which makes equatorial averaged thermocline depth a very useful predictor.

As for the models presented in the previous sections, the little difference between the cross-validated skills and the skill of the not cross-validated run, using the whole timeseries for the parameter fits and for the evaluation, suggests that 26 years provide sufficient data for the fits and that there is little artificial skill in the not cross-validated run.

2.5.3 The Delayed Recharge Oscillator Excited by Stochastic Forcing

Analogue to sections 2.2.3 and 2.3.3 the results of a model run of the delayed recharge oscillator model, with stochastic excitation representing short time-scale weather fluctuations, are presented in the following. With noise forcings acting on both the SST and thermocline depth equations, the model can be written as:

$$\begin{aligned} \frac{d}{dt}T_E &= -\gamma_T T_E + c h_E + \xi_T \\ \frac{d}{dt}h_E &= -\gamma_h h_E + k T_E - r T_E(t-\delta) + \xi_h \end{aligned} \tag{2.23}$$

where ξ_T and ξ_h are the net forcings acting on eastern Pacific SST and thermocline depth. As for the recharge oscillator, the variance and correlation of the noise forcings that are used in the following are fitted to mimic observed statistical properties, especially the total variance of Niño3 SST and averaged thermocline depth. The

variance of the noise forcings is chosen to meet $\sigma_{\xi_T} = 1.05\,\sigma_{\xi_h}$ and the correlation between the two noise forcings is 0.32 as for the recharge oscillator model. The other parameters are set according to the fit presented in the previous section. The model is integrated for $3 \cdot 10^4$ years.

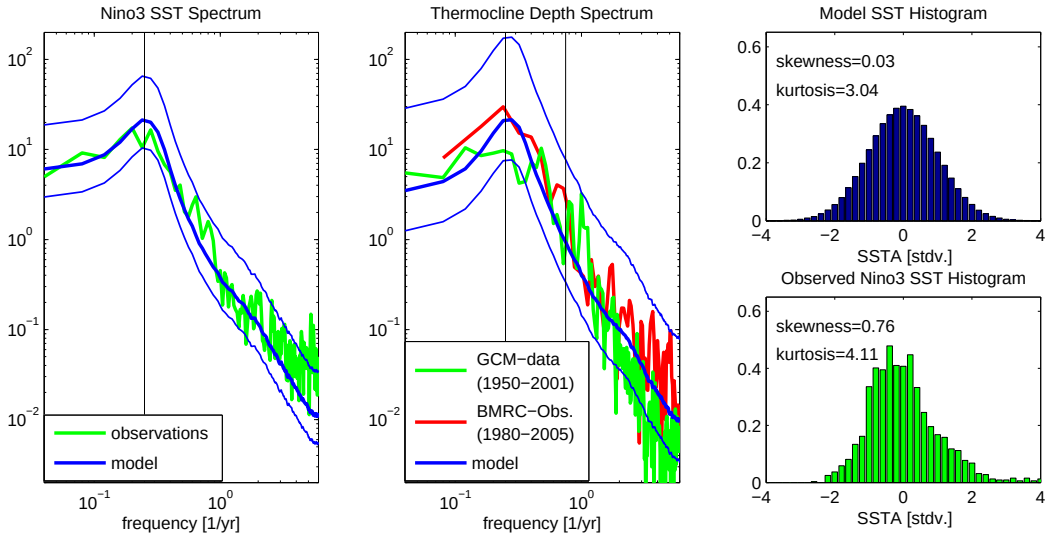

Figure 2.10: As Figure 2.6, but for the delayed recharge oscillator model and thermocline depth averaged over the Niño3 region.

Figure 2.10 compares the resulting power spectra and the SST frequency distribution to observational Niño3 SST data from 1870 to 2003 and the 20°C isotherm depth data from 1951 to 2001 that was used to fit the model parameters.

The SST spectrum reflects that the delayed recharge oscillator includes elements of both, the delayed oscillator and the recharge oscillator. Generally it can be seen that the model agrees well with observations. On longer timescales it is very similar to the SST spectrum of the recharge oscillator model, indicating that the recharge mechanism is most important on timescales in the order of the oscillation period of around four to five years. Unlike the recharge oscillator model, the delayed recharge oscillator model spectrum also indicates a weak secondary "peak" at a period of around six month, which can be seen more clearly in the delayed oscillator spectrum and agrees with observations. However, this secondary "peak" should probably not be taken as a criterion of the models ability to reproduce observational data, because it is too small to be clearly identifiable in the observations, and explains a negligible proportion of the variance.

Analogue to the basinwide equatorially averaged thermocline depth in the recharge oscillator model, the spectrum of the model eastern Pacific thermocline depth time-series of the delayed recharge oscillator tends to have a too pronounced peak at the El Niño period and too much variance on shorter timescales compared to the GCM

data. On the other hand, the model spectrum is in good agreement with the real observational BMRC data, even though the GCM data was used to fit the model parameters. A secondary peak at around half a year can also be found in the model thermocline depth spectrum. While it can hardly be found in the GCM data, it might be inferred from the observational BMRC data. However, too little observational data exists to accurately check the model thermocline depth spectrum against observations.

As for the models discussed before, the frequency distribution of the model SST is, unlike the observations, nearly Gauss shaped. Asymmetry and residuals of the eastern Pacific SST frequency distribution are gained if the model is extended by nonlinear surface-subsurface interaction. This is done in the following section.

Figure 2.9 also shows the cross-correlation between eastern Pacific SSTA and eastern Pacific thermocline depth anomalies resulting from the recharge oscillator model run (blue). As for the observations (green), the phase difference between SSTA and thermocline depth is smaller than for the recharge oscillator model using thermocline depth averaged over the whole equatorial Pacific instead of only the eastern part of the basin. Compared to the observations, the maximum correlation is still somewhat shifted to thermocline depth anomalies leading SSTA by about 3 months instead of about one month for the observational/forced GCM data.

2.6 A Nonlinear Extension of the Delayed Recharge Oscillator

There are different sources of nonlinearity in coupled ocean atmosphere models. BH89 showed in a Zebiak and Cane (1987) type model that the dominant nonlinearity for ENSO is the nonlinear coupling of SST on thermocline depth anomalies. The vertical temperature profile in the equatorial ocean is highly nonlinear, with a very strong temperature gradient at the depth of the thermocline and weaker gradients above and below the thermocline. Thus the feedback of thermocline depth on SST cannot be assumed to be linear, but to depend on the vertical temperature profile according to a nonlinear function. Schopf and Burgman (2006) propose a very simple model with a *tanh* shaped temperature profile to explain ENSO residuals and asymmetry. A simplified schematic temperature section of the equatorial Pacific with a tilted *tanh*-shaped thermocline is drafted in figure 2.11. Additionally three temperature profiles, one in the west, one in the east and one in the center of the basin are shown. A given upward or downward displacement of the thermocline at a specific position, caused by a change of thermocline tilt and/or a change of average thermocline depth will produce a subsurface temperature change proportional to the vertical temperature gradient, which is not constant. Assuming that the SST tendency is proportional to the subsurface temperature, the SST tendency due to thermocline depth anomalies is therefore generally nonlinear as well. Given a *tanh*-shaped vertical temperature

profile as sketched in figure 2.11, one can see that a more or less random up- and downward movement of the thermocline would lead to a positive skewed SST frequency distribution at 90^oW and a negatively skewed distribution at 160^oE. This effect is explained in more detail in Schopf and Burgman (2006) for a sinosoidal thermocline movement. However this qualitative result does not depend on the nature of the thermocline movement, as long as it is symmetric about the mean state. It only depends on the nonlinearity of the temperature profile.

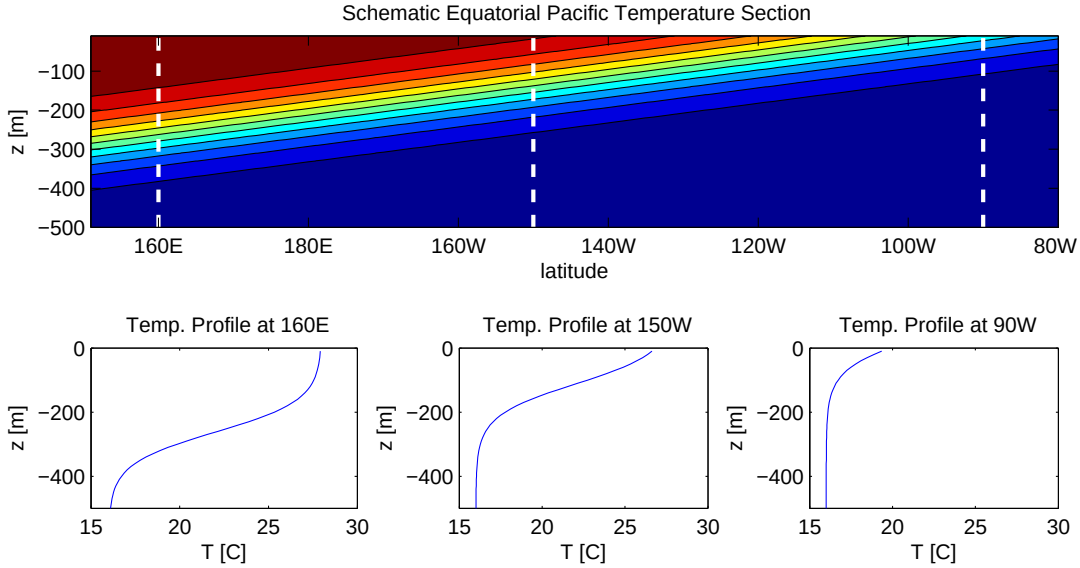

Figure 2.11: Simplified, schematic temperature section through the equatorial Pacific and depth profiles of temperature at different longitudes. The dashed white lines in the section above indicate the positions of the vertical profiles below

For the model presented in the following, the nonlinearity is not assumed to be *tanh* shaped. Instead the coupling is expanded up to the third order in thermocline depth anomalies, to allow the approximation of every kind of nonlinear coupling as long as thermocline displacements are small. The nonlinear delayed recharge oscillator can then be written in the form

$$\begin{aligned} \frac{d}{dt}T_E &= -\gamma_T T_E - c_0 + c_1 h_E + c_2 h_E^2 - c_3 h_E^3 \\ \frac{d}{dt}h_E &= -\gamma_h h_E + k T_E - r T_E(t-\delta) \end{aligned} \tag{2.24}$$

with the c_i , $i = 0..3$ denoting the Taylor expansion coefficients of the coupling function. The signs are chosen so that the expected parameter values are positive.

The parameters of this model are fitted as for the linear model, with the timelag fixed to δ=6 months. Table 2.5 gives the results of the parameter fits.

	1950-1975	1976-2001	1950-2001
γ_T	0.20 ± 0.06	0.18 ± 0.05	0.18 ± 0.04
c_0	0.06 ± 0.05	0.02 ± 0.04	0.03 ± 0.03
c_1	0.14 ± 0.08	0.22 ± 0.07	0.17 ± 0.05
c_2	0.04 ± 0.06	0.04 ± 0.03	0.035 ± 0.020
c_3	0.000 ± 0.019	0.014 ± 0.018	0.005 ± 0.012
γ_h	0.11 ± 0.05	0.09 ± 0.05	0.10 ± 0.04
k	0.10 ± 0.06	0.05 ± 0.05	0.07 ± 0.04
r	0.18 ± 0.04	0.13 ± 0.04	0.15 ± 0.03

Table 2.5: Fitted parameters and 95% confidence intervals of the nonlinear delayed recharge oscillator model for the Pacific in [month^{-1}]. The upper row gives the time periods of observational data used for the fits.

The coefficients of the linear terms do not differ significantly from the parameters fitted for the linear model. The nonlinearity reveals an asymmetrie matching a subsurface temperature profile as shown in the eastern Pacific temperature profile in figure 2.11. However, it should be realized that the nonlinear parameters exhibit quite big relative error estimates.

Analogue to the linear delayed recharge oscillator model, the nonlinear version is excited by stochastic forcing, representing short time-scale weather fluctuations. The noise forcing acting on T_E is chosen to have a standard deviation about 15% higher than the noise forcing on h_E. The correlation between the two forcings is about 0.32. The model is run for $3 \cdot 10^4$ years. The resulting power spectral densities do not differ significantly from those of the linear model (not shown). But the nonlinear model is able to explain some skewness and kurtosis of the frequency distribution. Figure 2.12 shows the frequency distribution for eastern Pacific SSTA resulting from the model run and the frequency distribution of observed Niño3 SSTA from 1870 to 2003.

It can be seen that unlike the linear models, the model containing a nonlinear surface-subsurface coupling reveals a skewed frequency distribution and a kurtosis higher than that of a Gauss distribution, but skewness and especially kurtosis are still weaker than in the observational data. Especially the kurtosis seen in the observational data can to its major part be explained by the seasonal cycle in standard deviation, which comes from the fact that the destabilising Bjerknes feedback seems to be active mainly from late spring to fall. Additionally there is a weak linear trend in the observed Niño3 SST variability with variance growing stronger.[9] Figure 2.12 c) shows the observed frequency distribution with the seasonal cycle and linear trend of standard deviation removed. Seasonality (and to a minor part the linear trend) is responsible for the

[9]Long term variability can also be made responsible for some of the kurtosis and skewness. However this shall not be adressed here in detail.

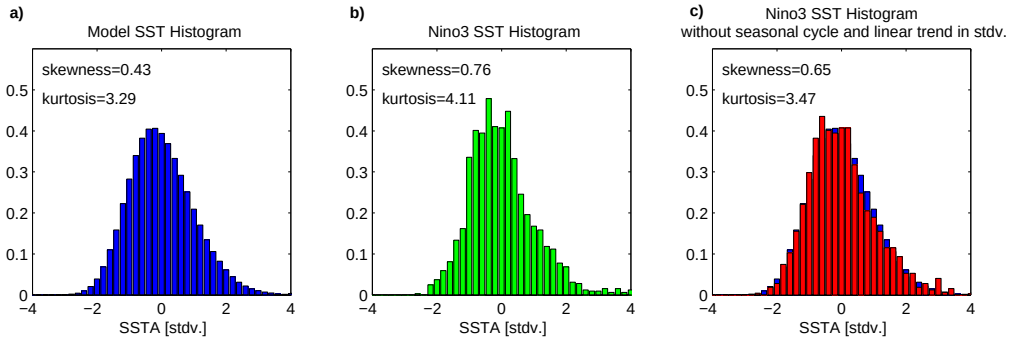

Figure 2.12: Frequency distribution for Niño3 SSTA. **a)** From the nonlinear delayed recharge oscillator model run. **b)** From HADISST Niño3 observational data (1870-2003). **c)** Red: As b) but with the seasonal cycle and linear trend in the standard deviation removed. Blue (behind): The model distribution as shown in a) for comparison.

major part of the kurtosis and some of the skewness of the observed timeseries. Since the model used in this chapter does not contain seasonality or a linear trend it has to be compared to the adjusted observational data with seasonal cycle and linear trend of standard deviation removed. There is still a little less skewness and kurtosis in the model data, which can also be seen in comparison to the model frequency distribution plotted in green behind the adjusted frequency distribution in figure 2.12 c). However, this difference is hardly significant and if model parameters are tuned within the estimated 95% confidence intervals, the observed skewness and kurtosis can easily be reproduced.

For the sake of completeness it should be added that very recently van Oldenborgh (personal communication) suggested that the important nonlinearity responsible for the observed skewness is the nonlinear coupling of the atmospheric wind stress on eastern Pacific SSTA, while Jin et al. (2007) find that state dependent noise forcing such as variability associated with westerly wind bursts, can also play an important role for the observed asymmetry of ENSO.

2.7 Seasonality

2.7.1 The Recharge Oscillator Model with Seasonal Dependent Parameters

Parameter Fits

In the following, some results are presented that were achieved by fitting the recharge oscillator model as described in section 2.3 using a fit that allows for a seasonal cycle in the parameter values. The seasonal fitting method is described in section 1.2.

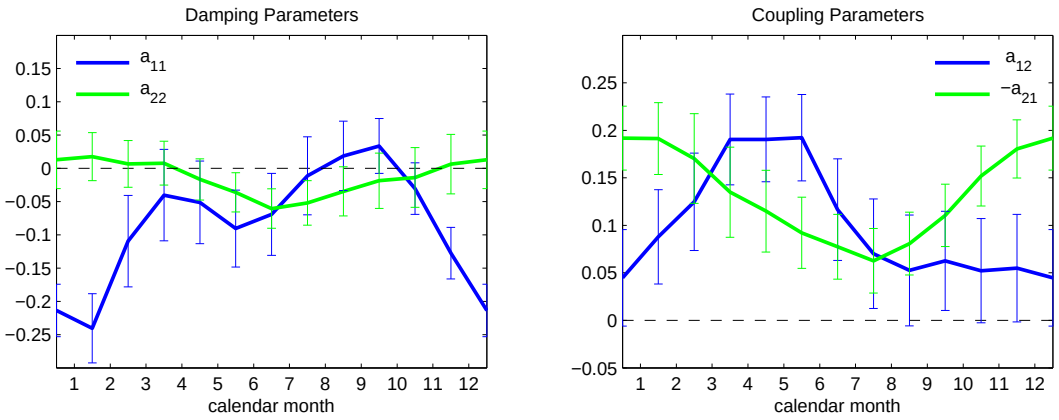

Figure 2.13: Seasonality of fitted parameters of the recharge oscillator model for the Pacific, with 95% significance interval estimated from the linear regression. All parameters are fitted to 1950-2001 data.

Figure 2.13 shows the seasonal cycle of the parameters as gained by the seasonal fitting method, using the numerical fit and the estimated 95% confidence interval. Niño3 SST and 20^{o}C isotherm depth data, described in section 1.1, for the time period from 1950 to 2001 were used for the fit.

As for the non seasonal-dependent model, we find that the damping of thermocline depth (a_{22}) is not significantly different from zero during three quarters of the year. The surface-subsurface coupling parameters a_{12} and a_{21} that are found to be equal in the non-seasonal fit can, however, hardly be considered to have the same seasonal cycle. Parameter a_{11} which is the temperature damping and includes the Bjerknes feedback (see section 2.3) shows high absolute values in the winter months whereas it is about zero from April to November indicating that during this time the positive Bjerknes feedback outweighs the damping. This is in good agreement with SSTA peaking towards the end of the year. a_{21} which describes the "recharging" of equatorial heat content as a reaction on eastern Pacific SST anomalies via changed zonal wind stress and wind stress curl (see Meinen and McPhaden (2000) or Neelin et al. (1998)) does have high absolute values mainly in the winter months. a_{12} which represents the coupling of eastern Pacific SST to averaged equatorial heat content shows a maximum in late spring and early summer.

The eigenvalues of the recharge oscillator model resulting from this parameters are shown in figure 2.14. A complex eigenvalue corresponding to an oscillatory eigenmode exists throughout the whole year, except of the December-January transition for which two purely damped modes are found. Phase progression is strongest in boreal spring. Except for the September-October transition where a positive but insignificant growth rate is found, the real part suggests that the oscillation is damped. The damping is strongest in boreal winter, whereas no significant damping exists in

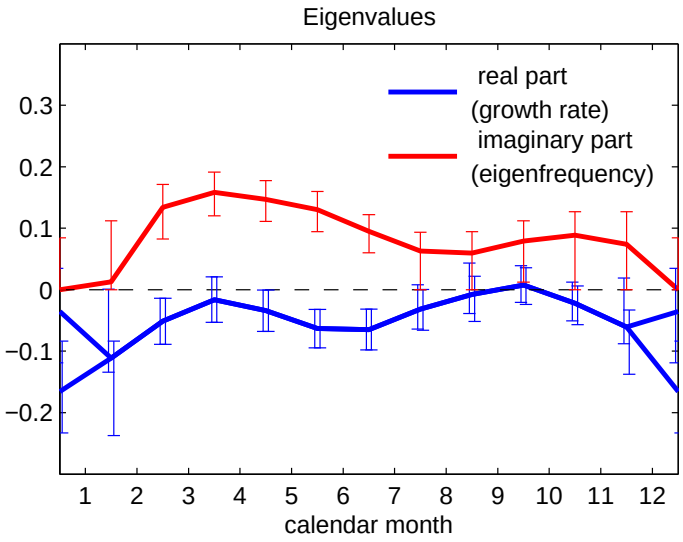

Figure 2.14: Seasonal cycle of the eigenvalues of the recharge oscillator with the parameters fitted to Pacific observational SSTA data and thermocline depth data from an NCEP forced GCM run, for the time period 1950-2001. Error bars denote 95% confidence levels.

late boreal summer and early boreal fall, in agreement with El Niño events peaking towards the end of the year.

The strong seasonality of the fitted parameters stresses the importance of seasonality. The forecast skills for Niño3 SSTA and thermocline depth of the seasonal dependent model are compared to those of the model without seasonality in figure 2.15. An improved SST forecast skill at least for SSTA can be observed for all time intervals compared to the non seasonal-dependent model. Considering the strong seasonal cycle of the parameter values, the improvement is quite small, which might be the case because the enhancement is in parts compensated by the reduced sample size available for parameter fits of monthly varying parameters. Against this hypothesis stands the fact that the cross-validated skills are not significantly worse than the skill of the fit using the whole time series. This indicates that the availability of more data does not improve the forecasts and that artificial skill is negligible.

Figure 2.16 shows the seasonal dependence of the forecast correlation skill for SSTA and thermocline depth compared to persistence (identical to the auto-correlation). In agreement with the results of McPhaden (2003) a strong persistence barrier in SST can be seen in boreal spring, while there is a persistence barrier for thermocline depth towards the end of the year. High SST prediction skill above persistence can be seen in the beginning of the year. This can be explained by the high persistence and predictability of thermocline depth anomalies during this time of the year and the strong surface to subsurface coupling in spring (represented by parameter a_{12} in figure 2.13). SST forecasts initialized from November till February on the other

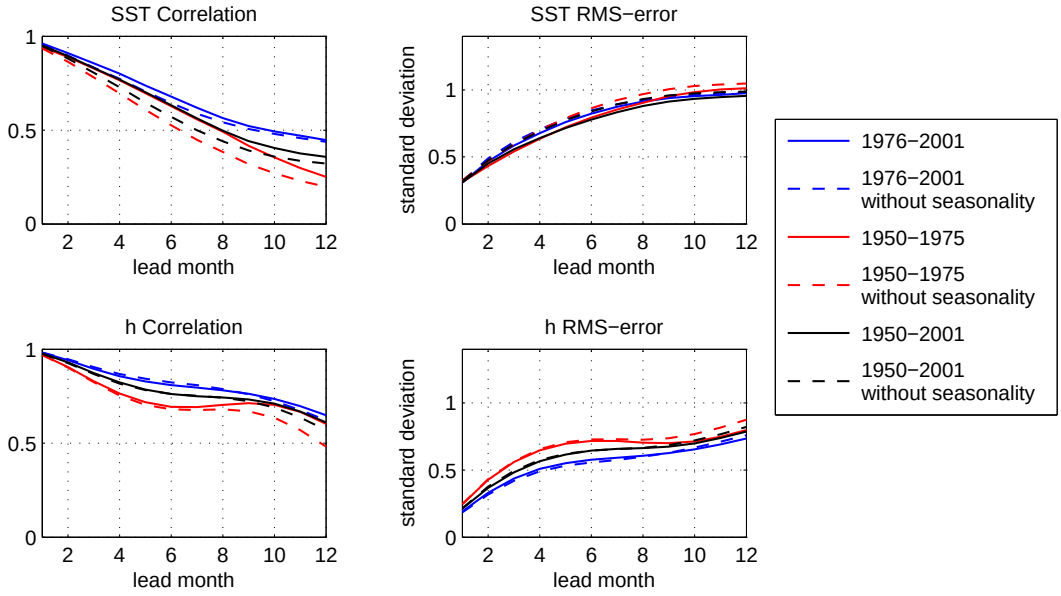

Figure 2.15: Forecast skill of the recharge oscillator model with seasonal dependent parameters for the Pacific. The coloured lines show cross-validated forecast skills. The time intervals given in the legend refer to the period used for the forecast skill evaluation, while in each case the other interval was used to fit the parameters. For the black line the whole time period was used for the parameter fit and for evaluation of forecast skill. The dashed lines show the corresponding forecast skill of the recharge oscillator model without seasonality.

hand do not reach a correlation skill of 0.5 or more for 6 months lead time. Thus useful predictions should be initialized in late spring or early summer. Prediction skill of thermocline depth anomalies is significantly higher than SST prediction skill throughout the year, with a less pronounced barrier towards the end of the year. However, as described in section 1.1 the thermocline depth data used here is GCM data, which might be less noisy than real observational data.

The Seasonal Dependent Recharge Oscillator Excited by Stochastic Forcing

Analogue to section 2.3.3 the recharge oscillator model with seasonal dependent parameters is integrated with stochastic excitation, representing short time-scale weather fluctuations. For simplicity the standard deviation of the noise forcing was chosen to be constant throughout the whole year. The correlation between the noise forcings on SST and thermocline depth was chosen similar to the nonseasonal model and the variance of the noise forcing is chosen to meet $\sigma_{\xi_T} = 1.8\,\sigma_{\xi_h}$ to reproduce the observed total variance. The model is integrated for $3 \cdot 10^4$ years.

The resulting power spectral densities for SST and thermocline depth are shown in

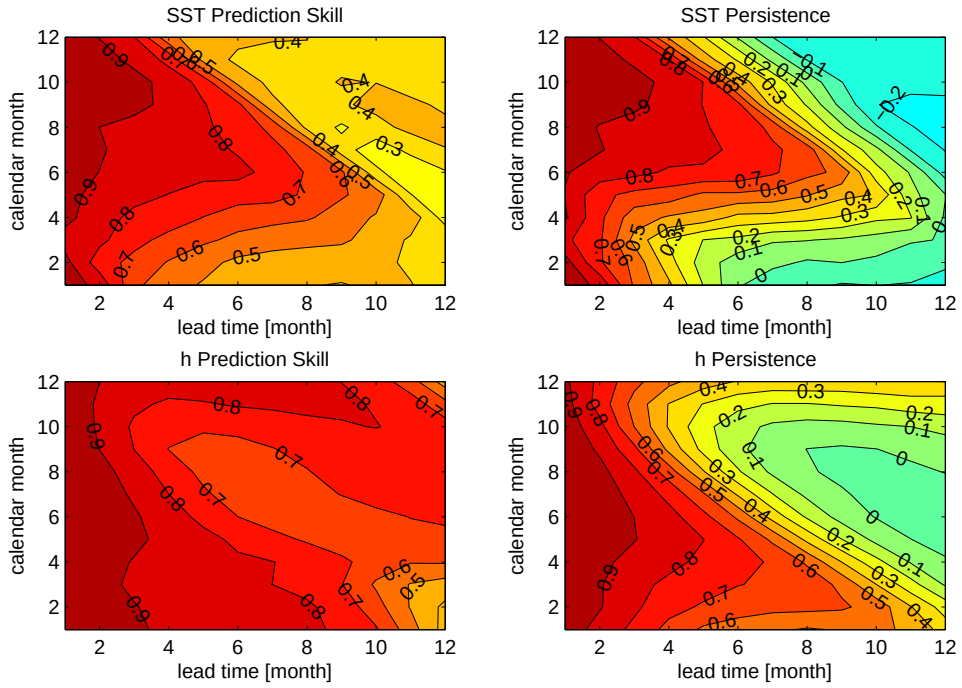

Figure 2.16: Seasonal dependence of forecast correlation skill of the recharge oscillator model with seasonality for the Pacific, compared to the auto-correlation (persistence skill). All data is for the time period from 1950 to 2001.

figure 2.17. Compared to the non-seasonal spectrum, additional minor peaks are found at higher frequencies. Particularly a secondary peak at a period of about $\frac{4}{3}$-years can be seen in the SST as well as in the thermocline depth spectrum. This peak can also be noticed in the observational SST spectrum. It can be explained by the modulation of the ENSO frequency $\omega \sim \frac{1}{4}\, yr^{-1}$ with the annual cycle $\Omega = 1\, yr^{-1}$, which corresponds to a superposition of the frequencies $\Omega + \omega = \frac{5}{4} yr^{-1}$ and $\Omega - \omega = \frac{3}{4}\, yr^{-1}$. The $\frac{4}{5}$ year peak can also be seen in the model thermocline depth spectrum, while an additional $\frac{4}{9}$ year peak, explained by interaction with the semi-annual cycle can be spotted in the model SST spectrum. The interaction between El Niño and the seasonal cycle is discussed in detail by Jin et al. (1996) using an ICM with annual forcing. They also find a $\frac{4}{3}$-year peak as a result of nonlinear interaction with the seasonal cycle.

The observed frequency distribution has a kurtosis of little more than 3.3 which is less than expected from the observational results presented in section 2.6. However, a direct comparison of the influence of the seasonal cycle on the observed kurtosis is not possible here, since no nonlinearity is included in the model presented here.

Figure 2.18 shows the seasonal cycle of standard deviation of Niño3 SST from the

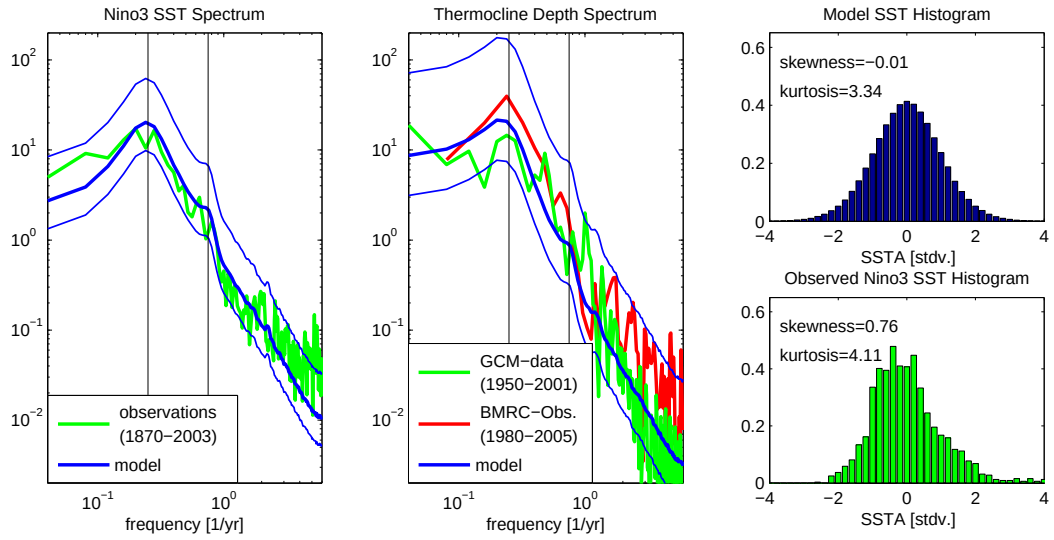

Figure 2.17: As Figure 2.6, but for the seasonal dependent recharge oscillator model. The thin vertical lines in the spectral density plots denote periods of four years and 4/3 years.

model compared to observations. It can be seen that the observed seasonal cycle, with maximum variance towards the end of the year and a break-in of variance during the winter months leading to a minimum in early spring, can well be reproduced by the model, even though no seasonality in the noise forcing was assumed.

Figure 2.19 shows the seasonal dependence of the Niño3 SST auto-correlation and the cross-correlation between Niño3 SST and equatorially averaged thermocline depth for the recharge oscillator model and for observations/GCM data. The observed auto-correlation with the characteristic spring persistence-barrier is well resembled by the recharge oscillator model. The observed cross-correlation reveals a positive correlation with thermocline depth leading SST and negative correlation with SST leading thermocline depth, with the phase difference shifting through the year. The SST lead time of zero correlation shifts from about -2 months in March to about 5 months in June. This can also be found in the model results. However, there are still some differences between the model and the "observations", but it should be remembered that for the cross-correlation GCM data for thermocline depth was used instead of real observations, so this has to be handled with care.

A Forecast Skill Comparison to a "State of the Art" Model

To allow for a comparison of prediction skills of different models, the same quantity has to be predicted for the same time period. If the models contain statistical parameters the same "training" data should also be available. Therefore, an experiment is

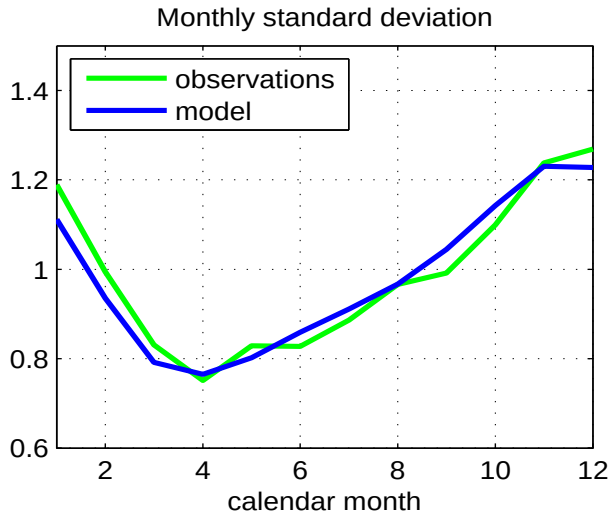

Figure 2.18: Seasonal dependence of standard deviation of Niño3 SST in observations (1950-2002) compared to the results of the seasonal dependent recharge oscillator model with constant stochastic excitation.

presented in the following using the recharge oscillator model which should allow for a comparison of the forecast skill to results of a much more complex hybrid coupled model, published by Dommenget and Stammer (2004).

In their model, SSTA averaged over the region $130^oW - 170^oW; 5^oS - 5^oN$, referred to as the EQ2 region in the following, is used instead of Niño3 SSTA. This region in the central Pacific provides a less noisy ENSO signal. Parameter fits and forecasts of the recharge oscillator model are therefore also performed using EQ2 instead of Niño3 SSTA here. Furthermore, observed 20^oC isotherm depth data, described in section 1.1 is used in this experiment instead of GCM data for the thermocline depth. 21 forecasts during the time period between 1993 and 1999 are performed by Dommenget and Stammer (2004) using different training periods . The skill of the recharge oscillator model is calculated from forecast runs starting from each month of the same time period, here. Since observational thermocline depth data is available only since 1980, the training periods used here for the recharge oscillator differ slightly from those used for the statistical atmosphere of the hybrid coupled model, with the latter being a little longer. (Further details about the model setting of Dommenget and Stammer (2004) can be found in their description of the "control" experiment.)

Figure 2.20 shows the forecast skills of the hybrid coupled model as published by Dommenget and Stammer (2004) compared to the forecast skills of the recharge oscillator model. The different training time periods are given in the legend. The red curve shows the forecast skill of the models using the longest training period. The forecast correlation skill of the two models is about similar for lead times up to 6 months. For longer lead times the hybrid coupled model becomes a little better.

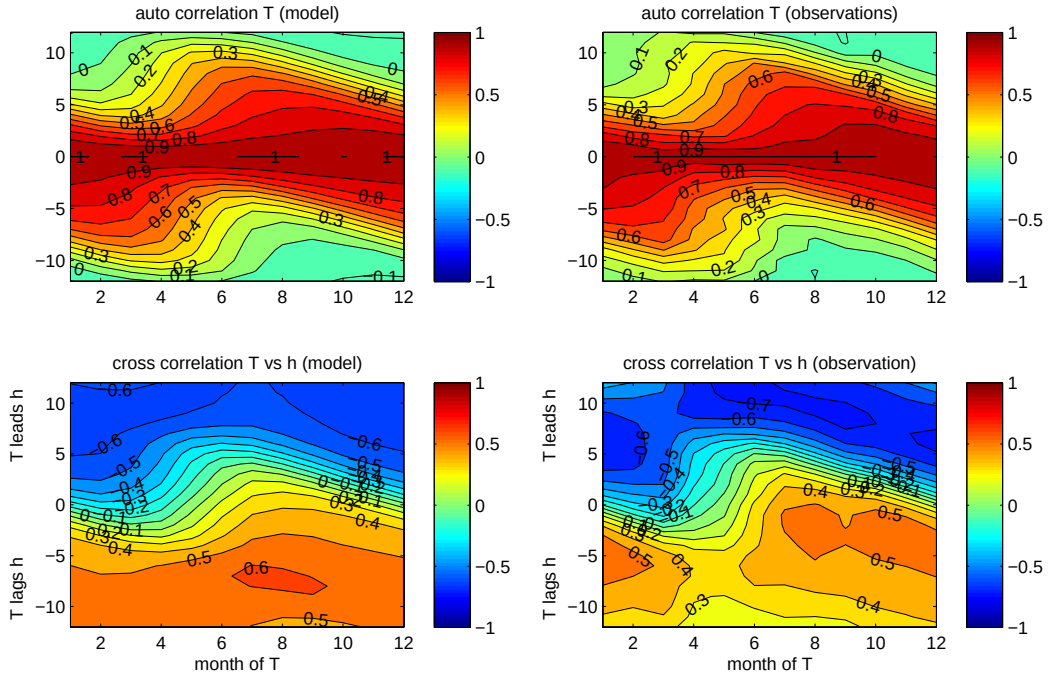

Figure 2.19: Seasonal dependence of Niño3 SST auto-correlation and cross-correlation between SST and mean thermocline depth of the recharge oscillator model with seasonality for the Pacific, compared to observational/GCM data. The time periods are 1870-2003 for the observed auto-correlations and 1950-2001 for the cross-correlations.

However, it should be realized that the training period overlaps with the time period that was used for the evaluation of forecast skills. Therefore, it has to be assumed that artificial skill is contained in both models. Since the more complex hybrid coupled model probably contains more degrees of freedom that are fitted to the training data it can also be expected to have higher artificial skill.

The green curve can approximately be considered to be cross-validated. Even though the training period used for the recharge oscillator model is shorter, its forecast skill is better than that of the hybrid coupled model. Again it should be remembered that the recharge oscillator has less degrees of freedom (small number of parameters) and therefore needs less training data. The blue curve makes clear that the hybrid coupled model does not provide useful fits if the training period is too short, even though the training period overlaps nearly completely with the forecasted time period.

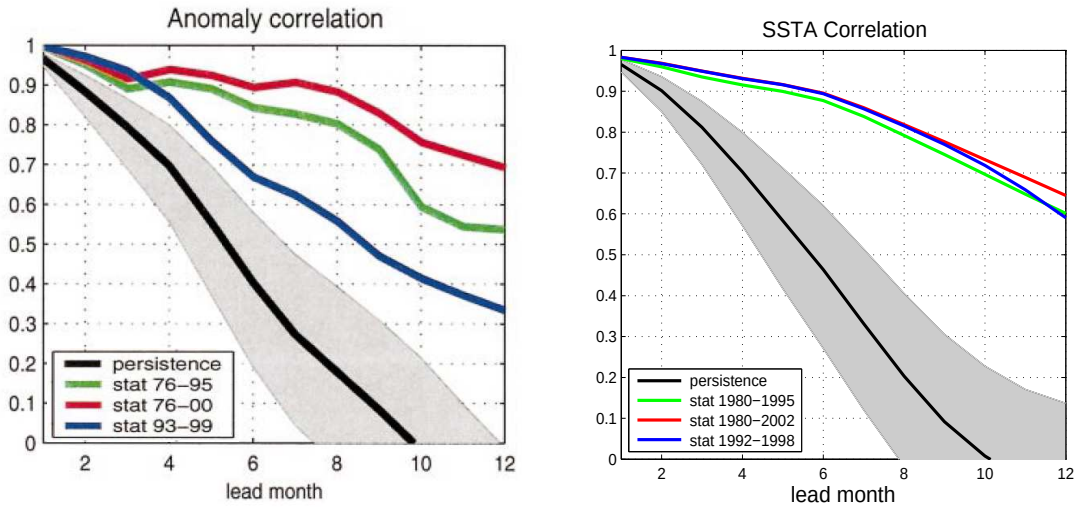

Figure 2.20: Forecast correlation skill for EQ2 SSTA of an hybrid coupled model as presented in Dommenget and Stammer (2004) (left) compared to the forecast skill of the recharge oscillator model with seasonality (right). All skills are evaluated in the time period from 1993 to 1999. The shaded regions show the statistical uncertainty (one standard deviation) of the SSTA persistence. For the estimates of the significance intervals 21 degrees of freedom are assumed in Dommenget and Stammer (2004) (corresponding to the number of forecast runs conducted for the skill evaluation) and 24 degrees of freedom (1 deg. of freedom/3months) are assumed for the results of the recharge oscillator.

2.7.2 A Seasonal Dependent Parameter Fit for the Simplest Recharge Oscillator Model

Burgers et al. (2005) showed that the recharge oscillator model can be further simplified to the simplest recharge oscillator model presented in section 2.3. This result is supported by the parameter fits performed in section 2.3.2. However, seasonal dependent parameter fits presented in the previous section indicated that this simplification can hardly be justified for seasonal dependent models. However, the smaller number of parameters makes the simplest recharge oscillator an interesting alternative if little data for parameter fits is available and if additional feedbacks (and thus additional parameters) shall be included in the model. Therefore, the abilities and shortcomings of the simplified models are analyzed in this section. As done for the full recharge oscillator model in the previous section, parameter fits for the simplest recharge oscillator model, described in section 2.4, are performed, using a fit that allows for a seasonal cycle in the parameter values.

Figure 2.21 shows the seasonal cycle of the fitted parameters and the 95% significance levels. Niño3 SST and 20^o isotherm depth GCM data, described in section 1.1, for the time period from 1950 to 2001 are used for the fit.

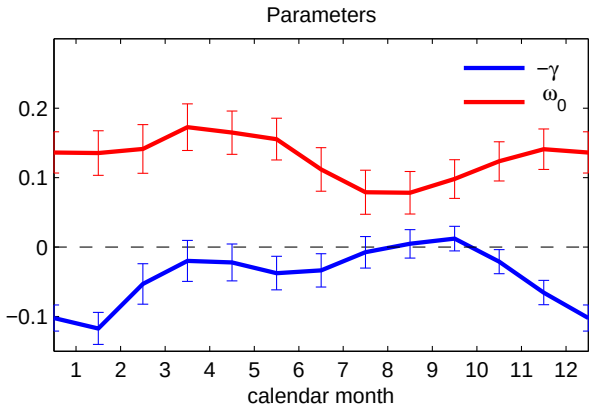

Figure 2.21: Seasonality of fitted parameters of the simplest recharge oscillator model for the Pacific, with 95% significance interval estimated from the linear regression. All parameters are fitted to 1950-2001 data.

The damping (γ) approximately equals the damping found in the eigenvalue analysis of the recharge oscillator model, which was to be expected since for months with a complex eigenvalue, the real part of the latter equals -γ in this model, with strong damping during late boreal fall and early winter and instability in late boreal summer and early fall. The coupling parameter (ω) is quite similar to the phase progression (imaginary part of the eigenvalue) in the recharge oscillator during boreal spring and summer but it does not show the breakdown during boreal winter that was found for the phase progression in the recharge oscillator model. The eigenvalues of the simplest recharge oscillator (not shown) on the other hand show little difference to those of the recharge oscillator model. This makes clear that this breakdown is explained by the strong damping during boreal winter, since the phase progression is given as $\omega^2 = \omega_0^2 - \gamma^2$ in the simplest recharge oscillator picture.

Looking at the forecast skill of the simplest recharge oscillator (not shown) we find that the forecast skill is slightly worse than that of the recharge oscillator, especially for thermocline depth predictions. For SST the difference cannot be considered significant.

A toy model run with stochastic excitation is performed with this model, as done before for the recharge oscillator model. The resulting power spectra (not shown) differ little from those found with the recharge oscillator model. However, the secondary peak at $\frac{4}{3}$ years is less pronounced. This is in agreement with the result that the seasonality of different statistical properties seems to be less pronounced in this simplified model. Figure 2.22 shows that the seasonal cycle of standard deviation is somewhat weaker than in observations, which is not the case for the full recharge oscillator model, as shown in section 2.3.3. However, the major part of the seasonal dependence of standard deviation is still included.

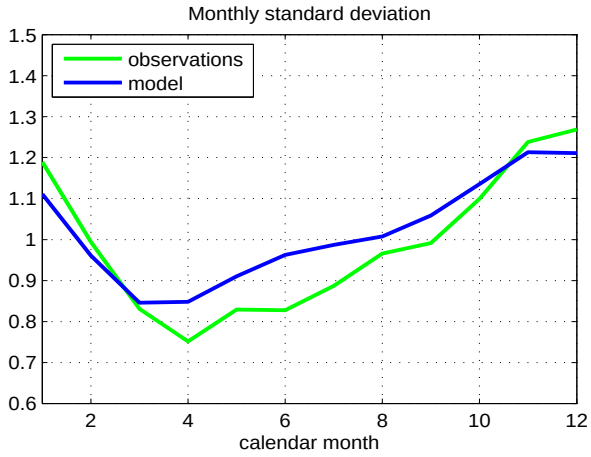

Figure 2.22: Seasonal dependence of standard deviation of Niño3 SSTA in observations (1950-2002) compared to the results of the seasonal dependent simplest recharge oscillator model with constant stochastic excitation.

The seasonal dependent cross and auto-correlations are shown in figure 2.23. While these are well reproduced by the recharge oscillator model (see section 2.3.3), the seasonality is too weak in the simplified model.

2.8 Summary and Discussion

The parameters of the delayed action oscillator model and the recharge oscillator model are fitted to observational data. For both models the resulting parameter sets belong to damped oscillatory regimes.

The recharge oscillator model can be transformed to one second order differential equation, which for the fitted parameters reveals a damped harmonic oscillation with an eigenfrequency corresponding to a 4-year period and a damping timescale of approximately two years. The delayed action oscillator on the other hand is described by a delayed differential equation. The general solution is therefore given by an infinite superposition of harmonic oscillations and is not harmonic itself. However, the model can be approximated by a harmonic oscillator, which for the parameters fitted in this study reveals a damped oscillation with a period of about two years and a damping timescale of about 20 months. The power spectral density of the eastern Pacific SSTA resulting from an integration of the (unapproximated) delayed action oscillator model with stochastic excitation, representing short-timescale "weather-noise", also shows a dominant period of around two years. But, it also reveals enhanced variance at a period of about 6 months. As expected from the eigenfrequency, the spectrum of an integration of the recharge oscillator model peaks at a period of around 4 years. The

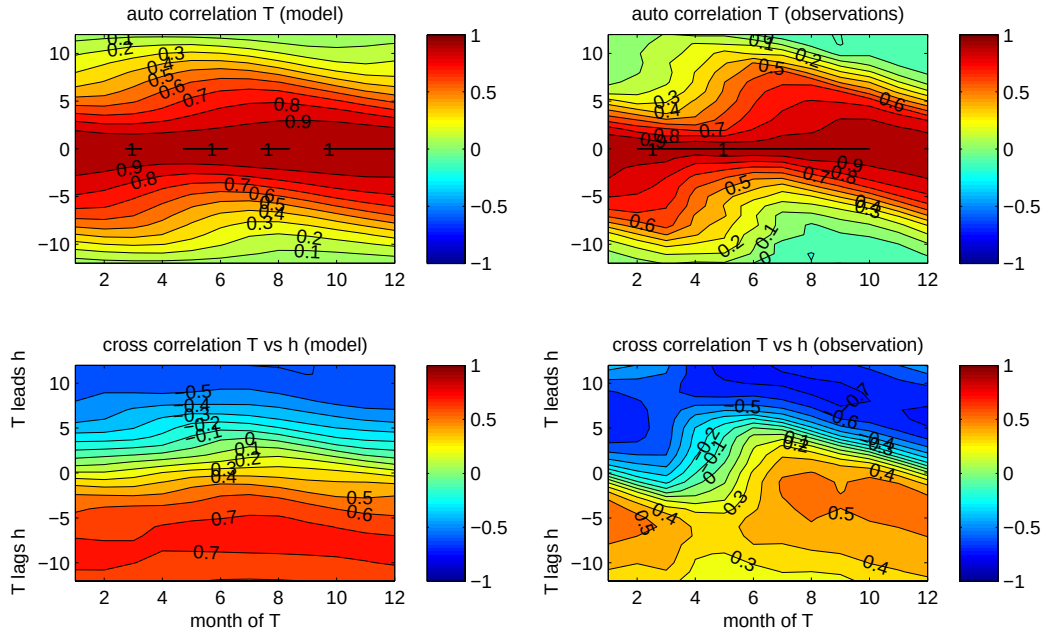

Figure 2.23: Seasonal dependence of Niño3 SSTA auto-correlation and cross-correlation between SSTA and equatorial averaged thermocline depth of the simplest recharge oscillator model with seasonality for the Pacific, compared to observational/GCM data for the time period from 1950 to 2001.

recharge oscillator model spectrum is in good agreement with the observed Niño3 SST spectrum which also peaks at a period of around 4 years. However, somewhat enhanced variance at a period of about 6 months can also be identified in the observational spectrum.

The recharge oscillator model also reproduces the observed cross-correlation between eastern Pacific SSTA and equatorially averaged thermocline depth, with thermocline depth anomalies leading SSTA anomalies by about 6 to 9 months and SSTA leading thermocline depth anomalies of opposite sign by about 8 to 12 months.

The recharge oscillator also turns out to be a better forecast model than the delayed action oscillator. It should be stressed that both models use two predictors for initialization, which are present-month SSTA and thermocline depth for the recharge oscillator model and present-month and lagged SSTA for the delayed oscillator.

As a natural generalization, the delayed recharge oscillator model is proposed which explicitly includes SST adjustment time as well as wave travel times. It simplifies to the delayed action oscillator in the limit of fast SST adjustment, whereas it simplifies to the recharge oscillator model in the limit of fast wave travel times. The results of this study suggest that the recharge oscillator model is the more reasonable

approximation than the delayed action oscillator.

While useful for theoretical considerations, the delayed recharge oscillator in the formulation presented here is not a good forecast model because eastern Pacific thermocline depth is used as a second variable. For the recharge oscillator model thermocline depth averaged over the whole equatorial Pacific is used instead, which is a more useful predictor.

The delayed recharge oscillator is extended by nonlinear coupling of SST on thermocline depth anomalies which is necessary to adequately take into account the highly nonlinear structure of the subsurface temperature profile. The fitted linear terms are not significantly different to the terms resulting from the fit not considering nonlinear coupling and the model still reveals a damped oscillation which is only slightly modified by the nonlinear terms. But the nonlinear coupling of SST on thermocline depth explains a major part of the skewness and part of the kurtosis of observed ENSO timeseries. The major part of the kurtosis and also part of the skewness of the observed ENSO timeseries results from the seasonal cycle in ENSO variability.

For the simple models proposed here, parameter fits reveal damped and more or less regular oscillatory regimes. Excited by white noise forcing, representing "weather noise", observed statistical properties of ENSO can be well described by these models. Nevertheless, it is the authors opinion, that no strict answer can be given to the question whether ENSO reveals a self sustained (regular or irregular) oscillation due to nonlinear dynamics within the "slow" components of the coupled system, or whether ENSO is in a damped oscillatory regime and variability is sustained by uncoupled, short timescale, "weather noise". While for the proposed simple models this separation of timescales is predetermined by the nature of the model, for the real world, such a strict separation into "slow" coupled components and "fast", "uncoupled" dynamics does not exist. But a strict definition of this separation would be necessary to define the ENSO regime.

Seasonal dependent parameter fits of the recharge oscillator model reveal that a damped oscillatory coupled SSTA-Ocean dynamics mode can be found nearly throughout the whole year. The imaginary part of the eigenvalues is in agreement with the results of Burgers et al. (2005), finding that "in spring phase progression is larger than the annual average, in fall it almost comes to a halt". The damping falls to zero in late summer whereas it has a maximum in winter, indicating a breakdown of the positive Bjerknes feedback. This is in accordance with the prevalent breakdown of El Niño events at the beginning of the year and the observed spring persistence barrier. The observed seasonal cycle in Niño3 SST variance as well as in the SSTA auto-correlation and in the cross-correlation between SSTA and thermocline depth is reproduced by the recharge oscillator model with stochastic excitation, even though the "weather-noise" is held constant throughout the year. This shows that the observed seasonality can be explained by the stability of the "slow" coupled dynamics only.

The annual mean properties of the model change little if seasonality is included. However, as indicated above, some kurtosis is produced in the frequency distribution of Niño3 SSTA, and, in agreement with Jin et al. (1996), an additional $\frac{4}{3}$-year spectral peak is found. The latter can be explained by nonlinear interaction with the seasonal cycle.

Finally, it was shown that the predictive skill of the recharge oscillator with seasonality, which is slightly better than that of the model without seasonality, is comparable to that of a much more complex hybrid coupled model. This supports the proposition that the recharge oscillator model contains the basic mechanisms that are important for the predictability of ENSO.

The simplest recharge oscillator, proposed by Burgers et al. (2005) as a further simplification of the recharge oscillator model, is well justified by parameter fits without consideration of the seasonal cycle. But it is not able to appropriately account for seasonality.

Chapter 3

Atlantic and Indian Ocean

3.1 Introduction

The atmosphere-ocean interactions responsible for the El Niño Southern Oscillation (ENSO) are generally understood and can be described by simple conceptual models, such as the recharge oscillator, as shown in the previous chapter. More recently, indications were found that a similar coupled mode also exists in the Atlantic Ocean (e.g. Zebiak (1993), Latif and Grötzner (2000), Keenlyside and Latif (2007)). Keenlyside and Latif (2007) show that all elements of the Bjerknes feedback, which allows for the growth of an initial perturbation via atmosphere-ocean interaction, are also active in the equatorial Atlantic, even though the feedbacks are weaker than in the Pacific Ocean and primarily restricted to boreal spring and summer. However, they do not analyze the existence of a delayed negative feedback which is necessary for the oscillatory behaviour of ENSO in the Pacific. In the recharge oscillator picture, this negative feedback acts via the discharge (recharge) of equatorial averaged heat content during an El Niño (La Niña) event.

Webster et al. (1999) and Saji et al. (1999) first suggested that a zonal dipole mode in the Indian Ocean is a reflection of atmosphere-ocean interaction intrinsic to the Indian Ocean. Whether or not this can be understood as an oscillatory mode of internal atmosphere-ocean dynamics in the Indian Ocean is currently still under discussion (e.g. Baquero-Bernal et al. (2002), Dommenget and Latif (2002), Behera et al. (2003), Dommenget and Latif (2003)).

In this chapter it shall be analyzed if the recharge mechanism, which turned out to be essential for oscillatory behaviour of ENSO, does also exist in the equatorial Atlantic and Indian Oceans and whether the atmospheric feedback there is strong enough to allow for oscillatory behaviour. This is done by fitting the recharge oscillator model to observational Atlantic and Indian Ocean data and analyzing the results in terms of the ability of the fitted models to describe the observations, and the implications

of the resulting parameters for equatorial Atlantic and Indian Ocean dynamics.

3.2 An Atlantic Recharge Oscillator?

In this section the existence of the recharge-discharge mechanism in the equatorial Atlantic area is analyzed by fitting the parameters of the recharge oscillator model, as discussed in section 2.3, to Atlantic Ocean observational data.

The model equations are given by (2.9) where T_E now denotes eastern Atlantic SSTA and h denotes thermocline depth averaged over the equatorial Atlantic basin.

The model parameters are fitted to 1951-2002 Atl3 ($20^oW - 0^oW, 3^oS - 3^oN$) SSTA data for T_E and 20^o isotherm depth data averaged over $50^oW - 20^oE, 5^oS - 5^oN$ for h. Since Keenlyside and Latif (2007) stress the importance of seasonality of the ocean-atmosphere interaction in the Atlantic, parameters are fitted depending on the calendar month of the year, as explained in section 1.2.

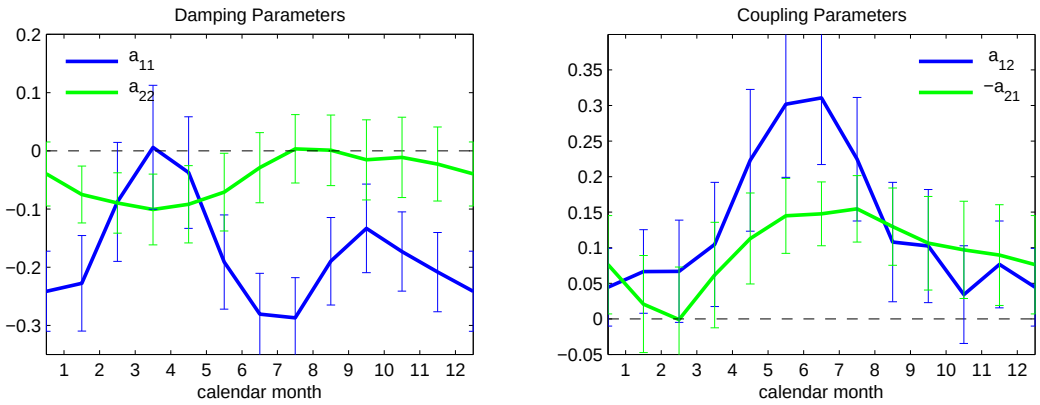

Figure 3.1: Seasonal cycle of the fitted parameters of the recharge oscillator model for the Atlantic Ocean, with 95% confidence intervals. All parameters are fitted to 1950-2001 data.

Figure 3.1 shows the seasonal cycle of the parameters of equation (2.9) resulting from the parameter fit to Atlantic Ocean data. As for the Pacific, the damping of thermocline depth is weak throughout the year, and significantly different from zero only during spring. The damping of SSTA is on average stronger than in the Pacific, but has a distinct minimum in late winter/early spring when it is not significantly different from zero. The coupling parameters between averaged thermocline depth and eastern Atlantic SSTA have the same sign as for the Pacific in the annual mean, with shallow (deep) thermocline anomalies causing a cooling (heating) of the SST and warm (cold) SSTA causing a shallowing (deepening) of the equatorial thermocline. This describes the recharge-discharge mechanism. Significant coupling parameters in both directions are found during boreal summer.

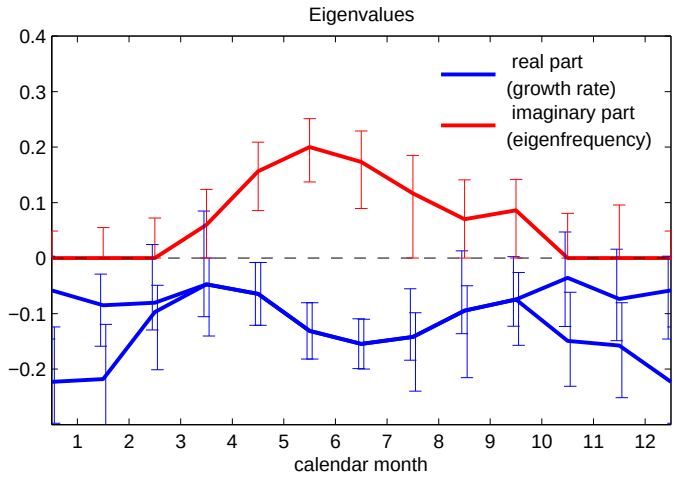

Figure 3.2: Seasonal cycle of the eigenvalues of the recharge oscillator with the parameters fitted to Atlantic observational SSTA data and thermocline depth data from an NCEP forced GCM run, for the time period 1950-2001. Error bars denote 95% confidence levels.

Figure 3.2 shows the seasonal cycle of the corresponding eigenvalues of equation (2.9) for the fitted parameters. It can be seen that an oscillatory mixed SST-thermocline depth mode exists from boreal spring till early fall, while the system is overdamped with two decaying eigenmodes in late fall and winter. While growth rates around zero are found in late summer and early fall in the Pacific, only decaying modes are found in the Atlantic throughout the whole year. The damping is smallest in early boreal spring, which is in agreement with the observed maximum in the variance of eastern Atlantic SSTA in early summer.

As done for the Pacific Ocean models, the recharge oscillator with the parameters fitted to Atlantic Ocean data and with additional stochastic excitation is integrated for $3 \cdot 10^4$ years. The noise forcing is constant throughout the year. The variance of the noise forcings are fitted to mimic the total variances of SSTAs and thermocline depth. They are chosen to meet $\sigma_{\xi_h} = 0.6 \cdot \sigma_{\xi_T}$ and assumed to be uncorrelated, for simplicity.

As for the Pacific, the resulting seasonal cycle of eastern Atlantic SST variance (not shown) is in agreement with observations, even though the noise forcing is constant throughout the year.

Figure 3.3 a) shows the annual cycle of the cross-correlation between Atl3 SSTA and averaged equatorial thermocline depth from observational/forced GCM data for the period 1951-2001. Analogue to the Pacific, positive correlation is found with thermocline depth anomalies leading SSTA and negative correlation with SSTA leading thermocline depth anomalies. However, correlation is smaller than in the Pacific. The highest positive correlation is found with early summer heat content anomalies

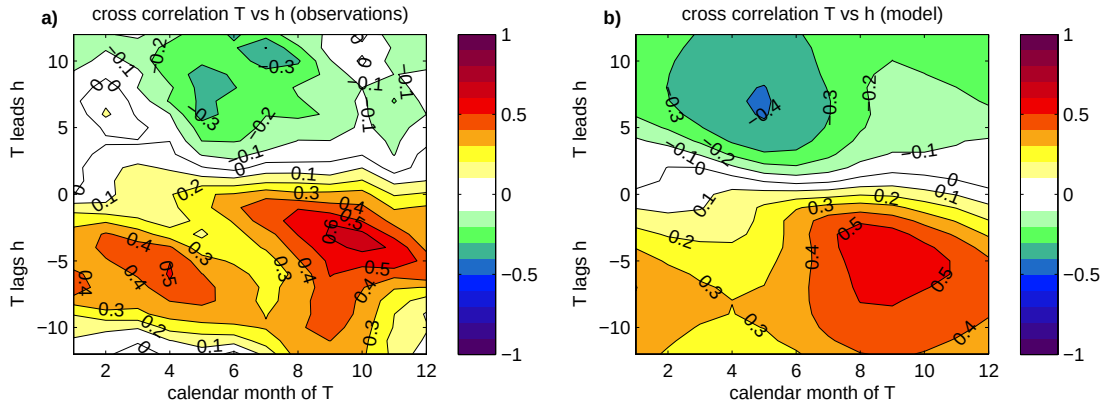

Figure 3.3: a) Annual cycle of the cross-correlation between observed Atl3 SSTA and equatorial Atlantic thermocline depth anomalies from an NCEP-forced GCM run, for the time period 1950-2001. Correlations of 0.3 are significant on a 95% level. **b)** The same for a $3 \cdot 10^4$ year run of the recharge oscillator model with stochastic excitation.

leading early fall SSTA and the highest negative correlation is found with early summer SSTA leading winter thermocline depth anomalies. This is in agreement with the maximum phase propagation in early summer, since the latter is directly related to the strength of surface-subsurface interactions. Except for a slight shift of maximum negative correlation to spring SSTA leading winter thermocline depth anomalies, the cross-correlation is well resembled in the recharge oscillator model integration, indicating that the elementary surface-subsurface interaction is well described by the simple model approach (Fig. 3.3 b).

Figure 3.4 a) shows the power spectral density of SST resulting from the model integration compared to the Atl3 SST spectrum from 1870-2003 observational data. The model spectrum as well as the observed SST spectrum reveal only little difference to red noise. Figure 3.4 b) shows that, compared to a fitted AR1 process, variance in the recharge oscillator model is increased on interannual timescales, with a peak frequency around 4 years.

As done for the Pacific in the previous chapter, the model is integrated in forecast mode using observed SST and thermocline depth data for initialization. Forecast runs are started from each month and integrated for one year. The resulting forecast correlation-skill is shown in figure 3.5 a). It can be seen that for both cross-validated time periods, forecast skill above persistence is found. It should be added that even better forecast skill could be expected if real observational thermocline depth data were available instead of the NCEP forced GCM data that is used here. This turned out to be the case for the Pacific for which some real observational data from the TOGA array exists, which was used for the forecast skill comparison in section 2.7.1. The model also has some predictive skill above persistence for thermocline depth

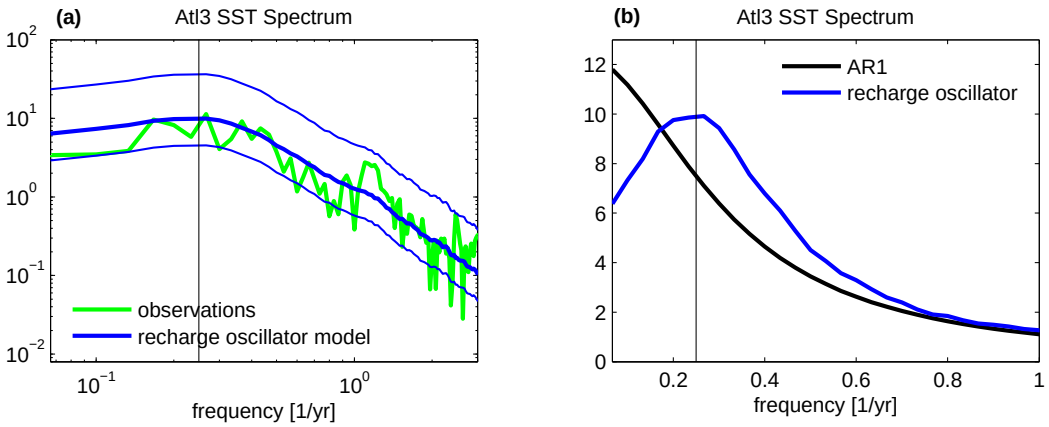

Figure 3.4: a) Eastern Atlantic SSTA spectrum of the recharge oscillator model with stochastic excitation (blue), compared to the observed Niño3 SSTA spectrum from 1870 to 2003 (green). The thin blue lines show the 95% confidence interval. **b)** The model spectrum (blue) compared to an AR1 process fitted to observational data (black) in a linear scale. The thin vertical black lines denote a frequency of four years in both plots.

anomalies (not shown). But, opposite to the Pacific, less predictive skill above persistence is found for thermocline depth anomalies than for SSTA.

To test the importance of internal atmosphere-ocean dynamics in the eastern equatorial Atlantic versus the remote forcing of ENSO, an AR1 model with an additional forcing from ENSO is fitted to observational SST data for the same time period. The model can be written as:

$$T_E(t + 1\,month) = \alpha \cdot T_E(t) + c_{AP} \cdot T_P(t) \tag{3.1}$$

where T_E is Atl3 SSTA and T_P is Niño3 SSTA. Parameters are fitted for each calendar month, as done for the recharge oscillator model. The forecast skill of this model (fig. 3.5 b) is hardly better than persistence, indicating that internal coupled atmosphere-ocean dynamics are more important in the eastern equatorial Atlantic than the remote forcing from ENSO.[1]

3.3 An Indian Ocean Recharge Oscillator?

To test for the existence of a recharge-discharge mechanism in the Indian Ocean, parameters of the recharge oscillator model are fitted to Indian Ocean observational data, as done for the Atlantic in the previous section. To filter out the strong

[1]Niño3 SSTA is not predicted in the forecast integrations of (3.1), but taken from observations, so this model contains artificial skill due to the knowledge of Niño3 SSTA.

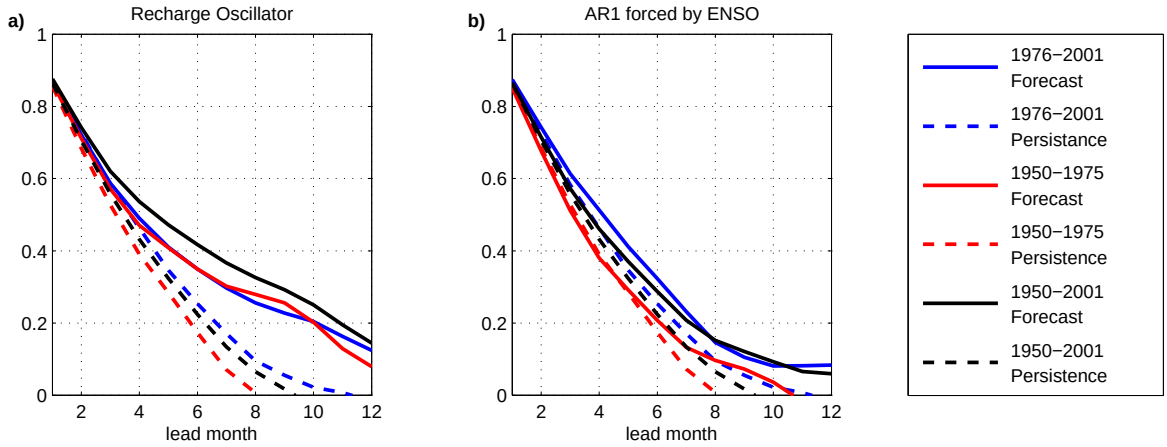

Figure 3.5: a) Forecast skill of the recharge oscillator model for the Atlantic. Shown is the anomaly correlation between predicted and observed Atl3 SSTA, compared to the observed auto-correlation (persistence). The coloured lines show cross-validated forecast skills. The time intervals given in the legend refer to the period used for the forecast skill evaluation, while in each case the other interval was used to fit the parameters. For the black line the whole time period was used for the parameter fit and for the evaluation of forecast skill. **b)** The same for an AR1 model with an additional coupling to observed Niño3 SSTA.

monopole response of the Indian Ocean SSTA to ENSO, the Indian Ocean Dipole mode (DMI) with reversed sign is used for T_E in equation (2.9), instead of a single area in the eastern basin as for the Pacific and Atlantic Oceans. The DMI is defined by Saji et al. (1999) as the difference in SST anomaly between the equatorial western Indian Ocean ($50^oE - 70^oE, 10^oS - 10^oN$) and the south-eastern tropical Indian Ocean ($90^oE - 110^oE, 10^oS - 0^o$). The reversed DMI is chosen to retain positive values for T_E for positive eastern Indian Ocean SSTA. Note that the qualitative results presented in the following change little, if only the eastern part of the dipole mode, or another index centered in the eastern equatorial Indian Ocean is chosen. 20^o isotherm depth data averaged over the whole equatorial strip ($40^oE - 110^oE, 5^oS - 5^oN$) is taken for h.

Figure 3.6 shows the seasonal cycle of the parameters of equation (2.9), resulting from the parameter fit to Indian Ocean data. Both damping parameters exceed the Atlantic damping parameters in the annual mean. While the damping of thermocline depth is approximately constant throughout the year, the SST damping has a minimum in boreal summer. The coupling of the DMI on thermocline depth anomalies a_{12} is not significantly different from zero throughout the whole year. Some significant coupling of equatorial averaged thermocline depth anomalies on DMI SSTA exists in boreal winter and summer, but it is of opposite sign as expected from the recharge-discharge mechanism, with eastern Indian Ocean SSTA causing thermocline depth anomalies of the same sign.

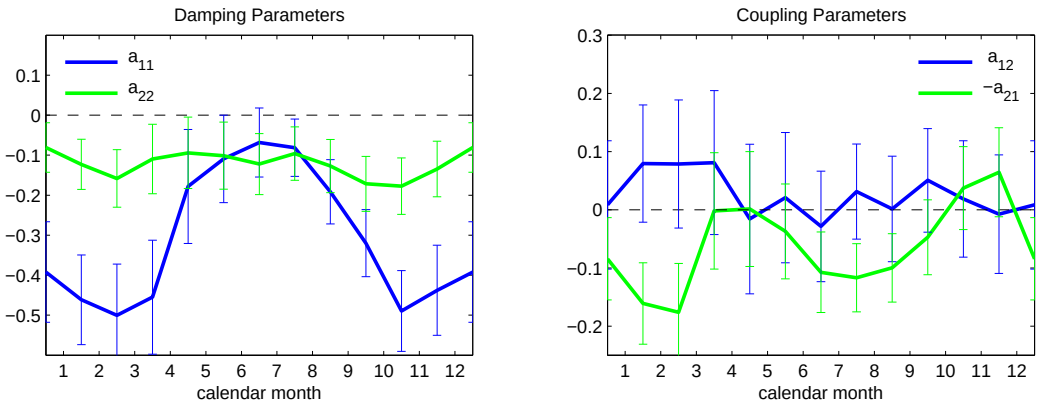

Figure 3.6: Seasonal cycle of the parameters of the recharge oscillator model fitted to Indian Ocean observational DMI data and thermocline depth data from an NCEP forced GCM run, for the time period 1950-2001. Error bars denote 95% confidence levels.

Figure 3.7 shows the seasonal cycle of the eigenvalues of equation (2.9) corresponding to the fitted parameters. Except for the June-July transition, two damped eigenmodes are found throughout the year. Looking at the corresponding eigenvectors (not shown), especially for boreal fall and winter, the amplitude of the stronger damped mode can be identified to be approximately a pure SST mode. The weaker damped eigenvalue on the other hand belongs to a mode that is approximately a pure thermocline depth mode. Indeed, comparing the eigenvalues to the SST and thermocline depth damping parameters a_{11} and a_{22} which are also shown in figure 3.7, one finds that for the major part of the year the two damping timescales match the damping of SST and the thermocline depth anomalies. The thermocline depth mode shows relatively little seasonality, with hardly significant minimal and maximal damping in boreal summer and fall, respectively. The SST mode is significantly stronger damped in boreal fall and winter. The weaker damping in boreal summer is in agreement with the variability of DMI peaking towards the end of summer. It has to be stressed that this reduced damping in boreal summer is not found for equatorial averaged Indian Ocean SSTA.

An oscillatory mixed SST-thermocline depth mode is found only for the June-July transition, but the imaginary part of the eigenvalue is not significantly different from zero. Moreover, the corresponding eigenvector reveals that eastern Indian Ocean SSTA is leading thermocline depth anomalies of the same sign, whereas in the Pacific and Atlantic Ocean eastern ocean SSTA is leading thermocline depth anomalies of opposite sign and thermocline depth anomalies are leading SSTA of the same sign. The phase relation describing the recharging/discharging during a La Niña/El Niño event is therefore not found for any month in the Indian Ocean. This is consistent with the reversed sign found for the coupling parameter a_{21}.

The model is integrated for $3 \cdot 10^4$ years using the fitted parameters and additional

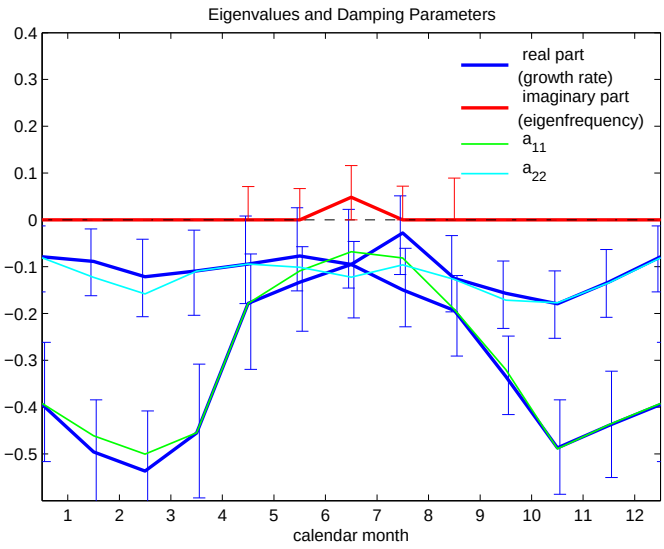

Figure 3.7: Seasonal cycle of the real and imaginary part of the eigenvalues (blue and red) and the damping parameters a_{11} and a_{22} (green and cyan) of the recharge oscillator fitted to Indian Ocean observational DMI data and thermocline depth data from an NCEP forced GCM run, for the time period 1950-2001. Error bars denote 95% confidence levels.

stochastic excitation. The noise forcing is constant throughout the year. The variances of the noise forcings are chosen to meet $\sigma_{\xi_h} = 0.65 \cdot \sigma_{\xi_T}$.

The DMI spectrum resulting from the model integration, as well as the observational spectrum (figure 3.8), do not reveal a peak frequency, which is consistent with the eigenvalues of the model revealing no significant phase progression. The model spectrum has somewhat enhanced variance on long timescales compared to an AR1 process, but no evidence for this can be found in the observations. Figure 3.9 a) shows the annual cycle of the cross-correlation between the (reversed) DMI and equatorial averaged thermocline depth from observational/forced GCM data for the period 1951-2001. The correlation is generally weaker than for the Atlantic. In opposition to the Atlantic and Pacific Ocean, in the annual mean, maximum correlation is found with -DMI leading thermocline depth anomalies of the same sign by about one month. This correlation is most pronounced in boreal fall. The cross-correlation can partly be reproduced by the recharge oscillator model, where we find maximum correlation with late summer positive (negative) SST anomalies leading a deepening (shallowing) of the thermocline in fall. This cross-correlation, which is of reversed sign to the correlation expected from the recharge-oscillator picture, is consistent with the results for the eigenvectors described above.

As done for the Pacific and Atlantic, the model is integrated in forecast mode using observed DMI and thermocline depth data for initialization. Forecast runs are started

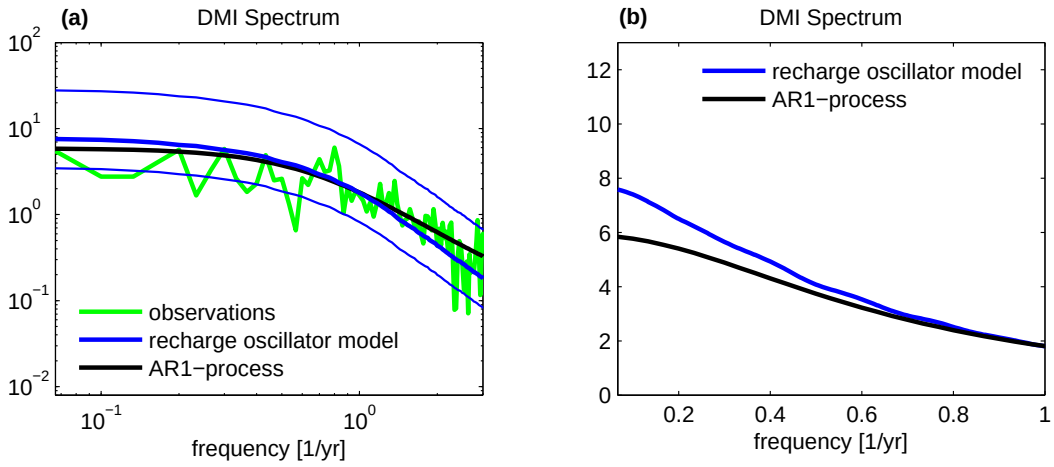

Figure 3.8: a) Indian Ocean DMI spectrum of the recharge oscillator model with stochastic excitation (blue), compared to the observed Niño3 SSTS spectrum from 1870 to 2003 (green). The thin blue lines show the 95% confidence interval. **b)** The model spectrum compared to an AR1 process fitted to observational data(black) in a linear scale. The thin vertical black lines denote a frequency of four years in both plots.

from each month and integrated for one year. The forecast skill for DMI is shown in figure 3.10 a). The recharge oscillator model does not have forecast skill above persistence for the DMI. To estimate to what extent the DMI is independent from ENSO, an AR1 model with an additional forcing from ENSO is fitted to observational DMI data, as done for the Atlantic in the previous section (figure 3.10 b). Skill above persistence is found especially on long lead times. It should be mentioned that this is not a real forecast run, since Niño3 SST is not modelled, but observational data is used for the "forecasts". The small, approximately constant forecast skill on long timescales is in agreement with the correlation of the DMI with Niño3 SSTA, which interestingly has a maximum value of -0.38 with DMI leading Niño3 SSTA by about two months for 1950-2001 HADISST data. The latter might indicate a feedback from DMI on ENSO. However, this shall not be the scope of this work. Figure 3.10 b) shows the results of the same model but for equatorial Indian Ocean SSTA ($5^oS - 5^oN, 40^oE - 110^oE$; hereinafter referred to as EqInd) instead of the DMI. It can be seen that the averaged equatorial Indian Ocean SSTA is to a large extent determined by ENSO. Note that the correlation skill for long lead times of this model is higher than the correlation between Niño3 and EqInd SSTA itself, which has a maximum of 0.61 with Niño3 SSTA leading EqInd SST by about three months, for 1950-2001 HADISST data.

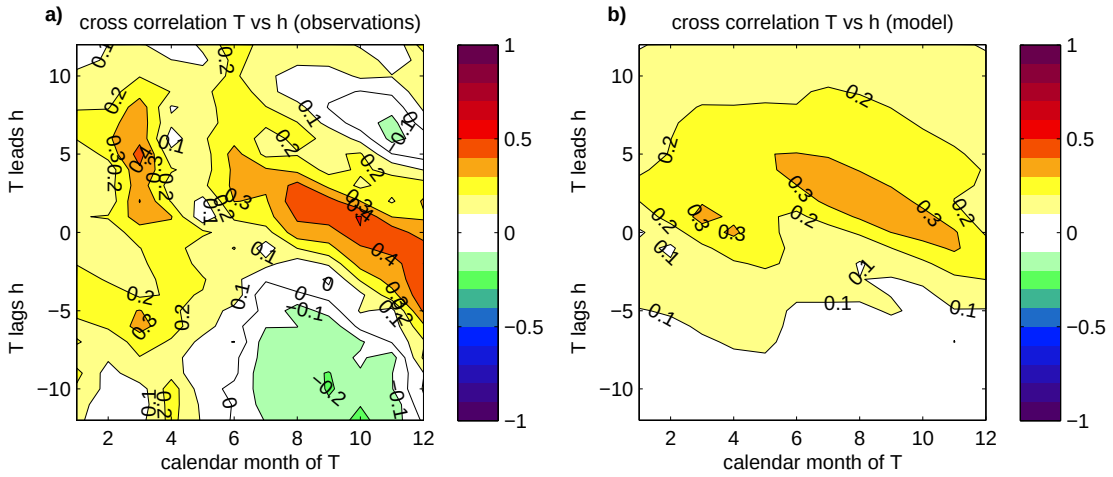

Figure 3.9: a) Annual cycle of the cross-correlation between -DMI and equatorial Indian Ocean thermocline depth anomalies from HADISST and NCEP-forced GCM data for the time period 1950-2001, repectively. Correlations of 0.3 are significant on a 95% level. **b)** The same for a $3 \cdot 10^4$ year run of the recharge oscillator model with stochastic excitation.

3.4 Summary and Discussion

Observed Atlantic Ocean variability can be described by the recharge oscillator model with parameters fitted to Atlantic Ocean observational data. A negative feedback for SSTA via a recharge/discharge of equatorial heat content is found to be active in the equatorial Atlantic. The feedbacks are found to be strong enough to reveal a damped oscillatory mixed ocean dynamics-SST mode from boreal spring to late boreal fall, while two purely damped eigenmodes are found during late boreal fall and summer. The spectrum of the recharge oscillator for the Atlantic reveals enhanced variance on timescales around 4 years, if compared to a red noise process. The results are in agreement with Zebiak (1993) who finds a damped oscillation with a period of about 4 years in a Zebiak and Cane (1987) -type model for the Atlantic. However, it is somewhat in disagreement with the results of Latif and Grötzner (2000) who find a quasi biennial mode in the equatorial Atlantic from observational data.

It was also shown that the recharge oscillator model, using equatorial averaged thermocline depth anomalies, has predictive skill above persistence for Atl3 SSTA, while a simple red noise model for Atl3 SSTA with an additional forcing from ENSO does hardly have any forecast skill above persistence. This shows that Atlantic subsurface information is a more useful predictor for eastern Atlantic SSTA than Niño3 SSTA, which in turn indicates that eastern Atlantic SST variability is primarily determined by coupled dynamics in the Atlantic basin itself.

The equatorial Indian Ocean variability turns out to be quite different from that

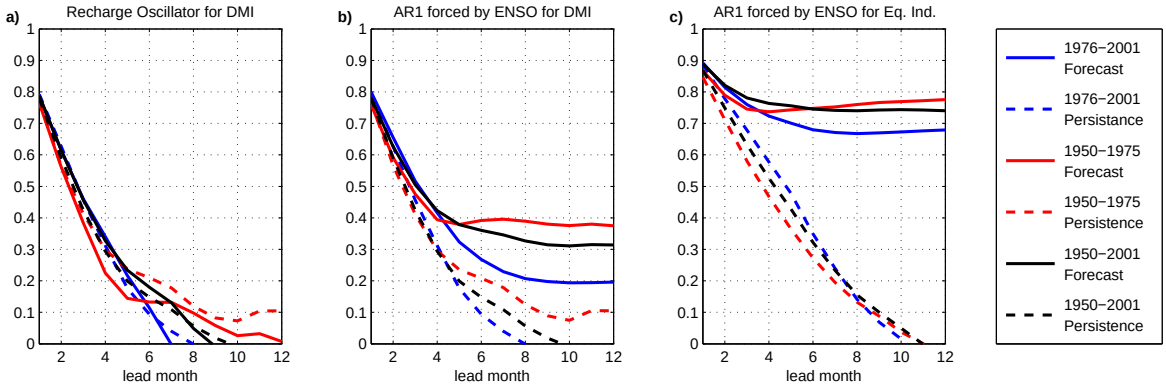

Figure 3.10: a) As figure 3.5 but for DMI predictions with the Indian Ocean recharge oscillator model. **b)** The same for an AR1 model with an additional coupling to observed Niño3 SSTA **c)** As b) but for equatorial Indian Ocean SSTA averaged over the whole basin ($5^oS - 5^oN, 40^oE - 110^oE$).

in the Pacific and Atlantic Oceans. A recharge-discharge mechanism of equatorial heat content, connected with the equatorial east-west SST gradient which is found in the Pacific and Atlantic Oceans, cannot be identified in the Indian Ocean. Since this delayed negative feedback is necessary for oscillation in the recharge oscillator picture, no significant oscillation is found in the model for the Indian Ocean.

The damping of the DMI mode is on average stronger than that of the eastern Atlantic SSTA, suggesting that a possible positive atmospheric feedback is at least smaller. However, it has a minimum in boreal summer, which is not found for the equatorial averaged Indian Ocean SSTA. This could indicate that during this time of the year some positive feedback comparable to the Bjerknes feedback might exist, which is suggested in different recent publications (see Chang et al. (2006) and references herein).

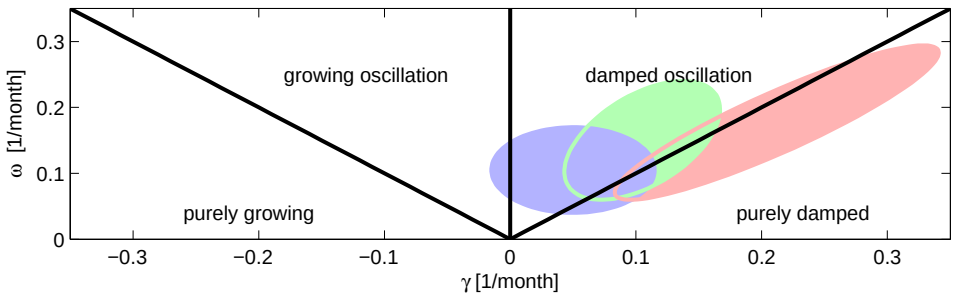

Figure 3.11: As figure 2.1, but with the parameter subspace found for the Pacific, Atlantic and Indian Ocean indicated in blue, green and red, respectively .

Figure 3.11 indicates the parameter subspaces of the oscillator equation (2.5) cor-

responding to the seasonal dependent recharge oscillator parameters found for the different oceans. The Pacific Ocean model is in a damped oscillatory regime during the major part of the year. The Atlantic model has a stronger damping but is still in an oscillatory regime at least for part of the year. The Indian Ocean Model, on the other hand, is purely damped throughout nearly the whole year. It should further be stressed that for the only month for which oscillatory eigenvalues are found in the Indian Ocean model, the signs of the SST-thermocline depth coupling parameters a_{12} and a_{21} are of reversed sign to what would be expected from the recharge oscillator picture.

Since the recharge oscillator mechanism is not active in the Indian Ocean, no predictive skill above persistence is found for the DMI using the recharge oscillator model. Some predictive skill for the DMI is found assuming a simple red noise process with an additional forcing from ENSO, which is, however, quite small compared to the high predictive skill that is found for the equatorial averaged Indian Ocean SSTA with a similar model. This confirms that the dominant mode of equatorial Indian Ocean variability is a monopol response to ENSO.

The results of this chapter suggest that while the equatorial Atlantic reveals coupled atmosphere-ocean dynamics quite similar to ENSO and is relatively independent from ENSO, the opposite seems to hold for the Indian Ocean.

Chapter 4

Tropical Oceans' Interaction

4.1 Introduction

While it is known that the Indian Ocean shows a strong response to ENSO (e.g. Venzke et al. (2000)), more recently, different studies also suggest a feedback of the Indian Ocean SSTA on ENSO. Analyzing observational data, Kug and Kang (2006) suggest a negative feedback of the tropical Indian Ocean on ENSO, with a warm Indian Ocean causing a decay of ENSO events via anomalous easterly winds in the western Pacific. CGCM experiments on the influence of the Indian Ocean on the ENSO cycle come to somewhat controversial results. Yu et al. (2002) find that ENSO variability is decreased and the frequency is slightly increased from a 4.4 to a 4 years period in a 42 year model integration, if the Indian Ocean is decoupled from the system. Wu and Kirtman (2004) agree that ENSO variability is decreased, but find that the frequency is also decreased if the Indian Ocean is decoupled. Dommenget et al. (2006) agree with the latter that the ENSO frequency is decreased, but find increased ENSO variability if the Indian Ocean is decoupled from the system.

While there is general agreement that the Atlantic sector is influenced by ENSO, with a particular strong response in the western subtropical Atlantic, some disagreement on the equatorial Atlantic's response to remote ENSO forcing exists. The weak instantaneous correlation between equatorial Atlantic and Niño3 SSTA has led to the suggestion that ENSO has no significant influence on the equatorial Atlantic (Zebiak (1993), Enfield and Mayer (1997)). However, seasonally stratified correlations, lag regressions and composite analyses come to conflicting results, concerning the response of equatorial Atlantic SST on ENSO (e.g. Saravanan and Chang (2000), Ruiz-Barradas et al. (2000), Huang (2004), Latif and Grötzner (2000)). Recently, Keenlyside and Latif (2007) stress a maximum negative correlation between Niño3 SSTA and eastern equatorial Atlantic SSTA with Atl3 leading Niño3 SSTA by about 6 months. This indicates a feedback from the Atlantic on ENSO, rising hope that ENSO predictions can be improved by explicitly including Atlantic SSTA.

Here, simple models are proposed as hypotheses for the interaction of the tropical Atlantic and Indian Oceans with ENSO. As in the previous chapters, the model parameters are fitted to observational data and the implications of the resulting parameters for the impact of the Indian and Atlantic Ocean on the ENSO cycle are analyzed. In the picture of this conceptual model, the different results of the CGCM studies for the influence of the Indian Ocean on the ENSO cycle can be explained on the basis of the biases of the CGCMs. Finally, a simple model including interactions between all tropical Oceans is proposed.

4.2 A Simple Model for the Tropical Oceans' Interactions with ENSO

A simple coupled model for the interactions of the Pacific and the Atlantic or Indian Ocean is proposed by Dommenget et al. (2006). It consists of the simplest recharge oscillator model suggested by Burgers et al. (2005) coupled to a linear damping model for the Atlantic/Indian Ocean. It proposes a feedback from the Atlantic/Indian Ocean on Pacific SST. Kug and Kang (2006) propose a similar model but with a feedback on western equatorial thermocline depth. In the following, the model as used by Dommenget et al. (2006) is extended by a feedback of Indian/Atlantic Ocean SSTA on averaged Pacific thermocline depth. It can be written as

$$\begin{aligned} \tfrac{d}{dt}T_P &= \omega_0 h_P - 2\gamma_P T_P + c_{PI/PA}T_{I/A} \quad + \xi_P \\ \tfrac{d}{dt}h_P &= -\omega_0 T_P + ch_{PI/PA}T_{I/A} \quad + \xi_h \\ \tfrac{d}{dt}T_{I/A} &= -2\gamma_{I/A}T_{I/A} + c_{IP/AP}T_P \quad + \xi_{I/A} \end{aligned} \tag{4.1}$$

where T_P is eastern Pacific (Niño3) SSTA, h_p denotes thermocline depth anomaly averaged over the equatorial Pacific and $T_{I/A}$ is equatorial Indian/Atlantic Ocean SSTA. The $c_{IP/AP}$ term describes the coupling of the Indian/Atlantic Ocean to Pacific SSTA whereas $c_{PI/PA}$ and $ch_{PI/PA}$ represent the feedback of Indian/Atlantic Ocean SSTA on Pacific SST and thermocline depth, respectively. ξ_{T_P}, ξ_h and $\xi_{T_I/A}$ again denote stochastic excitation, representing wind and heat flux forcing due to short time scale uncoupled atmospheric variability.

4.3 Indian Ocean-ENSO Interaction

The parameters of (4.1) are fitted to 1951-2002 EqInd and Niño3 SSTA data and 20^o isotherm depth data averaged over $120^oE - 80^oW, 5^oS - 5^oN$ for h. The data and fitting methods are described in chapter 1. To constrain the number of degrees

of freedom, no seasonal dependent parameter fit is performed here. The resulting parameters and estimated 95% confidence intervals for the whole time period 1950-2001 as well as for the time periods 1950-1975 and 1976-2001 are given in table 4.1.

	1950-1975	1976-2001	1950-2001
γ_P	0.052 ± 0.030	0.006 ± 0.021	0.022 ± 0.017
γ_I	0.161 ± 0.026	0.117 ± 0.021	0.135 ± 0.017
ω	0.117 ± 0.037	0.103 ± 0.029	0.106 ± 0.023
c_{PI}	0.001 ± 0.057	-0.084 ± 0.045	-0.053 ± 0.035
ch_{PI}	-0.056 ± 0.046	-0.045 ± 0.039	-0.052 ± 0.030
c_{IP}	0.309 ± 0.054	0.197 ± 0.040	0.242 ± 0.033

Table 4.1: Fitted parameters and 95% confidence intervals of the Pacific-Indian Ocean coupled model in [month^{-1}]. The upper row gives the time periods of observational data used for the fits.

c_{PI} and c_{IP} are different within the 95% confidence level for the 1950-1975 and 1976-2001 time periods, suggesting that the coupling of Indian Ocean SSTA on ENSO became weaker, while the feedback from the Indian Ocean on ENSO became stronger. It should be considered however, that the data quality for 1950-1975 has to be questioned, especially since no satellite data was available at that time. Besides, as mentioned in section 1.2 the significance levels might be somewhat underestimated. The strong coupling of equatorial Indian Ocean SSTA on Niño3 SSTA is in agreement with previous studies. Concerning the feedback of Indian Ocean SSTA on ENSO we find that a warm (cold) Indian Ocean causes a cooling (warming) in the eastern Pacific and a shallowing (deepening) of the equatorial averaged thermocline in the Pacific. A possible explanation are easterly (westerly) wind anomalies over the western equatorial Pacific and Indonesia, caused by a warm (cold) Indian Ocean SST, which can be found using partial correlation analysis. This wind anomaly could cause an upwelling (downwelling) in the western-central Pacific, which in turn causes a shallowing (deepening) of the averaged Pacific thermocline depth and a cooling (warming) in the eastern Pacific due to Kelvin wave propagation. This is speculative at this point but should be subject to further research.

To estimate the importance of the feedback of the Indian Ocean on ENSO to explain the observed cross-correlation, an alternative model is fitted to observational data that is similar to (4.1) except that no feedback of the Indian Ocean on the Pacific is included. The parameters fitted to 1950-2001 observational data are $\gamma_P = 0.040 \pm 0.011$, $\omega_P = 0.133 \pm 0.022$, $\gamma_I = 0.136 \pm 0.022$ and $c_{IP} = 0.25 \pm 0.04$.

Both models are integrated using the fitted parameters (for 1950-2001) and stochastic excitation. The noise forcings are fitted to mimic the total variance of SSTAs and thermocline depth. For the fully coupled model with feedback from the Indian Ocean on ENSO, they are chosen to meet $\sigma_{hp} = 0.6 \cdot \sigma_P$, $\sigma_I = 1.8 \cdot \sigma_P$ and the correlation

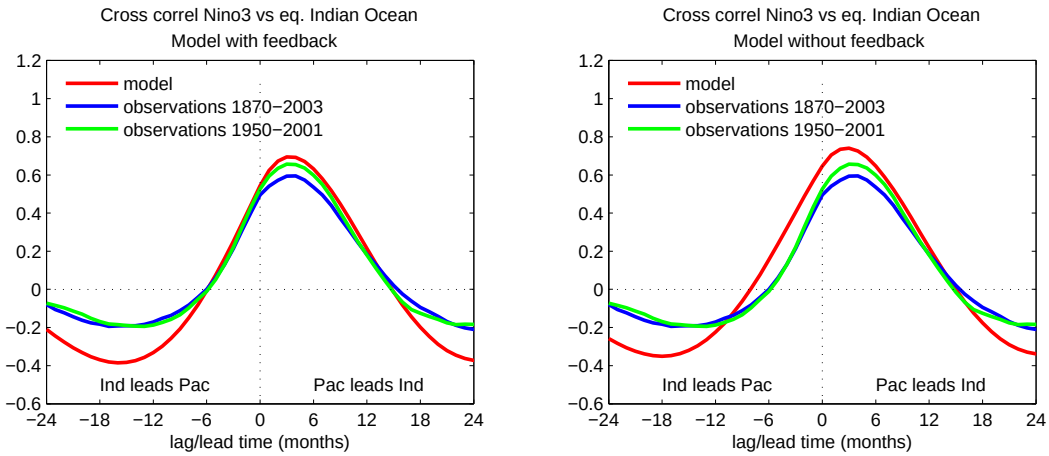

Figure 4.1: Left: Cross correlation between Niño3 SSTA and equatorial Indian Ocean SSTA for the Pacific-Indian Ocean coupled model (red) compared to observational SST data from the period 1870-2003 (blue) and 1950-2001 (green). Correlations above 0.27 (0.17) are significant at the 95% level, assuming 52 (134) degrees of freedom. Right: The same for the model without a feedback from the Indian Ocean on ENSO (The parameters for the two models are fitted separately).

between ξ_P and ξ_h is 0.5. For the model without feedback, they meet $\sigma_{hp} = 0.6 \cdot \sigma_P$, $\sigma_I = 1.45 \cdot \sigma_P$ and the correlation between ξ_P and ξ_h is 0.2. For simplicity ξ_{T_I} is assumed to be independent of the Pacific noise forcings. It should be noted that since the equations are written for normalized variables, the stronger noise forcings of Indian Ocean SSTA compared to Niño3 SSTA denote a higher signal-to-noise ratio in the Pacific, which is due to the fact that the major part of the Pacific SST variability is explained by the ENSO dynamics that are explicitly contained in the model.

Figure 4.1 shows the cross-correlation between Niño3 and EqInd SSTA for the two different models, resulting from $3 \cdot 10^4$ year model runs, compared to the observed cross-correlation. The cross-correlation of the fully coupled model fits well with observations, except for a little overestimation of the correlations especially with Indian Ocean SSTA leading Pacific SSTA. This is connected to the too regular behaviour of ENSO in this model. If a model without an Indian Ocean feedback on ENSO is fitted to observational data, it does not resemble the observed cross-correlation as well as the model with an Indian Ocean feedback, particularly with regard to the phase. But a negative cross-correlation with Indian Ocean SSTA leading Niño3 SSTA by about one or two years is also found in the model without a feedback from the Indian Ocean. This indicates that simple lagged correlation analysis or composite analysis as performed by Kug and Kang (2006) have to be interpreted carefully, since a lagged correlation with Indian Ocean SSTA leading Ninõ3 SSTA might as well exist in absence of a feedback.

The power spectral density of the coupled toy model given by equations (4.1) can be

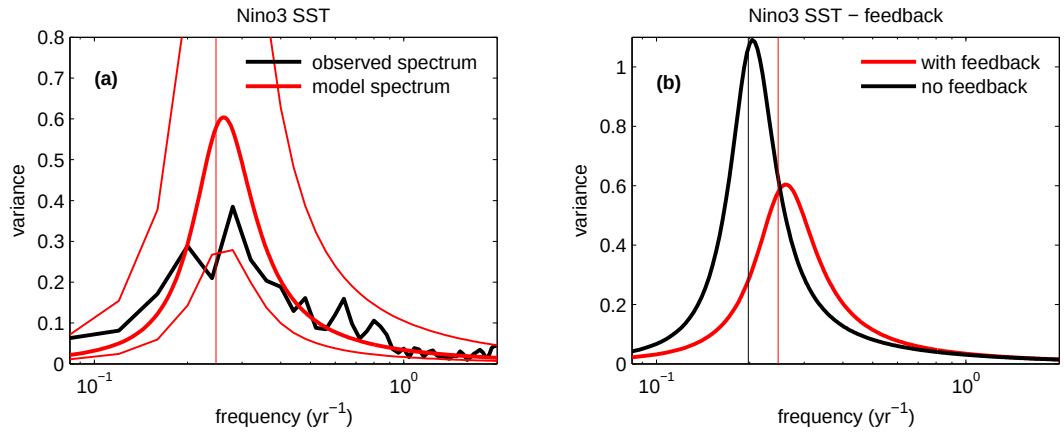

Figure 4.2: a) Niño3 SSTA spectrum of the Pacific-Indian Ocean coupled model (red) compared to HADISST observational data from 1870 to 2003 (black). The thin red lines show the 95% confidence interval. **b)** Model spectrum (red) compared to the spectrum of the same model, but with the feedback parameters c_{PI} and ch_{PI} set to zero (black). The thin vertical lines denote the eigenfrequencies, which are 48.5 month^{-1} for the fully coupled model and 60.5 month^{-1} if the feedback is switched off. (Plotted is frequency times power spectral density.)

calculated analytically.[1] It is found that if ξ_I is independent of the Pacific forcing and ξ_T and ξ_h are correlated in phase, the spectrum is independent of this correlation and can be written as:

$$P_{T_P T_P}(\omega) = \frac{\omega^2 (P_{\xi_P \xi_P} + c_{PI}^2 \frac{P_{\xi_I \xi_I}}{\omega^2 + 4\gamma_I^2}) + \omega_0^2 (P_{\xi_h \xi_h} + ch_{PI}^2 \frac{P_{\xi_I \xi_I}}{\omega^2 + 4\gamma_I^2})}{\left(\omega^2 - \omega_0^2 + \frac{\omega^2 c_{IP} c_{PI} + 2\gamma_I \omega_0 c_{IP} ch_{PI}}{\omega^2 + 4\gamma_I^2}\right)^2 + \left(2\gamma_P + \frac{\omega_0 ch_{PI} c_{IP} - 2\gamma_I c_{PI} c_{IP}}{\omega^2 + 4\gamma_I^2}\right)^2 \omega^2} \quad (4.2)$$

If white noise forcing is assumed, $P_{\xi_P \xi_P}$, $P_{\xi_h \xi_h}$ and $P_{\xi_I \xi_I}$ are constants. The spectrum of the simplest recharge oscillator is retained if the feedback parameters ch_{PI} and c_{PI} are set to zero. One can see that the feedback of the Indian Ocean acts as an additional red noise forcing on SST and thermocline depth proportional to c_{PI} and ch_{PI}, respectively. Independent from the nature of the forcing, the spectrum contains additional terms proportional to the product of the coupling and feedback parameters, $c_{IP} c_{PI}$ or $c_{IP} ch_{PI}$.

Figure 4.2 a) shows the spectrum compared to the observed Niño3 SST spectrum, calculated from 1870-2003 HADISST data. As for the model without feedback, discussed in section 2.3, it is in general agreement with observations, except for a tendency to a somewhat too pronounced peak and therefore a too regular behaviour in the model, which was already mentioned above.

[1] Regard appendix C for a cautionary note on the definition of spectra for processes continuous in time.

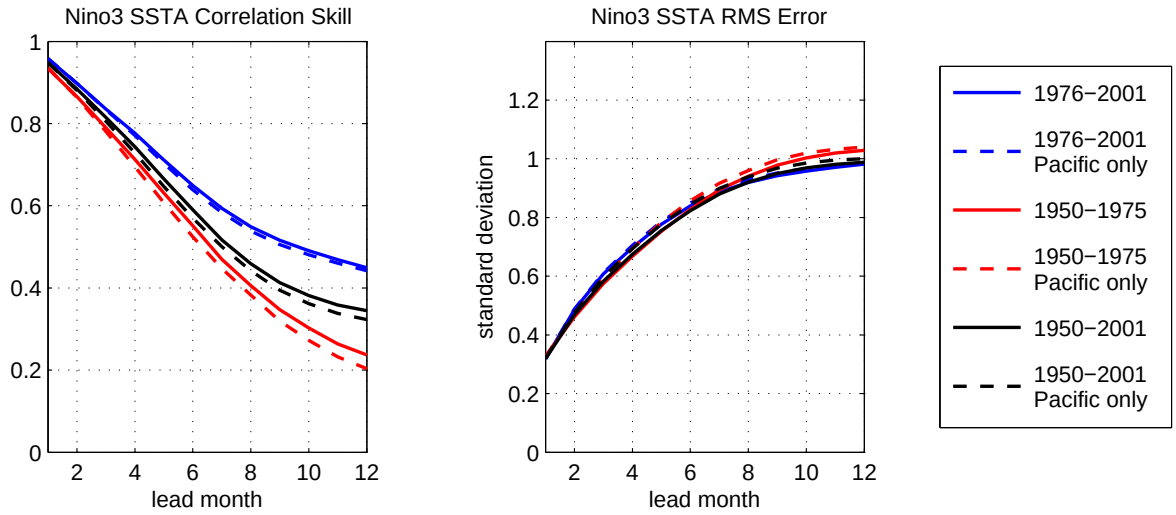

Figure 4.3: Forecast skill of the Pacific-Indian Ocean coupled model (solid lines), compared to the simplest recharge oscillator ENSO model, without explicit consideration of the Indian Ocean (dashed lines). The coloured lines show cross-validated forecast skills. The time intervals given in the legend refer to the period used for the forecast skill evaluation, while in each case the other interval was used to fit the parameters. For the black lines the whole time period was used for the parameter fit and for the evaluation of forecast skill. Left: Anomaly correlation between predictions and observations. Right: rms-error of predictitions in units of one standard deviation.

Figure 4.2 b) shows the influence of the Indian Ocean feedback on ENSO. If the feedback parameters are set to zero (which is equal to fixing Indian Ocean SSTA) the peak frequency shifts to lower frequencies and the variability is increased (the eigenfrequency shifts from $48.5\,month^{-1}$ to $60.5\,month^{-1}$ and the total variance is increased by 42%).

The above may arise hope that including the Indian Ocean in ENSO forecast models might improve ENSO predictions. Figure 4.3 shows that this is not the case. The forecast skill for Niño3 SSTA predictions of the coupled model is hardly better than the forecast skill of the simplest recharge oscillator model without a feedback of the Indian Ocean.

4.4 Atlantic Ocean-ENSO Interaction

Analog to the previous section, the coupled model described by equation (4.1) is now used to describe the interaction between the Atlantic Ocean and ENSO. The model parameters are fitted to 1950-2002 Atl3[2] and Niño3 SSTA data and 20^o isotherm depth data averaged over $120^oE - 80^oW, 5^oS - 5^oN$ for h. The data and fitting methods are described in chapter 1. The resulting parameters and estimated 95% confidence intervals using the whole time period 1950-2001 as well as for the time periods 1950-1975 and 1976-2001 are given in table 4.2

	1950-1975	1976-2001	1950-2001
γ_P	0.055 ± 0.025	0.033 ± 0.018	0.040 ± 0.015
γ_A	0.084 ± 0.022	0.067 ± 0.020	0.073 ± 0.015
ω	0.135 ± 0.033	0.128 ± 0.027	0.131 ± 0.021
c_{PA}	-0.001 ± 0.043	-0.043 ± 0.041	-0.025 ± 0.029
ch_{PA}	-0.037 ± 0.043	-0.017 ± 0.040	-0.028 ± 0.029
c_{AP}	0.054 ± 0.048	0.020 ± 0.037	0.030 ± 0.029

Table 4.2: Fitted parameters and 95% confidence intervals of the Pacific-Atlantic Ocean coupled model in [month^{-1}]. The upper row gives the time periods of observational data used for the fits.

All parameters are similar for the different time periods within the 95% confidence level, suggesting that the underlying processes can be assumed to be stationary. Focussing on the parameters describing the interaction between the two oceans, one finds weaker interactions than between Indian Ocean and Pacific. Especially the coupling of Atl3 SSTA on Niño3 SSTA (c_{AP}) is much weaker than the coupling of the Indian Ocean on ENSO. However, it is significantly different from zero, with an El Niño (La Niña) event causing a warming (cooling) in the Atl3 region. Concerning the feedback of Atlantic Ocean SSTA on ENSO we find that a warm (cold) Atlantic causes a cooling (warming) in the Niño3 region and a shallowing (deepening) of the equatorial averaged thermocline in the Pacific, similar to the feedback of the Indian Ocean on ENSO. Both feedback parameters are different from zero on a significance level of 90%.

A possible explanation are weakened (enhanced) easterlies in the eastern Pacific basin in response to a warm (cold) equatorial Atlantic, which can be identified using partial correlation analysis. This could produce upwelling (downwelling) Kelvin waves in the central basin, responsible for a cooling (warming) of SST in the Niño3 region. But this is speculation at this point and should be subject of further research.

[2]The qualitative results presented in the following are similar if a strip over the whole equatorial Atlantic is chosen instead of Atl3.

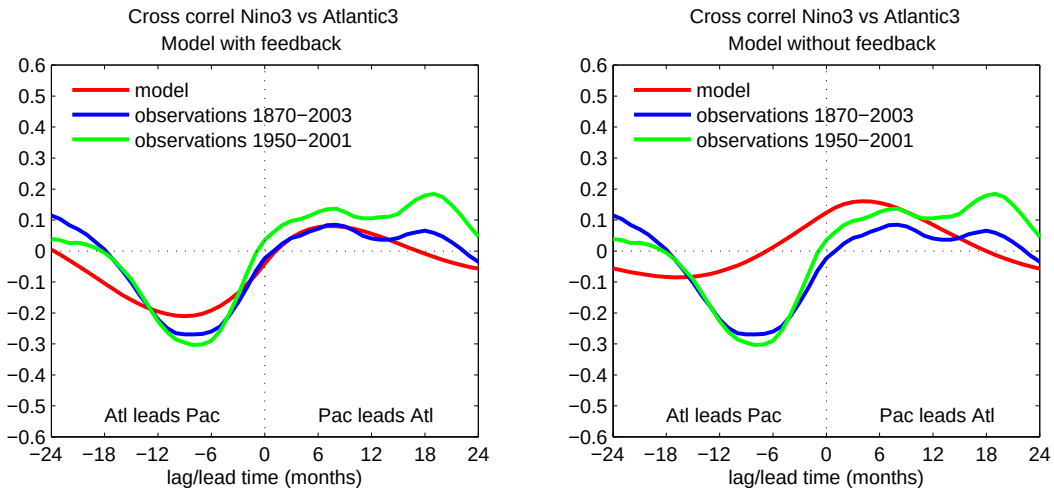

Figure 4.4: As figure 4.1 but for Niño3 SSTA and Atl3 SSTA.

As in the previous section, to estimate the importance of the feedback of the Atlantic on the Pacific, an alternative model is fitted to observational data that is similar to (4.1) except that no feedback is included. The fitted parameters are $\gamma_P = 0.040 \pm 0.011$, $\omega_P = 0.133 \pm 0.022$, $\gamma_A = 0.073 \pm 0.020$ and $c_{AP} = 0.037 \pm 0.040$.

Both models are integrated using the fitted parameters and stochastic excitation. The variance and correlation of the noise forcings are chosen to meet $\sigma_{\xi_{h_p}} = 0.6 \cdot \sigma_{\xi_{T_P}}$ and the correlation between ξ_{T_P} and ξ_{T_h} is 0.2. For the model with feedback $\sigma_{\xi_{T_A}} = 1.65 \cdot \sigma_{\xi T_P}$, while for the model without feedback $\sigma_{\xi_{T_A}} = 1.6 \cdot \sigma_{\xi T_P}$.

Figure 4.4 shows the cross-correlation of the two different models, resulting from $3 \cdot 10^4$ year model runs, compared to the observed cross-correlation. The cross-correlation of the model with feedback is in general agreement with observations, except for a significant positive correlation with Niño3 SSTA leading Atlantic SSTA by about 18 months which is found in the 1950-2001 observational data which is actually used for the parameter fit and is not reproduced by the model. However, this correlation does not exist in the older observational data, either. The model correlation indeed fits better to the observational cross-correlation calculated from the maximum available timeseries than to the shorter period used for the parameter fits. This might seem contra-intuitive at first glance but is reasonable if the model is assumed to be correct and the underlying physics are assumed to be stationary, since the the cross-correlation calculated from the shorter time series is simply more noisy then. In both, model and observational SSTA data, maximum correlation is found with positive (negative) Atl3 SSTA leading negative (positive) Niño3 SSTA. This lead-correlation, which was already mentioned by Keenlyside and Latif (2007), is not reproduced by the model without a feedback from the Atlantic on ENSO and raises hope for an improvement of ENSO predictions by including equatorial Atlantic

SSTA.

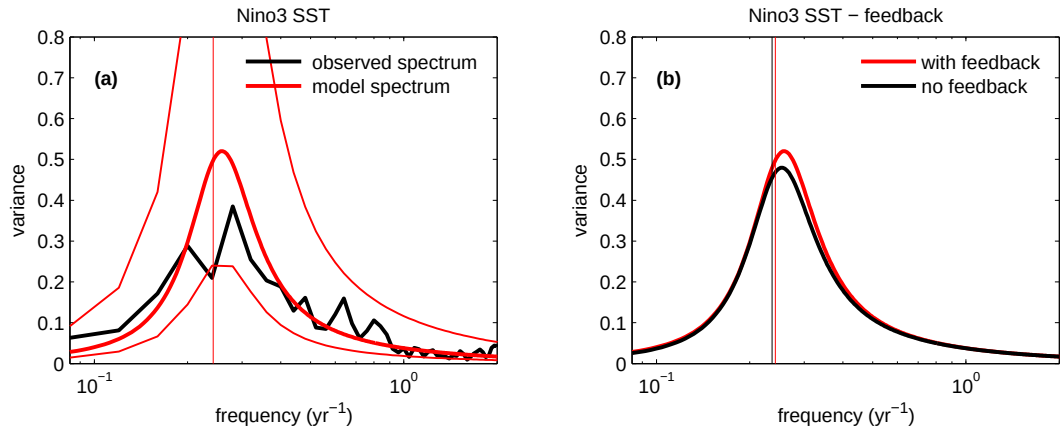

Figure 4.5: As figure 4.2 but for the Pacific-Atlantic model. (The eigenfrequencies are $49.5\,month^{-1}$ for the fully coupled model and $51\,month^{-1}$ if the feedback is switched off.)

Figure 4.5 a) shows the spectrum calculated from equation (4.2) with the parameters fitted for the Pacific-Atlantic coupled model, compared to the observed Niño3 SST spectrum, calculated from 1870-2003 HADISST data. As for the Pacific-Indian Ocean model and the Pacific only model (not shown), the model spectrum generally fits to observations. Figure 4.5 b) shows the influence of the Atlantic Ocean feedback on ENSO. Compared to the influence of the Indian Ocean feedback, the influence of the Atlantic Ocean feedback on ENSO variability is small. If the feedback is switched off (which means here that ch_{PA} and c_{PA} are set to zero) the total variance is reduced by 6% while the peak frequency (like the eigenfrequency) hardly changes at all. This result can be inferred from equation (4.2), remembering that, except for its relevance as an additional red noise forcing proportional to ch_{PA} and c_{PA}, the influence of the feedback on the Niño3 SST spectrum is proportional to $c_{AP}ch_{PA}$ and $c_{AP}c_{PA}$. While the feedback of the Atlantic Ocean on ENSO is smaller than the feedback of the Indian Ocean by "only" a factor of 2 , the coupling of the Atlantic Ocean on ENSO c_{AP} is at least by a factor of 4 smaller than the coupling of the Indian Ocean on ENSO, making the relevant products at least by a factor of 8 smaller than for the Indian Ocean-ENSO interactions.

Still, it has been found that some feedback from the Atlantic Ocean SSTA on ENSO exists. And unlike the Indian Ocean, the Atlantic SSTA itself is relatively independent from ENSO. Therefore, ENSO forecasts might be improved if the Atlantic Ocean is explicitely considered. Figure 4.6 compares the forecast skill of the coupled model to the forecast skill of the simplest recharge oscillator model without a feedback from ENSO. Even though the difference is small, some improvement is found for both cross-validated time periods on all lead times.

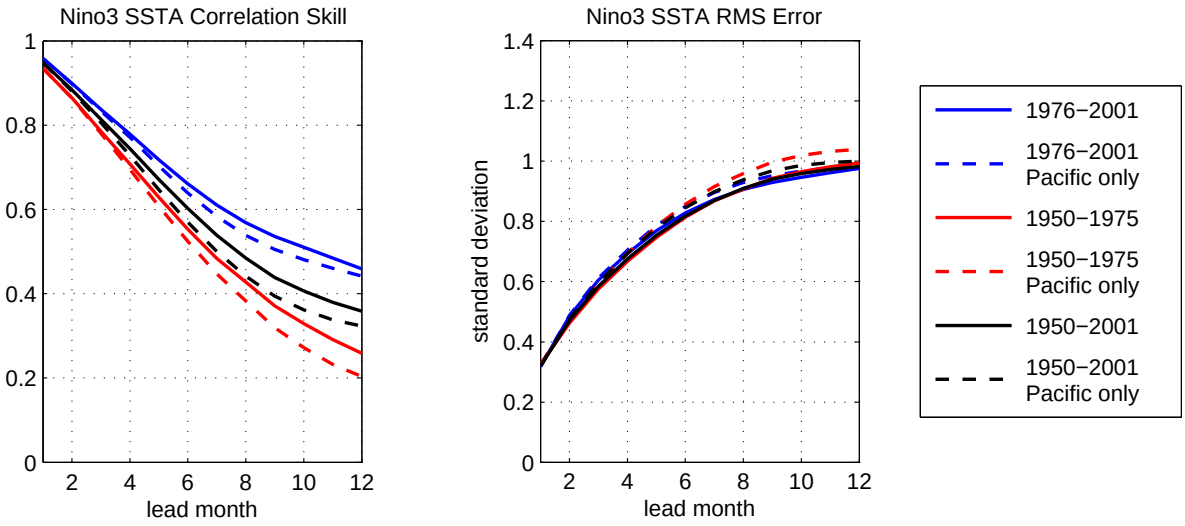

Figure 4.6: As figure 4.3 but for the Pacific-Atlantic coupled model.

4.5 A Coupled Model for the Interaction of All Tropical Oceans

Finally, a model containing all three tropical Oceans and allowing for interactions between all of them is proposed. The Pacific is again described by the simplest recharge oscillator model while Atlantic and Indian Ocean are described by red noise processes. The fully coupled model with stochastic excitation can be written as:

$$\begin{aligned}
\tfrac{d}{dt}T_P &= \omega_0 h_P - 2\gamma_P T_P + c_{PI}T_I + c_{PA}T_A \quad + \xi_P \\
\tfrac{d}{dt}h_P &= -\omega_0 T_P + ch_{PI}T_I + ch_{PA}T_A \quad + \xi_h \\
\tfrac{d}{dt}T_I &= -2\gamma_I T_I + c_{IP}T_P + c_{IA}T_A \quad + \xi_I \\
\tfrac{d}{dt}T_A &= -2\gamma_A T_A + c_{AP}T_P + c_{AI}T_I \quad + \xi_A
\end{aligned} \tag{4.3}$$

The parameters of (4.3) are fitted to EqInd, Atl3 and Niño3 SSTA data and 20^o isotherm depth data averaged over $120^oE - 80^oW, 5^oS - 5^oN$ for T_I,T_A,T_P and h_P, respectively. The data and fitting methods are described in chapter 1. The resulting parameters and estimated 95% confidence intervals for fits to 1950-2001 data as well as for the periods 1950-1975 and 1976-2001 are given in table 4.3.

All parameters except for c_{IA} are similar for the different time periods within the 95% confidence level, suggesting that the underlying processes can be assumed to be stationary. For c_{IA} the parameter fits suggest an increase of the coupling of the equatorial Indian Ocean on Atlantic SSTA. But since this increase is significant on no

	1950-1975	1976-2001	1950-2001
γ_P	0.051 ± 0.034	0.013 ± 0.025	0.024 ± 0.020
γ_I	0.165 ± 0.029	0.137 ± 0.026	0.147 ± 0.019
γ_A	0.084 ± 0.024	0.067 ± 0.023	0.074 ± 0.016
ω	0.117 ± 0.041	0.118 ± 0.034	0.107 ± 0.026
c_{PI}	0.000 ± 0.065	-0.067 ± 0.054	-0.046 ± 0.041
c_{PA}	-0.004 ± 0.047	-0.022 ± 0.046	-0.017 ± 0.032
ch_{PI}	-0.048 ± 0.047	0.000 ± 0.045	-0.047 ± 0.032
ch_{PA}	-0.026 ± 0.054	-0.015 ± 0.047	-0.016 ± 0.035
c_{IP}	0.306 ± 0.062	0.235 ± 0.049	0.255 ± 0.038
c_{AP}	0.046 ± 0.062	0.020 ± 0.049	0.024 ± 0.038
c_{IA}	0.030 ± 0.047	0.102 ± 0.046	0.070 ± 0.032
c_{AI}	0.012 ± 0.059	0.000 ± 0.051	0.009 ± 0.038

Table 4.3: Fitted parameters and 95% confidence intervals of the fully coupled model for the Tropical Oceans interactions in [month^{-1}]. The upper row gives the time periods of observational data used for the fits.

more than a 95% level, a physical reason cannot necessarily be assumed. Focussing on the parameters fitted for whole time period 1950-2001, the parameters that are also included in the Indian Ocean - ENSO coupled model are found to be little different if the Atlantic is also included. The coupling of the Pacific on Atlantic Ocean SSTA c_{PA} and ch_{PA} on the other hand is found to be smaller in this model compared to the Atlantic Ocean - ENSO model[3]. Moreover, a significant coupling of Indian Ocean on Atlantic SSTA is found, with warm (cold) SSTA in the Atl3 region causing SSTA of the same sign in the Indian Ocean. Considering this, the stronger coupling of the Pacific on Atlantic SSTA found for the model without explicit consideration of the Indian Ocean might be explained by an indirect coupling of the Pacific on Atlantic SSTA via Indian Ocean SSTA. The forecast skill for EqInd SSTA (not shown) cannot be improved by including a feedback from the Atlantic Ocean. This might be explained by the strong damping of Indian Ocean SSTA and the dominating forcing from ENSO. Considering, that the variables in the model are normalized by their standard deviations, the magnitude of the different terms in a model equation are given by the magnitude the corresponding parameters. Comparing the feedback from the Atlantic which is of magnitude $c_{IA} = 0.07$ to the other terms in the Indian Ocean SSTA equation which are of magnitude $\gamma_I = 0.15$ and $c_{IP} = 0.26$ it should have relatively little impact. Finally, it should be noted that, as mentioned in section 1.2, the confidence levels for the fitted parameters might be somewhat underestimated,

[3]It has to be noted, that the same data is used for the parameter fits of all models. Thus differences can be assumed to be significant, even though they lie within the confidence levels of the parameter fits.

which is of particular importance for models containing many parameters, since the numerical fit might become ambiguous and the differences between linear regression, using one timestep per month, and a numerical least-squares fit, using ten timesteps per month, becomes wide.

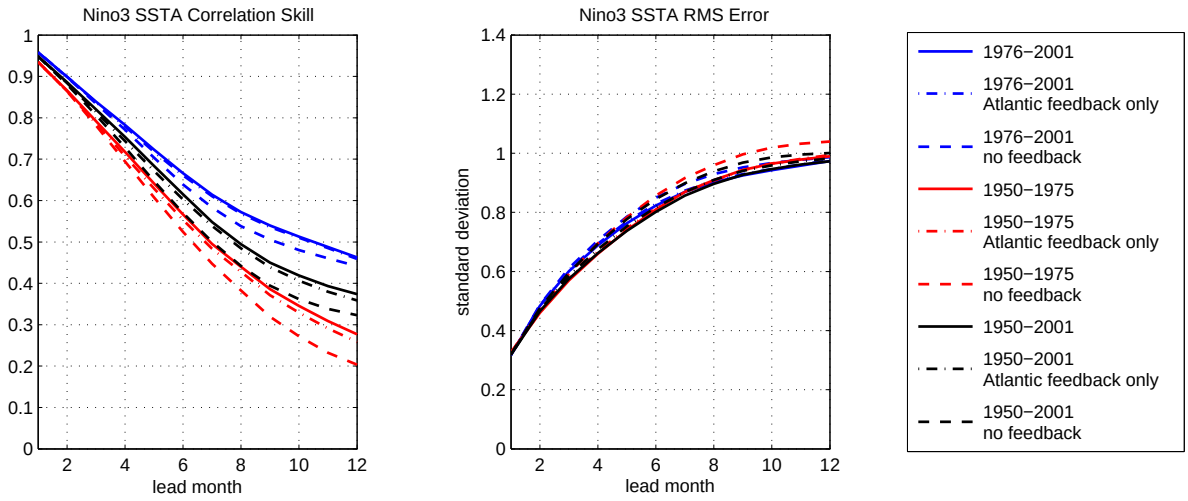

Figure 4.7: As figure 4.3 but for the Pacific-Atlantic-Indian Ocean coupled model compared to the model with a feedback from the Atlantic only and to the simplest recharge oscillator without any feedback from the Atlantic or Indian Ocean.

Figure 4.7 shows the prediction skill of the Pacific-Atlantic-Indian Ocean coupled model compared to the Pacific-Atlantic Ocean only model and to the simplest recharge oscillator without any feedback from the Atlantic or Indian Ocean. The skill of the fully coupled model is hardly better than for the Pacific-Atlantic Ocean coupled model. This was to be expected from the finding of section 4.3, that the explicit consideration of Indian Ocean SSTA does hardly improve the forecast skill for the Pacific.

As in the previous sections, the model is integrated using the fitted parameters and stochastic excitation. The variance and correlation of the noise forcings are chosen to meet $\sigma_{\xi_{h_P}} = 0.5 \cdot \sigma_{\xi_{T_P}}$, $\sigma_{\xi_{T_A}} = \sigma_{\xi_{T_I}} = 1.75 \cdot \sigma_{\xi T_P}$ and the correlation between ξ_{T_P} and ξ_{T_h} is 0.4, while the noise forcings of the different oceans are assumed to be independent, for simplicity. The resulting cross-correlations between SSTA of the different oceans are shown in figure 4.8. The cross-correlations between Niño3 and Atl3 as well as between Niño3 and EqInd are similar to those resulting from the Pacific-Atlantic and Pacific-Indian Ocean coupled models, respectively. The observed small correlation between EqInd and Atl3 is generally reproduced by the model, especially regarding the full 1870-2003 observational timeseries. It reveals a maximum correlation of about

0.2 at zero time lag. The negative correlation with Atl3 leading EqInd SSTA by more than about 8 months is somewhat contra-intuitive considering the positive coupling of the Indian Ocean on Atl3 SSTA c_{IA} in the model. This stresses again that simple lagged correlation analysis has to be interpreted carefully.

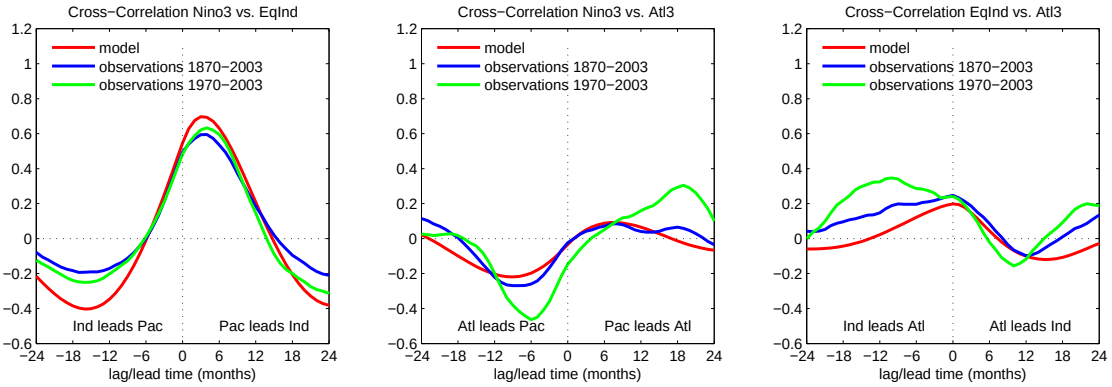

Figure 4.8: Left: Cross correlation between Niño3 and EqInd SSTA for the Pacific-Atlantic-Indian Ocean coupled model (red) compared to observational SST data from the period 1870-2003 (blue) and 1970-2003 (green). Center: Cross correlation between Niño3 and Atl3 SSTA. Right: Cross correlation between EqInd and Atl3 SSTA.

4.6 Summary and Discussion

Concerning the feedback of the Indian Ocean on ENSO, this study suggests that a warm (cold) Indian Ocean causes a cooling (warming) in the eastern Pacific and a shallowing of the equatorial averaged thermocline in the Pacific, presumably due to changes in the Walker circulation. If this feedback is switched off in the simple model proposed here, the ENSO period shifts from about 4 to about 5 years and the total variance of Niño3 SSTA is increased by about 40%. The feedback is in agreement with the results of Wu and Kirtman (2004) and Kug and Kang (2006). The resulting influence of the tropical Indian Ocean on ENSO periodicity is also in agreement with Wu and Kirtman (2004) and with Dommenget et al. (2006). However, while Wu and Kirtman (2004) find an amplifying influence of the Indian Ocean on ENSO variability in their GCM experiments, we find that the Indian Ocean damps ENSO variability, which is in agreement with Dommenget et al. (2006). So, even though the feedback found in this study is in agreement with Wu and Kirtman (2004), controversial results are found for the influence of the Indian Ocean on ENSO variability. To explain these controversial findings, different approximations for the Indian Ocean SST equation in (4.1) shall be regarded in the following.

If Indian Ocean SSTA is assumed to be primarily a slave to ENSO and if its adjustment timescale is short compared to the ENSO period, the Indian Ocean SST

equation can be approximated as

$$T_I \approx \frac{c_{IP}}{2\gamma_I} T_P \tag{4.4}$$

If on the other hand the Indian Ocean adjustment timescale is long compared to the ENSO period, the Indian Ocean SST equation can be approximated as

$$\frac{dT_I}{dt} \approx c_{IP} T_P \tag{4.5}$$

Finally, if the Indian Ocean-atmosphere dynamics are assumed to produce SSTA that are to a first approximation independent of ENSO the Indian Ocean approximately acts as an additional noise forcing and one can write

$$T_I \approx \hat{\xi}_I \tag{4.6}$$

where $\hat{\xi}_I$ is independent of T_P, but not necessarily white noise.

Using any of these approximations, and $d_{tt}T_I \approx -aT_I$ (where a is a positive constant) with approximation (4.5), equations (4.1) can be transformed to a second order differential equation for eastern Pacific SSTA:

$$\frac{d^2T_P}{dt^2} = -\omega_{eff}^2 T_P - 2\gamma_{eff}\frac{dT_P}{dt} + \ \xi_{eff} \tag{4.7}$$

where the eigenfrequency of the undamped system[4] ω_{eff}, the damping time scale γ_{eff} and the forcing ξ_{eff} are given as

$$\omega_{eff}^2 = \omega_0^2 - \frac{\omega_0 ch_{PI} c_{IP}}{2\gamma_I}\,, \quad \gamma_{eff} = \gamma_P - \frac{c_{PI}c_{IP}}{4\gamma_I}\,, \quad \xi_{eff} = \hat{\xi_P} \tag{4.8}$$

for the approximation (4.4),

$$\omega_{eff}^2 = \omega_0^2 - c_{PI}c_{IP}\,, \quad \gamma_{eff} = \gamma_P + \frac{\omega_0 ch_{PI}c_{IP}}{2a}\,, \quad \xi_{eff} = \hat{\xi_P} \tag{4.9}$$

for the approximation (4.5) and

$$\omega_{eff} = \omega_0\,, \quad \gamma_{eff} = \gamma_P\,, \quad \xi_{eff} = \hat{\xi_P} + c_{PI}\frac{d}{dt}\hat{\xi}_I + \omega_0 ch_{PI}\hat{\xi}_I \tag{4.10}$$

for the approximation (4.6). Where $\hat{\xi_P} = \frac{d}{dt}\xi_P + \omega_0\xi_h$ for all three cases.

With $c_{PI} < 0$, $ch_{PI} < 0$ and $c_{IP} > 0$, one can see that if the Indian Ocean is in phase with the Pacific (approximation (4.4)), it is responsible for a frequency shift to higher frequencies and a damping of ENSO variability. If on the other hand the Indian Ocean adjustment timescale is long compared to the ENSO frequency and

[4]The eigenfrequency of the damped system is given as $\omega^2 = \omega_{eff}^2 - \gamma^2$

therefore Indian Ocean SSTA lags Niño3 SSTA by 90^o (approximation (4.5)), the Indian Ocean would still be responsible for an increased ENSO frequency but for a reduced damping and therefore increased ENSO variability. Finally, independent Indian Ocean variability (approximation (4.6)) acts as an additional forcing on the Pacific and will therefore also increase Pacific Ocean variability, without having an influence on the ENSO period.

Observations show a high correlation of Indian Ocean SSTA with Niño3 SSTA with a phase lag that is very small compared to the ENSO frequency. This indicates that approximation (4.4) is justified. Therefore, increased ENSO variability and a longer ENSO period is found if the Indian Ocean is decoupled.

In the GCM used by Wu and Kirtman (2004) on the other hand, the simulated ENSO has a peak frequency of about 2.3 years and from their table 2, it can be deferred that the correlation between Indian Ocean SSTA and Pacific SSTA is smaller than in observations. This probably makes the approximations (4.5) or (4.6) fit better to Indian Ocean-ENSO interactions in the GCM. Both approximations lead to less ENSO varibility if the Indian Ocean is decoupled.

Even though it was shown that the Indian Ocean has a considerable influence on the ENSO cycle, the forecast skill for Niño3 SSTA of the simple models used here could hardly be improved by explicitly including the Indian Ocean feedback. This can be explained by the fact that, at least in this model, Indian Ocean SSTA predictability is primarily limited to the SSTA caused by ENSO. The feedback of ENSO-induced Indian Ocean SSTA back on ENSO, however, is implicitly included if the uncoupled recharge oscillator is fitted to Pacific data. This can also be seen considering approximation (4.4) which shows that the major effect of the Indian Ocean on ENSO is a shift of ENSO frequency and a strengthening of the damping. This is implicitly covered if the recharge oscillator model without an Indian Ocean feedback is fitted to Pacific data only.

The coupling of equatorial Atlantic SSTA on ENSO is found to be much weaker than the coupling of the Indian Ocean on ENSO. However, a significant interaction is found, with an El Niño (La Niña) event causing a warming (cooling) in the Atl3 region. Also a feedback from the equatorial Atlantic on ENSO is found with a warm (cold) Atlantic causing a cooling (warming) in the Niño3 region and a shallowing (deepening) of the equatorial averaged thermocline in the Pacific, which is similar to the feedback of the Indian Ocean on ENSO. However, the ENSO cycle is hardly influenced by this feedback. Solely a small reduction of Niño3 SSTA variability by about 6% is found if the Atlantic Ocean feedback is switched off in the simple model. This is in disagreement with the CGCM results of Dommenget et al. (2006), finding a considerable frequency shift to longer periods if the tropical Atlantic is decoupled, analog to the effect of the Indian Ocean feedback. These results can again be explained considering the approximations (4.4) to(4.6). Since in observational data a very weak coupling of the equatorial Atlantic on Niño3 SSTA is found, compared

to the coupling of the equatorial Indian Ocean on ENSO, the observed situation is well described by approximation (4.6). As shown by equation (4.10) the Atlantic does therefore not influence the eigenfrequency and damping of ENSO. However, the feedback from the Atlantic is responsible for an additional forcing, which increases ENSO variability. This increase is only weak, since the feedback from the Atlantic on ENSO is small. This slight additional noise forcing from the Atlantic is in agreement with the slightly reduced variance that is found if the Atlantic Ocean feedback is switched off. In the CGCM used by Dommenget et al. (2006) on the other hand, the equatorial Atlantic responds to Niño3 SSTA quite similar as the Indian Ocean, with a maximum correlation of about 0.7 with Niño3 SSTA leading Atlantic SSTA by about three months. This justifies approximation (4.4) which explains the frequency shift to longer periods (see equation (4.8)), assuming that a negative feedback on Pacific thermocline depth ($ch_{PA} < 0$), as found in the observations, also exists in the CGCM.

Even though the feedback from the Atlantic Ocean on ENSO is found to be weaker than the Indian Ocean feedback on ENSO, the forecast skill for Niño3 SSTA of the simple models used here could be improved somewhat because Atlantic SSTA itself is more independent from ENSO than Indian Ocean SSTA and might therefore be a more usefull additional predictor.

Finally, a parameter fit of a model containing the Pacific, Atlantic and Indian Oceans to observational data suggests an influence of eastern equatorial Atlantic on equatorial Indian Ocean SSTA. Further, the direct feedback of the Atlantic on ENSO is found to be smaller than in the model not considering the Indian Ocean, suggesting that part of this feedback might be indirect via the Indian Ocean. However, due to the high number of parameters in this model, this results have to be handled with care.

Generally, more research addressing the mechanisms of the interactions between the tropical oceans is necessary to support and explain the results of this study.

Appendix A

Eigenvalues of Differential Equations

A linear homogeneous ordinary differential equation (ODE) with constant coefficients be given as

$$y^{(n)}(x) = \sum_{k=0}^{n-1} a_k y^{(k)}(x) \tag{A.1}$$

with $y : \mathbb{R} \to \mathbb{C}$, $a_k \in \mathbb{C}$ and $y^{(k)}$ denoting the k'th derivative.

Defining $y_k := y^{(k-1)}$ for $k = 1..n$ this can be transformed to a system of first order ODEs

$$\underline{y}'(x) = \underline{\underline{A}}\,\underline{y}(x) \quad \text{with} \quad \underline{y} : \mathbb{R} \to \mathbb{C}^n \quad \text{and} \quad \underline{\underline{A}} \in \mathbb{C}^n \times \mathbb{C}^n \tag{A.2}$$

It is therefore apparent that every system of ODEs of the form (A.1) can as well be transformed to a system of first order ODEs of the form (A.2).

It can easily be verified that for all eigenvalues λ_i and corresponding eigenvectors $\underline{v}_i$ of $\underline{\underline{A}}$, solutions of (A.2) are given by

$$\underline{y}(t) = \underline{v}_i \exp(\lambda_i x) \; . \tag{A.3}$$

In climate sciences λ_i and $\underline{v}_i$ are thus commonly referred to as eigenvalues and eigenvectors or eigenmodes of the differential equation (A.2).

If $\underline{\underline{A}}$ is diagonalizable, the solutions (A.3) represent a fundamental system, which means that the solutions constitute a base for the solution space. If this is not the case, additional solutions can be found which becomes a little more complicated. However, since this does not happen to be the case in the examples of this study, it is not discussed in further detail here.

It should be added that, after discretizing in space, linear homogeneous systems of partial differential equations, such as linear reduced gravity models, can as well be transformed to ODEs of the form A.2. The eigenmodes then correspond to spatial patterns of the variables contained in the model.

Appendix B

A Correction to Jin (1997)

Jin (1997) proposes estimates for the parameters of the recharge oscillator model given by equation (2.8). The parameter γ is chosen "to give an SST change rate of 1.5^{o}C over 2 months (which is the upwelling timescale) per 10 m of thermocline depth anomaly over the eastern Pacific." This means $\gamma = 0.075 \frac{K}{m\,month}$. The parameters are nondimensionalized by scales of $[h]$=150 m, $[T]$=7.5 K and $[t]$=2 months. The corresponding nondimensional value of γ would be γ=3. Though, for the following discussion Jin (1997) uses the nondimensional value γ=0.75. Using $\gamma = 3$ without changing any other parameters would alter the discussion dramatically. In the eigenvalues of the system, however, γ occurs only in a product with the air sea coupling parameter $b = \mu\, b_0$, which is varied for his discussion via the so-called relative coupling coefficient μ. So a big part of the discussion would be unaltered if the tuning parameter was chosen by a factor 4 smaller. The high end estimation of b_0, on the other hand is meant to be physically motivated as well.

Concluding, even though the qualitative relevance of the paper is unaltered by this mistake, the quantitative results have to be handled with care.

Appendix C

The Power Spectral Density of a Random Process Continuous in Time

In climate science one usually only deals with discrete time series. However for theoretical studies it sometimes interesting to calculate spectra of random processes which are continuous in time. The aim is to find the power spectral density of the variables determined by a linear model of the following form

$$\frac{dx_k(t)}{dt} = \sum_{l=1}^{N} a_{kl} x_l(t) + \xi_k(t) \quad , \quad k = 1..N \tag{C.1}$$

with real coefficients a_{kl} and white noise forcing $\xi(t)$. Jin (1997) defines the power spectral density of such a process as the ensemble mean of the squared Fourier transform of the time series:

$$\left\langle |\tilde{x}_k(\omega)|^2 \right\rangle \quad \text{where} \quad \tilde{x}_k(\omega) = \int_{-\infty}^{\infty} x_k(t) \exp(-i\omega t) dt \tag{C.2}$$

and $\langle\rangle$ denotes the ensemble mean. However, the Fourier transform $\tilde{x}_k(\omega)$ is well defined only if $\int_{-\infty}^{\infty} |x_k(t)|\, dt < \infty$ which is generally not the case here. Indeed, the integral in (C.2) would diverge for all processes considered in this study.

Instead, defining

$$x_k^T(t) = \begin{cases} x_k(t) & for \ -\frac{T}{2} < t < \frac{T}{2} \\ 0 & else \end{cases} \quad , \tag{C.3}$$

the power spectral density can be defined as:

$$P_{xx}(\omega) = \lim_{T\to\infty}\left(\frac{\left\langle \left|\tilde{x}^T(\omega)\right|^2 \right\rangle}{T}\right) \tag{C.4}$$

with

$$\tilde{x}^T(\omega) = \int_{-\frac{T}{2}}^{\frac{T}{2}} x(t)\exp(-i\omega t)dt = \int_{-\infty}^{\infty} x^T(t)\exp(-i\omega t)dt\ . \tag{C.5}$$

According to the Wiener-Khinchin Theorem as proven in Couch (2001) this definition of the spectrum is equal to the Fourier transform of the auto-correlation function.

Defining ξ_k^T analog to x_k^T and using (C.1) we get:

$$\frac{dx_k^T(t)}{dt} = \sum_{l=1}^{N} a_{kl}x_l^T(t) + \xi_k^T(t) \quad , \quad k = 1,..N \qquad \forall\, t : |t| \neq \tfrac{T}{2}\ . \tag{C.6}$$

With $x_k^T(t) = \frac{1}{2\pi}\int_{-\infty}^{\infty}\tilde{x}_k^T(\omega)\exp(i\omega t)d\omega$[1] one obtains

$$\int_{-\infty}^{\infty} i\omega\tilde{x}_k^T\exp(i\omega t)d\omega = \int_{-\infty}^{\infty}\left(\sum_{l=1}^{N} a_{kl}\tilde{x}_l^T + \tilde{\xi}_k^T\right)\exp(i\omega t)d\omega \quad , \quad k = 1,..N\ . \tag{C.7}$$

This is true if and only if

$$i\omega\tilde{x}_k^T = \sum_{l=1}^{N} a_{kl}\tilde{x}_l^T + \tilde{\xi}_k^T \quad , \quad k = 1,..N\ . \tag{C.8}$$

This can be solved to get

$$\tilde{x}_k^T(\omega) = \sum_{l=1}^{N} c_{kl}(\omega)\tilde{\xi}_l^T(\omega) \quad , \quad k = 1,..N \tag{C.9}$$

with complex functions $c_{kl}(\omega)$. Using this result one can calculate the spectra by multiplying (C.9) with its complex conjugate dividing by T and taking the ensemble mean and the limit $t \to \infty$.

[1] Strictly speaking, this as well as the following equalities have to be understood between elements of the L^1 space, which means, that functions are identified if they are equal outside of a set of measure 0.

With the cross-spectral density defined similar to the power spectral density as $P_{xy} = \lim_{T\to\infty}\left(\frac{\langle \tilde{x}^T \tilde{y}^{T*}\rangle}{T}\right)$ the power spectral densities are given as

$$P_{x_k x_k} = \sum_{l=l}^{N}\sum_{m=1}^{N} c_{kl}c_{km}P_{\xi_l\xi_m} \quad , \quad k = 1,..N \; . \tag{C.10}$$

Thus the spectra can be written as linear combinations of the spectra and cross spectra of the noise forcings.

Note, that a white noise process continuous in time would always have infinite variance, since it has a constant power spectral density by definition and the total variance is given by the integral over the power spectrum. Any physically reasonable process is "white" only up to a certain frequency. But, since the high frequency end of the spectra examined in this study is generally damped proportional to $\frac{1}{\omega^2}$, we are only interested in the power spectral densities of the noise forcings in the low frequency range which are assumed to be constant.

List of Figures

List of Tables

Bibliography

Baquero-Bernal, A., M. Latif, and S. Legutke, 2002: On dipolelike variability of sea surface temperature in the tropical Indian Ocean. *J. Climate*, **15 (11)**, 1358–1368.

Battisti, D. S. and A. C. Hirst, 1989: Interannual variability in a tropical atmosphere-ocean model: influence of the basic state, ocean geometry and nonlinearity. *J. Atmos. Sci.*, **46 (12)**, 1687–1712.

Behera, S. K., S. A. Raoa, H. N. Saji, and T. Yamagata, 2003: Comments on "A cautionary note on the interpretation of EOFs". *J. Climate*, **16**, 1087–1093.

Bjerknes, J., 1964: Atlantic Air-Sea Interaction. *Adv. Geophys.*, **10**, 1–82.

Burgers, G., F.-F. Jin, and G. J. van Oldenborgh, 2005: The simplest ENSO recharge oscillator. *Geophys. Res. Lett.*, **32**, L13 706, doi:10.1029/2005GL022951.

Chang, P., T. Yamagata, P. Schopf, S. K. Behera, J. Carton, W. S. Keesler, G. Meyers, T. Qu, F. Schott, S. Shetye, and S.-P. Xie, 2006: Climate fluctuations of tropical coupled systems - The role of ocean dynamics. *J. Climate*, **19 (20)**, 5122–5174.

Couch, L. W., 2001: *Digital and Analog Communications Systems*. 6th ed., Prentice Hall.

Dommenget, D. and M. Latif, 2002: A cautionary note on the interpretation of EOFs. *J. Climate*, **15**, 216–225.

———, 2003: Reply. *J. Climate*, **16**, 1094–1097.

Dommenget, D., V. Semenov, and M. Latif, 2006: Impacts of the tropical Indian and Atlantic Oceans on ENSO. *Geophys. Res. Lett.*, **33**, L11 701, doi: 10.1029/2006GL025871.

Dommenget, D. and D. Stammer, 2004: Assessing ENSO simulations and predictions using adjoint ocean state estimation. *J. Climate*, **17 (22)**, 4301–4315.

Enfield, D. B. and D. A. Mayer, 1997: Tropical Atlantic sea surface temperature variability and its relation to El Niño-Southern Oscillation. *J. Geophys. Res.*, **102**, 929–945.

Hasselmann, K., 1976: Stochastic climate models, Part I, Theory. *Tellus*, **28**, 473.

Huang, B., 2004: Remotely forced variability in the tropical Atlantic ocean. *Climate Dyn.*, **23**, 133–152.

Jin, F., J. Neelin, and M. Ghil, 1996: El Nino Southern Oscillation and the annual cycle: Subharmonic frequency-locking and aperiodicity. *Physica D*, **98**, 442–465.

Jin, F.-F., 1997: An equatorial recharge paradigm for ENSO, Part 1: Conceptual model. *J. Atmos. Sci.*, **54**, 811–829.

Jin, F.-F., L. Lin, A. Timmermann, and J. Zhao, 2007: Ensemble-mean dynamics of the ENSO recharge oscillator under state-dependent stochastic forcing. *Geophys. Res. Lett.*, **43**, L03 807, doi:10.1029/2006GL027372.

Keenlyside, N. S. and M. Latif, 2007: Understanding equatorial Atlantic interannual variability. *J. Climate*, **20**, 131–142.

Kug, J.-S. and I.-S. Kang, 2006: Interactive feedback between ENSO and the Indian Ocean. *J. Climate*, **19 (9)**, 1784–1801.

Latif, M. and T. P. Barnett, 1995: Interactions of the tropical oceans. *J. Climate*, **8**, 952–964.

Latif, M. and A. Grötzner, 2000: The equatorial Atlantic oscillation and its response to ENSO. *Climate Dyn.*, **16**, 213–218.

Levitus, S., R. Burgett, and T. P. Boyer, 1994: *World Ocean Atlas, 1994*, Salinity, NOAA Atlas NESDIS 3, Vol. 3. Natl. Oceanogr. Data Cent., Sliver Springs, Md., 111 pp.

Marsland, S., H. Haak, J. Jungclaus, and M. Latif, 2003: The Max-Planck-Institute global ocean/sea ice model with orthogonal curvilinear coordinates. *Ocean Model.*, 91–127.

McPhaden, M., 2003: Tropical Pacific Ocean heat content variations and ENSO persistence barriers. *Geophys. Res. Lett.*, **30 (9)**, 1480, doi:10.1029/2003GL016872.

Meinen, C. S. and M. J. McPhaden, 2000: Observations of Warm Water Volume Changes in the Equatorial Pacific and Their Relationship to El Niño and La Niña. *J. Climate*, **13**, 3551–3559.

Neelin, J. D., D. S. Battisti, A. C. Hirst, F.-F. Jin, Y. Wakata, T. Yamagata, and S. E. Zebiak, 1998: ENSO theory. *J. Geophys. Res.*, **103**, 14 261–14 290.

Penland, C. and P. D. Sardeshmukh, 1995: The optimal growth of tropical sea surface anomalies. *J. Climate*, **8 (8)**, 1999–2024.

Rayner, N. A., D. E. Parker, E. B. Horton, C. K. Folland, L. V. Alexander, D. P. Rowell, E. C. Kent, and A. Kaplan, 2003: Global analyses of sea surface temperature, sea ice, and night marine air temperature since the late nineteenth century. *J. Geophys. Res.*, **108 (D14)**, 4407, doi:10.1029/2002JD002670.

Ruiz-Barradas, A., J. A. Carton, and S. Nigam, 2000: Structure of interannual-to-decadal climate variability in the tropical Atlantic sector. *J. Climate*, **13**, 3285–3297.

Saji, N., B. Goswami, P. Vinayachandran, and T. Yamagata, 1999: A dipole mode in the tropical Indian Ocean. *Nature*, **401 (6751)**, 360–363.

Saravanan, R. and P. Chang, 2000: Interaction between tropical Atlantic variability and El Niño-Southern Oscillation. *J. Climate*, **13**, 2177–2194.

Schopf, P. S. and R. J. Burgman, 2006: A simple mechanism for ENSO residuals and asymmetry. *J. Climate*, **19 (13)**, 3167–3179.

Suarez, M. J. and P. S. Schopf, 1988: A delayed action oscillator for ENSO. *J. Atmos. Sci.*, **45 (21)**, 3283–3287.

Venzke, S., M. Latif, and A. Villwock, 2000: The coupled GCM Echo-2. Part II: Indian Ocean response to ENSO. *J. Climate*, **13 (8)**, 1371–1383.

von Storch, H. and F. W. Zwiers, 1999: *Statistical Analysis in Climate Research*. Cambridge University Press.

Webster, P., A. Moore, J. Loschnigg, and R. Leben, 1999: Coupled ocean-atmosphere dynamics in the Indian Ocean during 1997-98. *Nature*, **401 (6751)**, 356–360.

Wu, R. and B. P. Kirtman, 2004: Understanding the impacts of the Indian Ocean on ENSO variability in a coupled GCM. *J. Climate*, **17 (20)**, 4019–4031.

Xue, Y., A. Leetmaa, and M. Ji, 2000: ENSO prediction with Markov models: The impact of sea level. *J. Climate*, **13 (4)**, 849–871.

Yu, J.-Y., C. R. Mechoso, J. C. McWilliams, and A. Arakawa, 2002: Impacts of the Indian Ocean on the ENSO cycle. *Geophys. Res. Lett.*, **29 (8)**, 1204, doi: 10.1029/2001GL014098.

Zebiak, S. E., 1993: Air-sea interaction in the equatorial Atlantic region. *J. Climate*, **6**, 1567–1586.

Zebiak, S. E. and M. A. Cane, 1987: A model El Niño-Southern Oscillation. *Mon. Wea. Rev.*, **115**, 2262–2278.

Acknowledgments

First and foremost I would like to thank Dietmar Dommenget who gave me good advice and still enough freedom. Thanks as well to Noel Keenlyside and Mojib Latif.

Thanks to Alex for interesting mathematical discussions, to Andi and the other physicists in Heidelberg, and to Astrid, Mirjam and Tim for our interdisciplinary coffee breaks and many other things...

Finally, special thanks to my parents for their support and their trust in me at all times.

Erklärung

Hiermit erkläre ich, dass ich die vorliegende Diplomarbeit selbständig verfasst und keine anderen als die angegebenen Quellen und Hilfsmittel verwendet habe. Ich versichere, dass diese Arbeit noch nicht an anderer Stelle zur Erlangung eines akademischen Grades vorgelegen hat.

Kiel, 15. Juni 2007

Malte Jansen